BTB-KELCH PROTEINS AND TAK1 KINASE
IN IMMUNE FUNCTION

APPROVED BY SUPERVISORY COMMITTEE

Zhijian Chen, Ph.D.

Daniel Garry, M.D., Ph.D.

Joachim Herz, M.D.

James Thomas, M.D.

DEDICATION

To my parents, my wife, and my twin boys.

BTB-KELCH PROTEINS AND TAK1 KINASE IN IMMUNE FUNCTION

by

Hong-Hsing Liu

DISSERTATION

Presented to the Faculty of the Graduate School of Biomedical Sciences
The University of Texas Southwestern Medical Center at Dallas
In Partial Fulfillment of the Requirements For the Degree of

DOCTOR OF PHILOSOPHY

The University of Texas Southwestern Medical Center at Dallas
Dallas, Texas
August, 2006

ACKNOWLEDGEMENT

I would like to acknowledge my mentor, Dr. Zhijian J. Chen, my committee chairman, Dr. Daniel Gary, and ex-program chair, Dr. George N. DeMartino for their trust. I would also acknowledge Dr. Thomas Wilkie, Dr. Chandra Mohan, and Dr. Joseph A. Hill for their help at the right time.

BTB-KELCH PROTEINS AND TAK1 KINASE
IN IMMUNE FUNCTION

Publication No. _____

Hong-Hsing Liu, Ph.D.
The University of Texas Southwestern Medical Center at Dallas, 2006

Supervising Professor: Zhijian Chen, Ph.D.

BTB-kelch proteins are putative components of E3 ligases with a BTB domain at the N terminus and several kelch repeats at the C terminus. KLHL6 and mKELCH are two members of this family. Conditional ablation of *Klhl6* in B cells resulted in mild developmental phenotypes in bone marrow precursors. The number of peripheral B cells was decreased by half, and responded defectively in germinal center formation after antigen stimulations. mKELCH is a novel protein cloned from hearts. Knocked-in *LacZ* expressed predominantly at muscles and several photosensitive organs.

TAK1 is a member of MAPKKK. Deletion of TAK1 prevented the maturation of $CD4^+$ or $CD8^+$ single positive thymocytes, leading to reduction of T cells in peripheral tissues. Thymocytes lacking TAK1 failed to activate NF-κB and JNK, and were prone to apoptosis upon stimulation. All three mouse models have provided important evidences in elucidating biological functions for each protein *in vivo*.

TABLE OF CONTENTS

LIST OF FIGURES

LIST OF TABLES

LIST OF ABBREVIATIONS

7-AAD	7-amino-actinomycin D
BACK	BTB and C-terminal Kelch
BCR	B Cell Receptor
BTB	Broad-Complex Tramtrack Bric-à-brac
CDD	Conserved Domain Database
E1	Ubiquitin-activation Enzyme
E2	Ubiquitin-conjugating Enzyme
E3	Ubiquitin Ligase Complex
EMSA	Electrophoretic Mobility Shift Assay
FACS	Fluorescence Activated Cell Sorting
Floxed	Flanked by *loxP* Sequences
IκB	Inhibitor of NF-κB
IKK	IκB Kinase
IL-1β	Interleukine-1β
JNK	c-Jun N-terminal Kinase
MAPKKK	Mitogen-activated Protein Kinase Kinase Kinase
NCBI	National Center for Biotechnology Information
NF-κB	Nuclear Factor Kappa B
PKCθ	Protein Kinase C-θ
PMA	Phorbol 12-myristate 13-acetate
RACE	Rapid Amplification of cDNA Ends
RIP	Receptor Interacting Protein
SCF	Skp1-Cul1-F-box
TAK1	TGFβ-activated Kinase 1
TCR	T Cell Receptor
TLR	Toll-like Receptor

TNFα	Tissue Necrosis Factor α
X-Gal	5-bromo-4-chloro-3-indolyl-beta-D-galactopyranoside

PRIOR PUBLICATIONS

[1] Hong-Hsing Liu†. Current Diagnosis & Treatment. Current Medicine, ING. (Chinese Version); Churchill Livingstone (English Version), Roy Pounder and Mark Hamilton edition, 1998. ISBN: 957-666-554-X †Translator for Chinese Version.

[2] Hong-Hsing Liu, Wuh-Liang Hwu, Chainllie Young, Wang-Tso Lee, Jyh-Chou Yang, Muh-Shy Chen, and Yu-Zen Shen. Phenotypic Polymorphism Associated with the T8993G Mutation of the Mitochondrial ATPase 6 Gene in a Family. Acta Paediatrica Sinica, 40(1):126–126, April 1999.

[3] Hong-Hsing Liu, Ming-Tai Lin, Chien-Chih Chang, Jou-Kou Wang, Mei-Hwan Wu, Ming-Kwang Shyu, Chien-Nan Lee, and Fon-Jou Hsieh. Postnatal outcome of fetal cardiac echogenic foci. J Formos Med Assoc, 101(5):329–336, May 2002.

[4] Jens Kroll†, Xiaozhong Shi†, Arianna Caprioli†, Hong-Hsing Liu†, Claudia Waskow, Keng-Mean Lin, Toru Miyazaki, Hans-Reimer Rodewald, and Thomas N Sato. The BTB-kelch protein KLHL6 is involved in B-lymphocyte antigen receptor signaling and germinal center formation. Mol Cell Biol, 25(19):8531–8540, Oct 2005. †Equal Contribution.

[5] Qinmiao Sun†, Lijun Sun†, Hong-Hsing Liu, Xiang Chen, Rashu B Seth, James Forman, and Zhijian J Chen. The Specific and Essential Role of MAVS in Antiviral Innate Immune Responses. Immunity, 24(5):633–642, May 2006. †Equal Contribution.

[6] Hong-Hsing Liu, Min Xie, Michael D Schneider, and Zhijian J Chen. Essential role of tak1 in thymocyte development and activation. Proc Natl Acad Sci U S A, 103(31):11677–11682, Aug 2006.

CHAPTER ONE
Introduction to BTB-kelch Proteins

BTB-kelch proteins usually have one BTB domain at the N terminus and several kelch repeats at the C terminus. They are present at genomes from viruses, plants, fungi to mammals. Among metazoan animals, BTB-kelch proteins represent the major expansion of the kelch-repeat superfamily. 70% (50/71) of the human kelch-repeat proteins have one BTB domain at the N-terminus [74]. *Lztr-1* is an exception which has kelch repeats at the N-terminus and two BTB domains at the C-terminus [64]. A recent bioinformatic study identified an additional sequence conservation between both terminal domains, the BACK domain [99]. 53 out of 55 BTB-kelch proteins in the human genome preserve this sequence motif between the N-terminal BTB domain and the C-terminal kelch repeats. Although BTB-kelch proteins represent a major protein family among metazoan animals, biological functions for most of such proteins have remained undefined.

BTB Domain

Identification and Structure

The BTB domain was first identified in *Drosophila* [128]. All of the three founder genes, *BR-C, ttk,* and *bab* are involved in *Drosophila* development. The conserved sequences are around 115 amino acids in length. Some zinc-finger transcription factors carry the BTB domain as well [7]. The crystal structure of the BTB domain from promyelocytic leukemia zinc finger protein revealed a tightly intertwined dimer (Figure 1.1). Around one-fourth of the monomer surface was involved in intermolecular contact, suggesting an obligate homodimer configuration.

Molecular Function

Part of the structure of Skp1 protein is very similar to BTB domain [90]. Skp1 is involved in the assembly of SCF E3 complex, which ligates ubiquitin to specific substrates for proteasome-dependent degradation. In 2003, several groups independently provided evidence that BTB domain is an adaptor for cullin-3-based E3 ligase [38, 39, 73, 122]. BTB domain combines the function of Skp1 and F box proteins in cullin-1-based E3 ligases [see review 72]. Recently some physiological substrates for BTB-based E3 complex have been revealed [24, 51, 117, 125]. Interestingly, at least in one case BTB domain directly links to E1 instead of cullin proteins in mediating ubiquitin ligation [3].

BACK Domain

This intervening domain between the N-terminal BTB domain and the C-terminal kelch repeats was identified through bioinformatic studies [99]. Most of the BTB-kelch proteins in the human genome preserve this sequence motif. Although there are no structural data for functional predictions, the BACK domain in Keap1 is responsible for sensing carcinogens and oxidants with several sulfhydryl groups at this region [29]. In addition, cullin-based ubiquitin ligation might need BACK domain as a scaffold to align the activated ubiquitin and a protein substrate.

Kelch Domain

Identification and Structure

Kelch motif was found in *Drosophila* as a sixfold tandem element [78]. Structurally it belongs to the β-propeller superfamily [see review 1]. Usually kelch motif repeats itself 6 to 8 times to form a bowl-shaped propeller (Figure 1.2). Each blade of the propeller has 4 anti-parallel β strands. A propeller has three potential interacting surfaces: the top, the

bottom, and the circumference. Between blades are various loops. Two structures of kelch repeats have been solved. One is galactose oxidase from *Hypomyces rosellus* (PDB 1GOF), and the other is the kelch domain from Keap1 (PDB 1U6D). For galactose oxidase, the substrate lies upon the top surface. Instead, the Keap1 kelch domain interacts with the Nrf2 substrate at a loop near the bottom surface. An intriguing feature of the Keap1 kelch domain is the strong positive charge surface near the bottom (Figure 1.3).

Molecular Function

As might be expected from the huge number of kelch-repeat proteins in the genomes, a lot of cellular functions are related to this family [see review 1]. In brief, they affect cytoskeleton organization, gene expression, and even human diseases; their subcellular localizations also span from extracellular space, cytoplasm, to nuclei.

Enzymes

Galactose oxidase uses the top surface of the kelch propeller as a catalytic surface to oxidize primary alcohols to aldehydes [62]. In *Arabidopsis* and *Plasmodium falciparum* kelch repeats function as phosphatases [53, 63]. However, there have been no evidence for enzymatic functions in kelch-repeat proteins of higher animals.

Novel G_β Subunits

Two groups have independently found kelch-repeat proteins as novel G_β mimics to Gpa2 in yeasts [9, 43]. Gpa2 used to be an orphan G_α protein without known G_β or G_γ partners. These groups provided both functional and biochemical evidences that kelch-repeat proteins can be a *bona fide* G_β protein. Interestingly G_β proteins usually carry a WD40 domain, which also belongs to the β-propeller superfamily. So far there has been no evidence that higher animals use kelch-repeat proteins as G_β mimics.

Substrate Adaptor for Proteasome

Structurally the BTB domain resembles Skp1-F-box in cullin-1-based E3 ligases [90]. Functionally the BTB domain interacts with cullin-3 [38, 39, 73, 122]. Compared

to the configurations of cullin-1-based E3 complexes, the C-terminal kelch repeats could function as a substrate catcher for cullin-3-based ubiquitin ligases. Indeed, Keap1 is an example of BTB-kelch proteins which mediates proteasome-dependent degradation through cullin-3-based complexes [24, 51, 125].

Examples of BTB-kelch Proteins

Kelch

Kelch is the prototype protein in kelch-repeat family [78]. In *Drosophila*, *kelch* mutants are sterile because of impaired cytoplasm transport from nurse cells to oocytes. Kelch colocalizes with actin, and functions as an organizer for ring canal assembly during oogenesis. In mutants assembly of ring canals are defective and cytoplasm transport is thus compromised between oocytes and nursing cells.

Keap1

Keap1 was identified through yeast two hybrids as a cytoplasmic repressor for Nrf2 [49]. Nrf2 is an essential transcription factor in response to oxidants. Under normal conditions, Nrf2 is constantly degraded. Under stressed conditions, Nrf2 translocates to the nucleus and turns on detoxifying genes. Keap1 plays a critical role in this regulation. Recent evidence has shown that this regulation depends on Keap1-cullin-3-based E3 complexes [24, 51, 125]. Several sulfhydryl groups at BACK domain of Keap1 were proposed to be the direct sensor for oxidants [29]. Knockout animals of Keap1 have phenotypes from constitutive Nrf2 activation with resultant postnatal lethality [113].

Gigaxonin

Gigaxonin is the pathogenic gene for giant axonal neuropathy [11]. Patients suffer from symptoms both at the central and the peripheral nervous systems. The main pathology is generalized disorganization of cytoskeletal intermediate filaments. Several potential

substrates for proteasome-dependent degradation have been identified, including the light chain of microtubule-associated protein 1B, tubulin folding cofactor B, and microtubule-associated protein 8 [3, 28, 117]. However, none of these substrates have been shown to depend on cullin-3 for ubiquitin ligations.

Discussion

Substrate specificity

Gigaxonin seems able to recognize many cytoskeleton-related proteins for degradation [3, 28, 117]. It is known that β-transducin repeats-containing proteins (β-TrCP) also recognizes several phosphorylated targets for proteasome-dependent degradation [see review 128]. The recognized motif for β-TrCP includes $DS^PG\Psi XS^P$, where S^P stands for phosphoserine, Ψ stands for a hydrophobic residue, and X represents any amino acids. Keap1-Nrf2 interaction depends on a short essential motif ETGE [52]. It would be intriguing to investigate the phosphorylation status of the threonine residue in ETGE motif. All of these facts imply the motif-based recognition for proteasome substrates. Because the motif sequences are not long, potential redundancy among BTB-kelch proteins could be expected.

BTB Domain Revisited

It is known BTB domains from some transcription factors can form heterodimers [7]. However, it is not known if this interaction can occur among BTB-kelch proteins. If heterodimers did exist among BTB-kelch proteins, the functional relationship between kelch-mediated protein targets would be intriguing. In addition to dimerization, the BTB domain is involved in Golgi localization in the case of Lztr-1 [64]. It is not known if N-terminal BTB domains could have similar functions.

Kelch Domain Revisited

BTB-kelch proteins can be divided into groups based on kelch repeat alignments [99]. It is not known if there are any functional significance for these divisions. One group has an Arginine in the beginning of each kelch repeat. Potentially these Arginine residues could form a positive electrostatic surface for the kelch propeller. It is interesting to note that $G_{\beta 1}$ has instead a negative electrostatic charge on the G_{α}-facing surface [114]. The significance of these findings deserve more detailed investigations.

Figures

All figures were rendered with PyMOL [26].

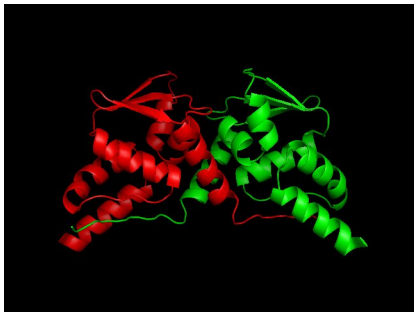

Figure 1.1 Ribbon diagram of BTB domain

BTB domain from promyelocytic leukemia zinc finger protein (PDB 1BUO) is shown in ribbon rendering. One monomer is colored red and the other is green.

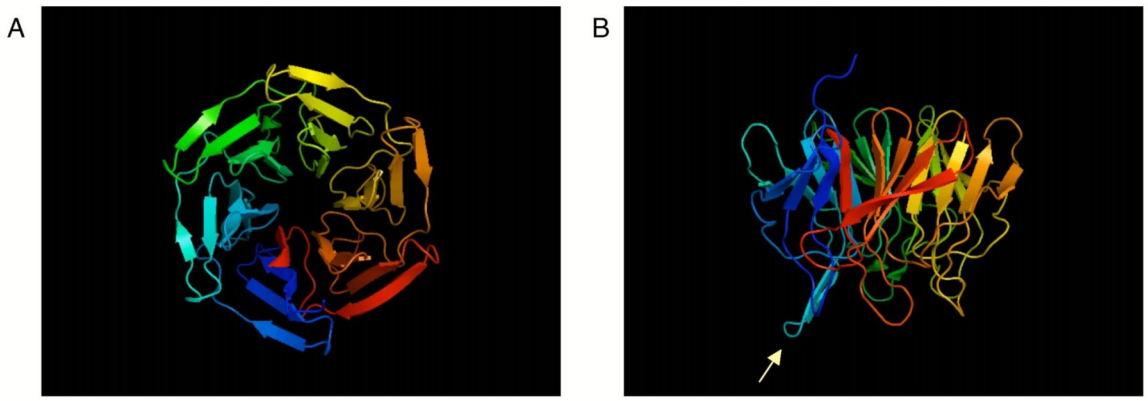

Figure 1.2 Ribbon diagrams of kelch domain

(A) Top view of Keap1 kelch domain, which has 6 blades in the β-propeller. (B) Side view of Keap1 kelch domain. The loop (arrow) near the bottom surface is the interacting motif to Nrf2.

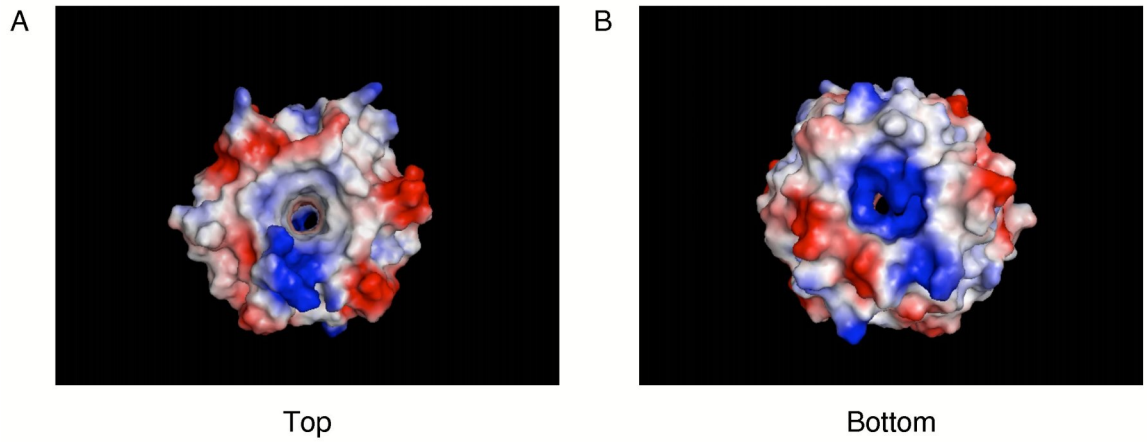

FIGURE 1.3 ELECTROSTATIC POTENTIAL OF KELCH DOMAIN

(A) Top view of electrostatic potential of Keap1 kelch domain. Red is negative charge, and blue is positive charge. (B) Bottom view of electrostatic potential of Keap1 kelch domain. Be aware of strong positive charge surface around the bottom hole.

CHAPTER TWO
KLHL6

Introduction

KLHL6 is a BTB-kelch protein, isolated by virtue of its expression in embryonic but not adult endothelial cells. By subtraction hybridization between cDNAs from E15.5 embryonic and adult endothelial cells, *Klhl6* was cloned from mouse spleen lambda ZAP II library (Stratagene). In adult mice, instead, we detected high levels of expression in hematopoietic and lymphoid organs. The same gene was recently shown to be highly expressed in sheep Peyer's patch and human tonsil B cells [41]. Based on this specific expression pattern in adult mice, it has been suggested that KLHL6 might be involved in B-cell functions, notably the germinal center reaction [41]. Indeed B cells from *Klhl6* conventional knockout mice had defects in response to antigen stimulation both *in vivo* and *in vitro* (J. Kroll). To further analyze if *Klhl6*-null phenotypes are B-cell autonomous or not, we took a genetic approach to conditionally knockout *Klhl6* in B cells. We found that all phenotypes from bone marrow precursors till lymph node B cells were reproducible in B-cell specific knockout mice. These included impaired upregulation of CD21 expression among bone marrow immature cells, reduced numbers of peripheral B cells, and compromised germinal center formation after antigen challenge. Biochemical studies also showed lower calcium mobilization and CD69 surface expression after anti-IgM stimulation. It seemed the threshold for BCR signaling was elevated in KLHL6-null B cells.

Materials and Methods

Generation of Floxed *Klhl6* mice

The bacterial artificial chromosome (BAC) genomic clone for the *Klhl6* gene was obtained from Research Genetics and the targeting vector was constructed as shown in Figure 2.3. Briefly, the first exon of *Klhl6* was replaced by a fragment containing a floxed first exon followed by an Flp recombination target-flanked *PGK::neo* cassette. The *PGK::neo* cassette was later removed by crossing chimera to hACTB::FLPe.9205 mice [79]. Electroporation, embryonic stem (ES) cell culture, and Southern blot screening were performed as previously described [102]. Some *neo*-free floxed mice were crossed to *CAG::Cre* mice to make Δ alleles [86]. Mice were genotyped by PCR using the following primer pairs: cctgtgcaggaaatccgttc and aagggtccttccaagctcctc (for the wild type and the floxed alleles; the former is 140 bp, and the latter is 217 bp); cctgtgcaggaaatccgttc and gcgggcctcttcgctattac (for the *LacZ* allele); cctgtgcaggaaatccgttc and cagcaaacaaatcagactgagc (for the Δ allele). The PCR conditions were: 94°C for 30 seconds; 58°C for 30 seconds; and 72°C for 1 minute; 35 cycles.

Genetic Background and Age of the Mice

The mice were studied on CD1 and 129/svEms-+Ter$^{?}$/J mixed backgrounds. The studies were conducted with adult mice at 6 to 10 weeks of age raised at the animal center of University of Southwestern Medical Center at Dallas.

Flow Cytometry

Splenocytes or lymph node cells were isolated by mechanically dissociating mouse spleens through 100μm nylon mesh (BD Bioscience) in the FACS staining buffer (5% fetal bovine serum in phosphate-buffered saline). Bone marrow cells were collected from femurs and tibias. Antibodies against B220 (RA3-6B2), CD21 (7G6), BP-1 (6C3), CD24 (M1/69), CD43 (S7), CD23 (B3B4), CD40, CXCR5, CD69, GL7 and immunoglobulin M (IgM) (II/41) coupled to allophycocyanin, phycoerythrin, fluorescein isothiocyanate, or biotin as appropriate were from BD Bioscience. Streptavidin coupled to peridinin chlorophyll protein (BD Bioscience) was used as the secondary reagent. At least half million total cells were analyzed for each experiment. Cells were stained on ice in FACS buffer for 15 minutes and washed once before analyzing or adding the secondary reagent. In the latter case, cells

were stained for another 15 minutes on ice followed by another washing step. Cells were detected by FACSCalibur or FACScan (Becton Dickinson) flow cytometers and analyzed using CellQuest software.

Footpad Assay

Ovalbumin (50μg in 50μl PBS) with 50μl complete Freund's adjuvant was injected in one hind footpad of each mouse. The other footpad was injected with PBS with complete Freund's adjuvant as a negative control. Mice were anesthetized 10 days after the injection, and perfused with 4% paraformaldehyde-PBS. Popliteal lymph nodes were dissected, fixed for 4 hours at 4°C in 4% paraformaldehyde-PBS, incubated overnight in 18% sucrose at 4°C, and embedded in OCT. Sections (8μm) were blocked in 3% bovine serum albumin-PBS in room temperature for 1 hour and incubated overnight at 4°C with 0.1 μg/ml peanut fluorescein isothiocyanate (FITC)-lectin (Sigma L-7381) in 3% bovine serum albumin-PBS. This lectin staining identifies germinal center B cells in lymph nodes [15]. The stained samples were washed, mounted in VECTASHIELD (Vector Laboratories), and examined with an Axioplan microscope (Zeiss) equipped with fluorescence filters. Germinal center B cells in lymph nodes were measured by staining with anti-GL7 together with anti-B220 antibodies (BD Bioscience).

RT-PCR Analysis of KLHL6 Expression

B cells were sorted at H.-R. Rodewald's and C. Waskow's lab according to the cell surface markers reported by Hardy et al. [44] and by Carsetti [17]. The cDNAs were synthesized from total RNA isolated from approximately 20,000 cells from each indicated developmental stage. The primers used for KLHL6 were 5'-AGA CCA GGA GAG TGT GCA TGG-3' and 5'-CGT TGA TGG CAG GAC AAA GAG-3'. The primers for glyceraldehyde-3-phosphate dehydrogenase (GAPDH) were obtained from Clontech. PCR was performed at 94°C (5 minutes), 35 cycles at 94°C (30 seconds), 58°C (30 seconds), 72°C (45 seconds), and 72°C (10 minutes) in the end.

CD69 Profile after Anti-IgM Stimulation

Spleens were removed from the mice and splenocytes were isolated by mechanical dissociation. B cells were purified by depletion of non-B cells using the mouse B-cell isolation kit (Miltenyi Biotec) according to the manufacturer's protocol. The purity of the resulting B-cell fraction (99%) was confirmed by FACS with anti-B220-phycoerythrin and anti-IgM-FITC antibodies. Approximately 10^6 cells per 96-well plate were seeded in Dulbecco's modified Eagle's medium containing 10% fetal bovine serum, antibiotics, and β-mercaptoethanol. One hour later, the cells were stimulated with various concentrations of anti-IgM. 48 hours later cells were subject to flow cytometric analysis for CD69 expression.

Assays for Intracellular Free Calcium Levels

These assays were performed by Dr. XZ. Shi in the lab. Calcium concentrations were measured by the protocol (PP00000011) of the Alliance for Cellular Signaling (http://www.signaling-gateway.org). B cells isolated by a B-cell isolation kit (Miltenyi Biotec 130-090-862) were resuspended at 5 x 10^6 cells/ml in SIMDM (Iscove's modified Dulbecco's medium supplied with 2 mM L-glutamine, 55 μM β-mercaptoethanol, 0.025% Pluronic F-68, and 0.1 mg/ml bovine serum albumin) containing 12 μl/ml Fluo-3 (4 μM) (Molecular Probes) and 12 μl/ml Pluronic F-127 (0.08%) (Molecular Probes). Cells were distributed into six-well ultra-low-attachment plates (Corning) at 2 ml/well. Incubated at 37°C and 5% CO2 for 30 min, cells were resuspended in fresh SIMDM for another 30 min, pelleted down and resuspended in Hanks' balanced salt solution-bovine serum albumin (Hanks' balanced salt solution supplied with 25 mM HEPES, 1 mg/ml bovine serum albumin, pH 7.4) at 8.3 x 10^6 cells/ml. The final cell suspension was distributed into 96-well black-walled plates at 90 μl/well and equilibrated in the fluorescence chamber for 5 minutes. Baseline fluorescence was measured for 10 minutes. 10 μl of the F(ab')$_2$ fragment of goat anti-mouse IgM or anti-CD19 was added to start the stimulation. The fluorescence was measured by Fluoroskan Ascent microplate fluorometer (Thermo-Labsystems) and analyzed by Ascent software (Thermo-Labsystems).

For measurements of intracellular calcium levels within individual cells, splenocytes were washed with 10% fetal bovine serum-PBS, resuspended at 10^7 cells/ml in load-

ing medium (10% fetal bovine serum-RPMI 1640), and incubated with 5 μg/ml Indo-1 AM (Molecular Probes) for 30 min at 37°C. The cells were stained with phycoerythrin-conjugated anti-B220 monoclonal antibody for 30 min on ice, washed with Hanks' balanced salt solution twice, and resuspended in loading buffer at 10^7 cells/ml. Calcium flux was triggered by adding a F(ab')$_2$ fragment of goat anti-mouse IgM (Jackson ImmunoResearch Laboratories) or anti-CD19 antibody (MB19-1, BD Biosciences). The calcium fluxes were recorded in real time using a FACSVantage SE instrument (BD Biosciences) and analyzed by FACSDiva (BD Biosciences).

Bioinformatic Analysis

Multiple alignments were calculated by ClustalW [22] and outputted as shaded drawings by BOXSHADE (http://www.ch.embnet.org/software/BOX_form.html). Protein domains were identified by Pfam protein families database [8].

Statistics

Student's t-Tests were used for statistical analyses. Data were presented as average ± standard deviation.

Results

Discovery and Expression

Discovery

We had originally identified *Klhl6* as a gene that is differentially expressed in embryonic but not in adult vascular endothelial cells. Sequence comparison showed that KLHL6 is a BTB-kelch protein which is highly conserved from Zebrafish to Humans (Figure 2.1.A).

It contains a BTB domain at the N terminus and six kelch repeats at the C terminus. It also has the intervening BACK domain between both termini. The typical GG doublets are apparent in each kelch motif (Figure 2.1.B), though the first kelch repeat was unrecognized by Pfam protein families database [8]. In spite of specific expression of KLHL6 in embryonic vasculature, analysis of conventional *Klhl6* knockout mice revealed apparently normal blood vessel development and function (J. Kroll and data not shown). Others have recently reported that KLHL6 is expressed predominantly in sheep Peyer's patch and human tonsil B lymphocytes [41].

Expression

To extend this analysis more systematically to various stages of B-cell ontogeny, B-cell progenitors were purified from bone marrow of normal mice according to Hardy's scheme [44]. B cells develop from fraction B (B220$^+$ CD43$^+$ CD24$^+$ BP-1$^-$), via C (B220$^+$ CD43$^+$ CD24$^+$ BP-1$^+$), D (B220$^+$ CD43$^-$ IgM$^-$), and E (B220$^+$ CD43$^-$ IgM$^+$) to F (B220^{high}CD43$^-$ IgM$^+$). In this order, B to E represent immature and newly generated B cells, while cells in F represent recirculating mature B cells to the bone marrow. Reverse transcription-PCR (RT-PCR) analysis showed similar expression of KLHL6 throughout B-cell development (Figure 2.2). Splenic B cells were sorted into transitional 1 (T1) (B220$^+$ HSA^{high} CD21$^-$ CD23$^-$), transitional 2 (T2) (B220$^+$ HSA^{low} CD21$^+$ CD23$^+$), marginal zone (Mz) (B220$^+$ CD21$^+$ CD23$^-$), and follicular (Fo) (B220$^+$ HSA$^{-/low}$ CD21^{low} CD23^{low}) B-cell subsets [19, 59]. Again, all of these B-cell populations expressed KLHL6 (Figure 2.2).

Floxed Allele

Conventional knockout mice of *Klhl6* had phenotypes of reduced B-cell numbers, compromised proliferation after anti-IgM stimulation, and impaired germinal center formation after antigen challenge *in vivo* (J. Kroll and data not shown). To test if these phenotypes could be explained in a B-cell-autonomous manner, a floxed allele of *Klhl6* was engineered by homologous recombination in mouse embryonic stem cells.

Targeting Construct

A pair of *loxP* sequences were inserted at the first exon before ATG and the first intron. Following the intron *loxP* sequence was a *FRT*-flanked *PGK::neo* cassette, which is removable by yeast-derived recombinase Flipase [4]. The lengths of short-arm and long-arm for homologous recombination are 1.5 kb and 5.2 kb, respectively (Figure 2.3.A). The targeted allele can be differentiated from the wildtype allele by Southern blotting after Spe I digestion. The external probe can detect the wildtype allele at 19.7 kb but the floxed allele at 18.2 kb (Figure 2.3.B).

Floxed Mice

Electroporation, culture and selection for homologous recombination among embryonic stem cells are described in Materials and Methods. Out of 295 *neo*-resistant stem cell clones, 2 recombined homologously. The targeted clones were injected into blastocysts, only one of which contributed more than 90% of cellularity to 7 chimeric mice. The only one chimera with germline transmission was mated directly to hACTB::FLPe.9205 mice to remove the *neo* cassette [79]. The *neo*-free floxed mice were further mated to *CD19::Cre* mice for B-cell specific knockout of *Klhl6* [77]. Except for the B-cell phenotypes, no other abnormalities were found in floxed animals. Some *neo*-free floxed mice were crossed to *CAG::Cre* mice to make Δ alleles [86].

B Cell Specific Excision

Tail and B cell genomes from the same heterozygous animal carrying *CD19::Cre* were subject to Southern blotting analysis (Figure 2.3.C). Clearly the floxed allele was only excised in the B cell genome, but not in the tail genome. In the meanwhile, the wildtype allele remained untouched by the Cre recombinase.

Phenotypes

B-cell phenotypes were present at several developmental stages. From early bone marrow precursors till lymph node germinal centers, all of the phenotypes were B-cell autonomous.

Bone Marrow Development

Based on Hardy's scheme [44], bone marrow B cell precursors develop from fraction B ($B220^+$ $CD43^+$ $CD24^+$ $BP\text{-}1^-$), via C ($B220^+$ $CD43^+$ $CD24^+$ $BP\text{-}1^+$), D ($B220^+$ $CD43^-$ IgM^-), and E ($B220^+$ $CD43^-$ IgM^+) to F ($B220^{high}$$CD43^-$ IgM^+). Although KLHL6 is expressed through the whole developmental stages (Figure 2.2), there are no apparent differences before stage F, the fraction containing mature B cells recirculating from periphery into bone marrow (Figure 2.4). However, if taken into consideration of transitional cells (IgM^{high} $CD21^{intermediate}$) [18], CD21 upregulation in this population was less apparent in any of *Klhl6*-null mice (arrow position of -/-, Δ/Δ, or *loxP/loxP;CD19::Cre* in Figure 2.5).

Splenic Development

As shown in Figure 2.4, there were less mature B cells (F fraction) in *Klhl6-null* mice. Direct analysis on splenic B cells showed a roughly 50% decrease in either conventional knockout or B-cell specific knockout animals (Figure 2.6). We next analyzed splenic B cells at different developmental stages. Similar to precursors in bone marrow, splenic B cells need to develop through several additional steps, including transitional 1 ($B220^+$ $CD23^-$ IgM^{high} $CD21^{low}$, T1), transitional 2 ($B220^+$ $CD23^+$ IgM^{high} $CD21^{high}$, T2), marginal zone ($B220^+$ $CD23^-$ IgM^{high} $CD21^{high}$, MZ), and mature follicular cells ($B220^+$ $CD23^-$ IgM^{low} $CD21^{high}$, Fo) [19, 59]. In *Klhl6*-null animals populations at T1, T2 or Fo stages were reduced significantly to around 50% (Table 2.1), but cells at Mz stage were not reduced to the same extent. Therefore their relative abundances were grossly preserved (Figure 2.7).

Anti-IgM Stimulation

Proliferation of *Klhl6*-null B cells in response to anti-IgM stimulation was severely compromised (J. Kroll and data not shown). To extend the analysis to single cells, we (J. Kroll and H.-H. Liu) stimulated purified splenic B cells with different concentrations of anti-IgM and analyzed their surface expression of CD69, which is an early activation marker for lymphoid cells [see review 103]. At the concentration of 5 μg/ml, expression profile of CD69 in *Klhl6* heterozygous B cells was overlapping with the expression profile at 10 μg/ml (Figure 2.8.A). Therefore stronger stimulation at 10 μg/ml did not shift the profile further.

Instead, CD69 was barely expressed on *Klhl6*-null B cells stimulated at 5 μg/ml, though the expression was upregulated to a higher level after anti-IgM was concentrated to 10 μg/ml. Notably the CD69 profiles between knockout and heterozygous B cells at 10 μg/ml anti-IgM level were essentially overlapping (Figure 2.8.B). These data were compatible with the hypothesis that BCR signaling threshold on *Klhl6*-null B cells was elevated, and cells' response could be compensated by strengthening the stimulation.

Germinal Centers

It has previously been reported that KLHL6 is expressed in sheep Peyer's patch and human tonsil B cells, suggesting that KLHL6 expression may be associated with the germinal center (GC) reaction [41]. To test this idea directly, mice were immunized in bilateral hind footpads with chicken ovalbumin or PBS. 10 days later, GC B cells ($B220^+$ $GL7^+$) were quantitated by flow cytometry. As shown in Table 2.2, GC B cell numbers in lymph nodes were much higher in wildtype animals after ovalbumin stimulation. In *Klhl6*-null mice, GC reactions still existed but expanded to a much lower extent. In *loxP/loxP;CD19::Cre* mice, GC reactions were also compromised (Figure 2.9.A). Quantification by flow cytometry revealed a 228-fold versus 19-fold increase of $B220^+$ $GL7^+$ GC B lymphocytes per lymph node in response to ovalbumin injections in *loxP/loxP* and *loxP/loxP;CD19::Cre* mice, respectively. The compromised GC formation in KLHL-null B cells were independent of other related receptors such as CD40 or CXCR5, which were essentially comparable between heterozygous and homozygous animals (Figure 2.9.B).

Mechanism Hypothesis

Similar compromised GC formation could be found in either *Cd19* or *Cd21* knockout mice [37, 76], which were involved in the threshold control for BCR signaling [see review 65]. It is also known that the CD19/CD21 complex has synergistic effect in calcium mobilization with B cell receptors [20, 109]. Because *Klhl6*-null mice had impaired GC reactions *in vivo* and elevated thresholds for CD69 expression *in vitro*, it is possible KLHL6 is another molecule involved in threshold control for BCR signaling. It is not known if KLHL6 has any interactions with CD19/CD21 complex, but preliminary data showed that CD19 cocapping

still occurred with BCR after anti-IgM stimulation upon *Klhl6*-null B cells (data not shown).

Increased Use of Lambda Light Chain

B cell receptors need to go through selections both in the bone marrow and in the spleen [54, 59]. There are two light chain loci for mice, kappa and lambda. Unlike humans, mice utilize kappa chains before lambda chains in establishing BCR repertoire [80]. If the threshold for BCR signaling is elevated, it would be expected to see more lambda light chain use in the periphery because of higher failing rates after putative "positive" selections for B cells. This expectation is indeed documented in *Cd19* knockout mice [95]. Similarly lambda light chains were used more frequently in *Klhl6*-null mature B cells (Figure 2.10). Early immature *Klhl6*-null B cells ($B200^+$ IgM^-) had comparable use of lambda light chains to wildtype B cells. However, the use frequency gradually increased with maturation of *Klhl6*-null B cells.

Impaired Calcium Response

To gain information as to whether BCR-signaling pathways were affected by the loss of KLHL6, Dr. XZ. Shi had studied calcium response to anti-IgM stimulations *in vitro* upon splenic B cells. As a population, *Klhl6*-null B cells showed a markedly reduced increase in the level of intracellular Ca^{2+} in response to anti-IgM stimulation compared to wild-type B cells (Figure 2.11.A). To determine the frequencies of B cells which exhibited such low Ca^{2+} response, stimulation-dependent changes in intracellular calcium levels in individual cells were measured by flow cytometry. This analysis demonstrated an impaired anti-IgM response in a substantial fraction of *Klhl6*-null B cells (Figure 2.11.B). Notably such compromised responses were partially compensated when the strength of anti-IgM stimulation was increased to 10 μg/ml.

Discussion

KLHL6 was expressed throughout all stages of B-cell development. In the bone marrow, upregulation of CD21 in transitional cells ($B220^+$ IgM^{high}) were less apparent.

In the periphery, several subsets of B cells were reduced to around 50%. Responses to stimulations were defective both *in vivo* and *in vitro*. GC formation after ovalbumin challenge was compromised. Thresholds for CD69 expression on anti-IgM stimulated B cells were elevated. Importantly, all the phenotypes were B-cell autonomous. Although precise biochemical defects in *Klhl6*-null B cells are not known, it is possible that loss of KLHL6 resulted in higher thresholds for BCR signaling.

BCR Signaling Threshold

Biochemical studies showed defective calcium response to anti-IgM stimulations in *Klhl6*-null B cells. The defect could be partially compensated by higher strengths of stimulations at 10 μg/ml (Figure 2.11.A). Similarly CD69 expressed normally when anti-IgM stimulations were raised to 10 μg/ml (Figure 2.8). The CD19/CD21 complex has been known to be involved in fine-tuning BCR signaling threshold [see review 65]. Knockout mice of either *Cd19* or *Cd21* have similar defects in GC formations [37, 76]. Loss of CD19 results in more frequent use of lambda light chains [95], which was also true for *Klhl6*-null B cells (Figure 2.10). Although primitive studies showed that CD19 cocapping with BCR was normal after anti-IgM stimulations (data not shown), further detailed studies on CD19 signaling would be helpful.

CD19 Signaling and Calcium

Ligation of CD19 is important in assembly of a signaling complex for Vav and phosphatidylinositol 3-kinase (PI3K) pathways [120]. Vav is a nucleotide exchange factor for G-protein Ras [40], while PI3K is important for calcium mobilization via interactions between phosphatidylinositol 3,4,5-trisphosphate and the Src-homology 2 domain on phospholipase C gamma [75]. Because Vav is important in T cell development [110] and we did not find apparent abnormalities in *Klhl6*-null T cells, the involvement of Vav in the biochemical defect is less likely. In contrast, phosphorylation of CD19 Y484 and Y515 are important for PI3K activation [13], and the latter is important for calcium mobilization. Therefore further studies on PI3K activity as well as phosphorylation status at indicated tyrosine residues on CD19 of *Klhl6*-null B cells would be warranted.

Relationship to E3 Ligase

Recently some BTB-kelch proteins have been shown to be components of E3 ligases [5, 24, 51, 117, 125]. KLHL12 negatively regulates Wnt signaling by targeting Dishevelled for degradation [5]. It would be possible KLHL6 also targets some negatively-regulating components in BCR signaling for proteasome-dependent degradation. Without KLHL6-mediated degradation, the presumed substrate level might be high and exerted a stronger negative effect. If the degradation was BCR-signaling dependent, KLHL6 might be able to positively feedback to those B cells which successfully signal through BCR. Alternatively, E3 might use ubiquitins for other signaling functions [see review 100], though such roles have not been reported for any of BTB-kelch proteins. Lastly, possibilities could not be ruled out that KLHL6 could have functions other than E3. If binding partners could be found for KLHL6, which might be BCR-signaling dependent, those possible functions of KLHL6 could be more readily investigated.

Conclusion

Knockout of KLHL6 in B cells has provided evidence in B-cell autonomous phenotypes from bone marrow precursors, peripheral mature B cells, and germinal center formations in lymph nodes. It is also another *in vivo* model demonstrating various involvements of BTB-kelch proteins in mammalian biology after Gigaxonin [11], Keap1 [113], and KLHL10 [124].

Acknowledgment

I thank Dr. Toru Miyazaki, Dr. Chandra Mohan, and Dr. Richard H. Scheuermann for their kind discussions and analyses with experimental data. I also thank John Shelton for his help with histological preparations.

Figures

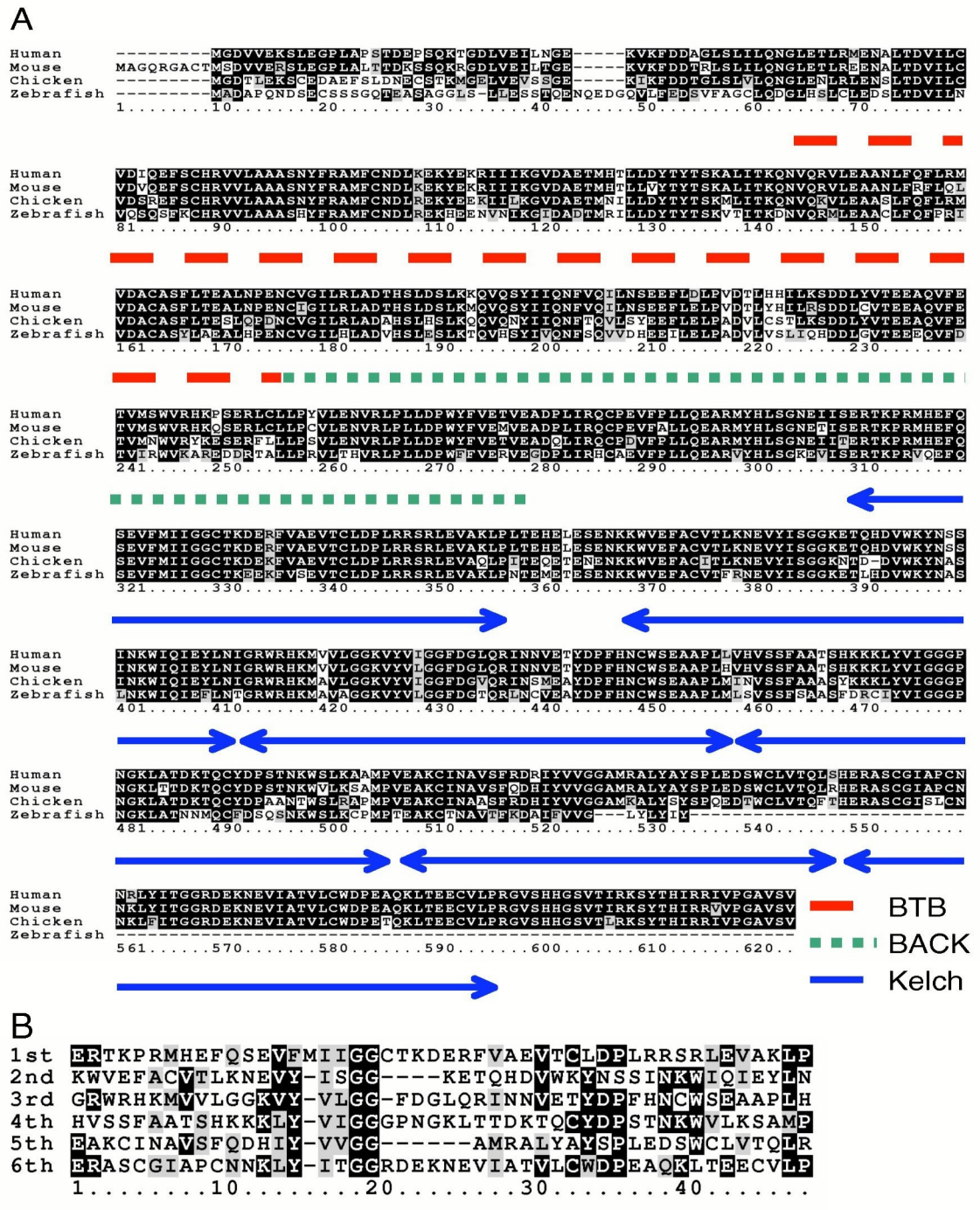

Figure 2.1 Multiple alignment of KLHL6

(A) KLHL6 homologs from Zebrafish, Chicken, Mouse, and Humans were aligned by ClustalW [22] and illustrated by BOXSHADE. Protein domain structures were identified by Pfam protein families database [8] and by manual inspection for the first kelch repeat. One BTB domain was identified at the N terminus, followed by the BACK domain, and six kelch repeats at the C terminus. Each domain or repeat was delineated by color lines. (B) 6 kelch repeats were aligned one by one. The typical GG doublets in kelch motif were apparent for every kelch repeat of KLHL6.

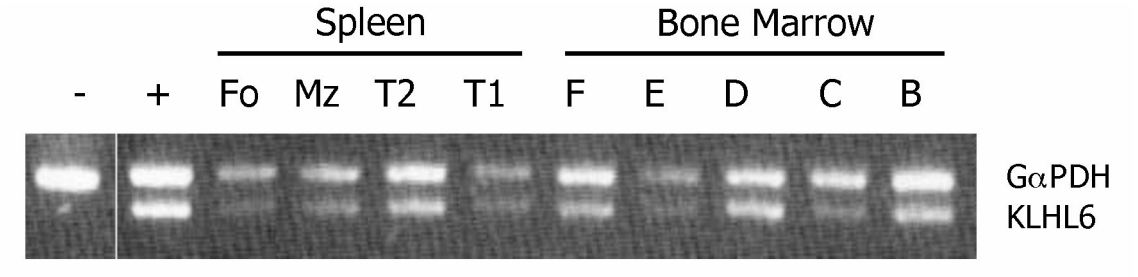

FIGURE 2.2 KLHL6 EXPRESSION AT B-LINEAGE DEVELOPMENTAL STAGES

B cells at different developmental stages were sorted according to the cell surface markers as reported by Hardy et al. [44] and by Carsetti [17]. The cDNAs were synthesized from total RNA and subject to PCR amplification for both KLHL6 and GAPDH. KLHL6 is expressed at all developmental stages from bone marrow precursors till splenic B cells. Negative control for KLHL6 was obtained from splenic cDNA of *Klhl6*-null mice.

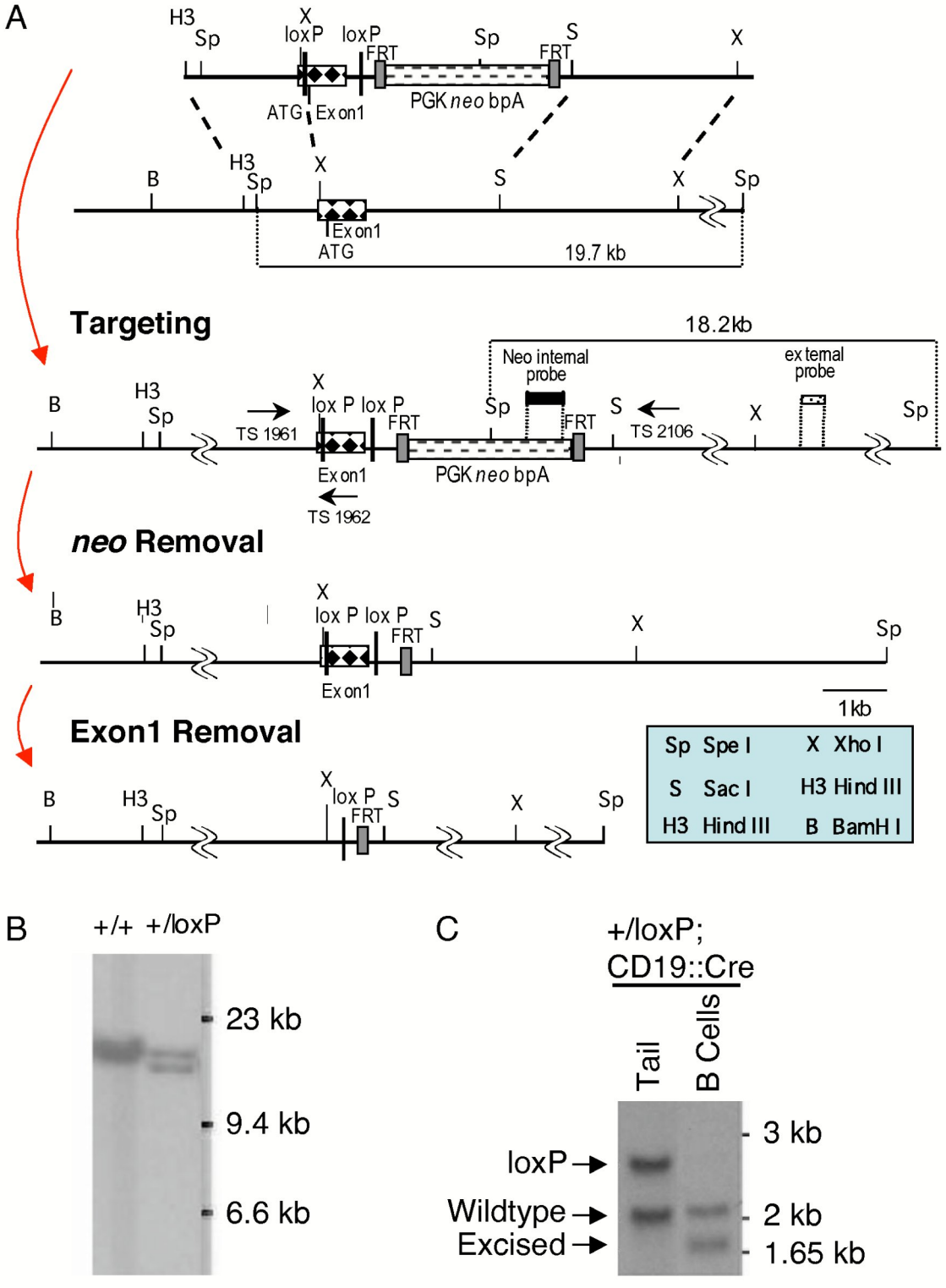

Figure 2.3 Floxed allele targeting in embryonic stem cells

(A) The first exon of KLHL6 was floxed by a pair of *loxP* sequences. One was inserted just before ATG starting codon, and the other was inserted into the first intron. The latter was followed by a *FRT*-flanked *PGK::neo* cassette, which is removable by yeast-derived recombinase Flipase [4]. The floxed allele can be differentiated from wildtype allele by Southern blotting after Spe I digestion with the 3' external probe. (B) Southern blotting showed one clone of embryonic stem cells which had successfully substituted the floxed allele for one wildtype allele after homologous recombination. (C) Tail and B cell genomes from the same heterozygous mouse carrying *CD19::Cre* were subject to Southern blotting analysis. The floxed allele was only excised in the B cell genome, but not in the tail genome. In the meanwhile, the wildtype allele remained untouched by the Cre recombinase.

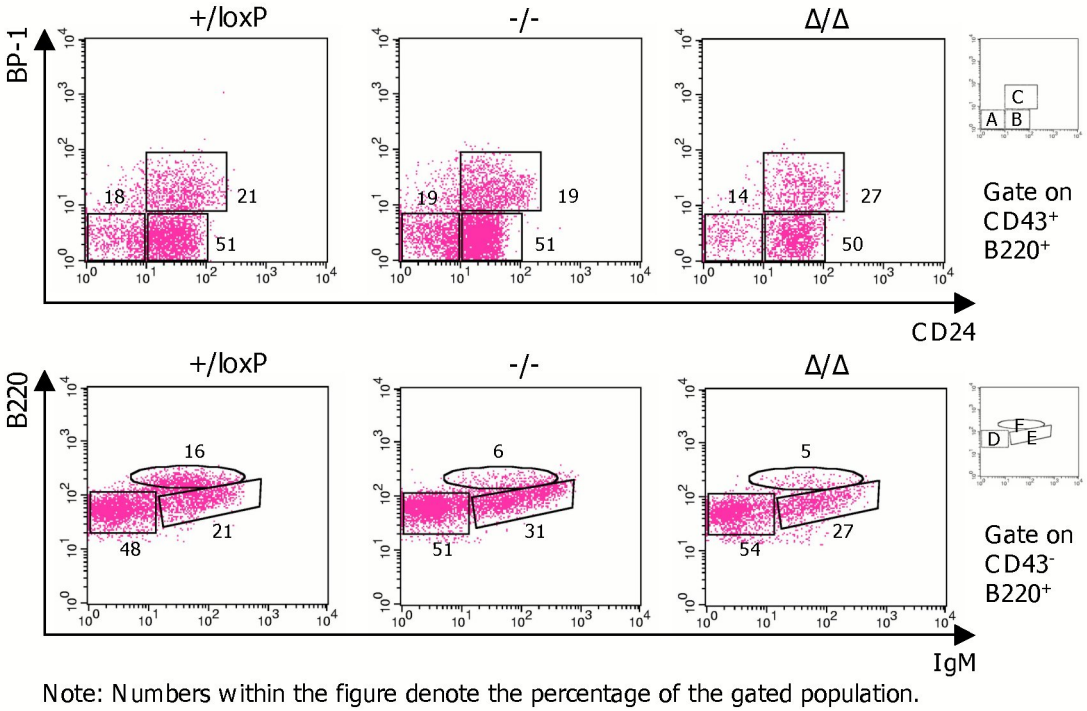

FIGURE 2.4 B-LINEAGE DEVELOPMENT IN BONE MARROW

Bone marrow B cell precursors were analyzed by flow cytometry according to Hardy's scheme [44], which develop from fraction B ($B220^+$ $CD43^+$ $CD24^+$ $BP\text{-}1^-$), via C ($B220^+$ $CD43^+$ $CD24^+$ $BP\text{-}1^+$), D ($B220^+$ $CD43^-$ IgM^-), and E ($B220^+$ $CD43^-$ IgM^+) to F ($B220^{high}CD43^-$ IgM^+). In this order, B to E represent immature and newly generated B cells, while cells in fraction F represent recirculating mature B cells to the bone marrow. It is apparent that less mature B cells were present in bone marrow of *Klhl6*-null mice (-/- or Δ/Δ).

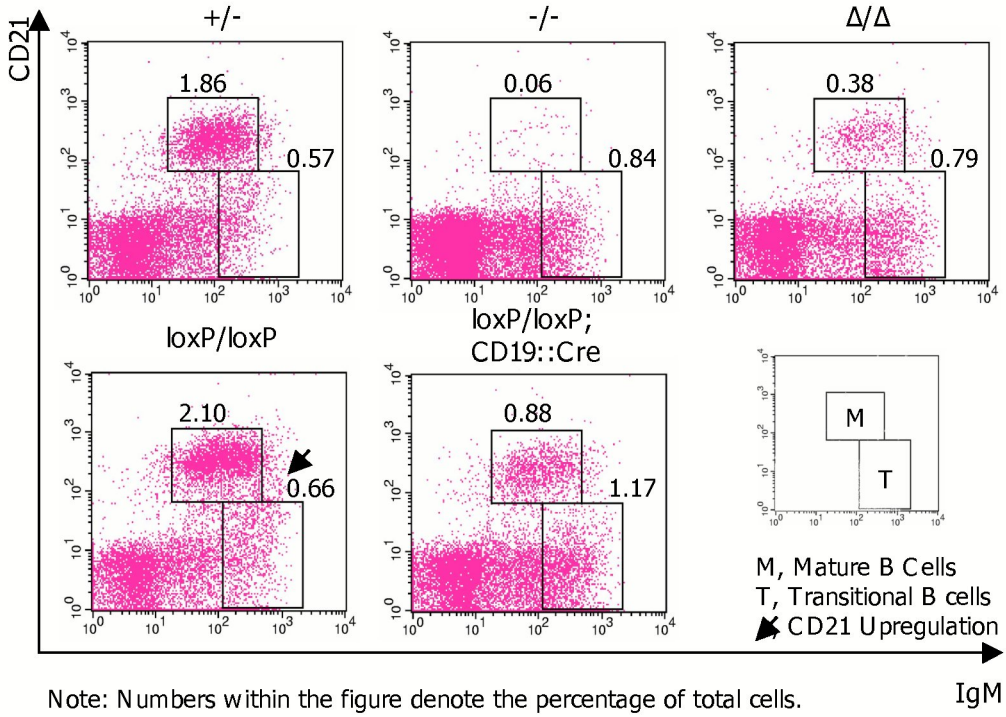

FIGURE 2.5 IMPAIRED UPREGULATION OF CD21 IN TRANSITIONAL CELLS

Transitional B cells in the bone marrow (IgM^{high} $CD21^{intermediate}$) were analyzed by flow cytometry with surface markers reported by Carsetti et al. [18]. CD21 upregulation was less apparent in any of *Klhl6*-null mice (arrow position of -/-, Δ/Δ, or *loxP/loxP;CD19::Cre*). It is also apparent that fewer mature B cells were detected in any of these *Klhl6*-null animals (area M in the inlet).

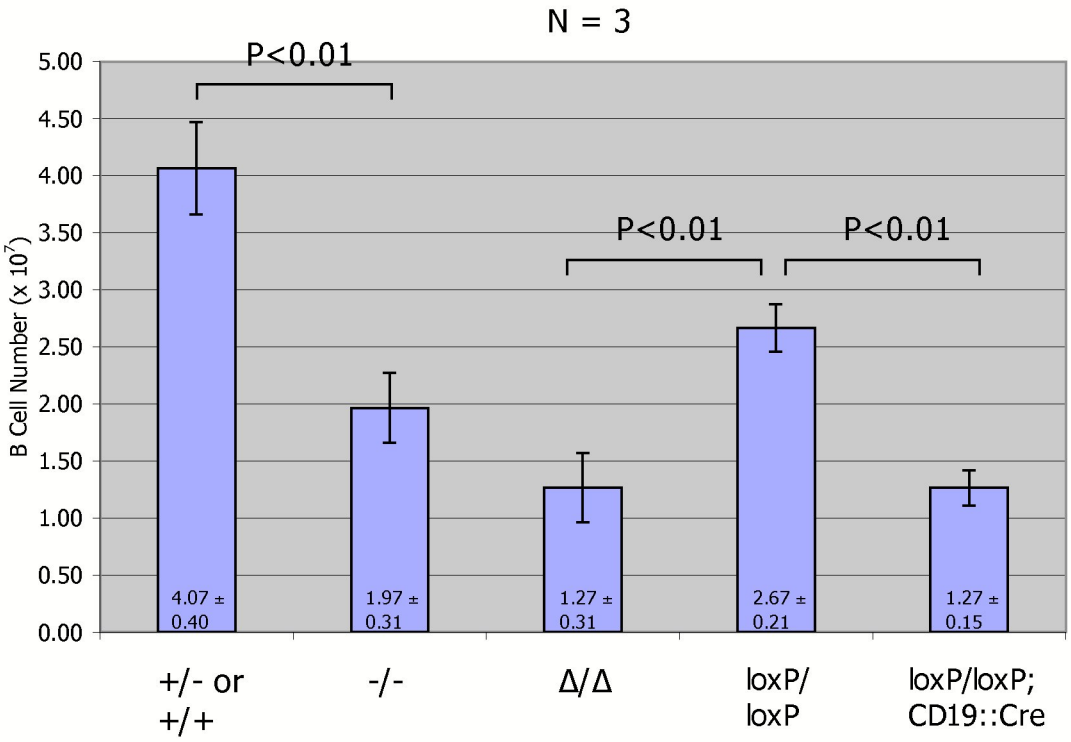

FIGURE 2.6 DECREASED SPLENIC B CELLS

Splenic B cells were calculated as $B220^{+}$ cells among all splenocytes. In conventional *LacZ*-knockin mice, homozygous animals had B cell numbers at around 50% of wildtype or heterozygous animal controls. The same reduction was also true for B-cell specific knockout mice (*loxP/loxP;CD19::Cre*). Three animals were included in each group.

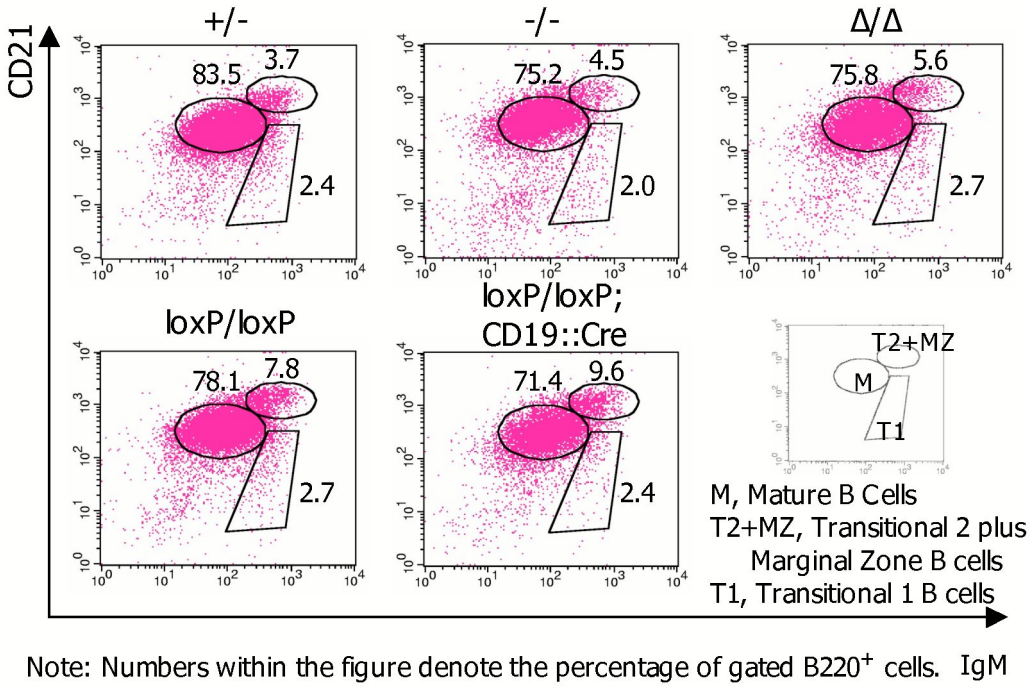

Note: Numbers within the figure denote the percentage of gated B220$^+$ cells.

FIGURE 2.7 B-LINEAGE DEVELOPMENT IN SPLEENS

Splenic B cells were analyzed according to surface markers as reported previously [19, 59], which included transitional 1 (B220$^+$ IgM^{high} CD21^{low}, T1), transitional 2 (B220$^+$ IgM^{high} CD21^{high}, T2) plus marginal zone (B220$^+$ IgM^{high} CD21^{high}, MZ), and mature follicular cells (B220$^+$ IgM^{low} CD21^{high}, Fo). The relative abundance between theses B cell subsets were grossly preserved.

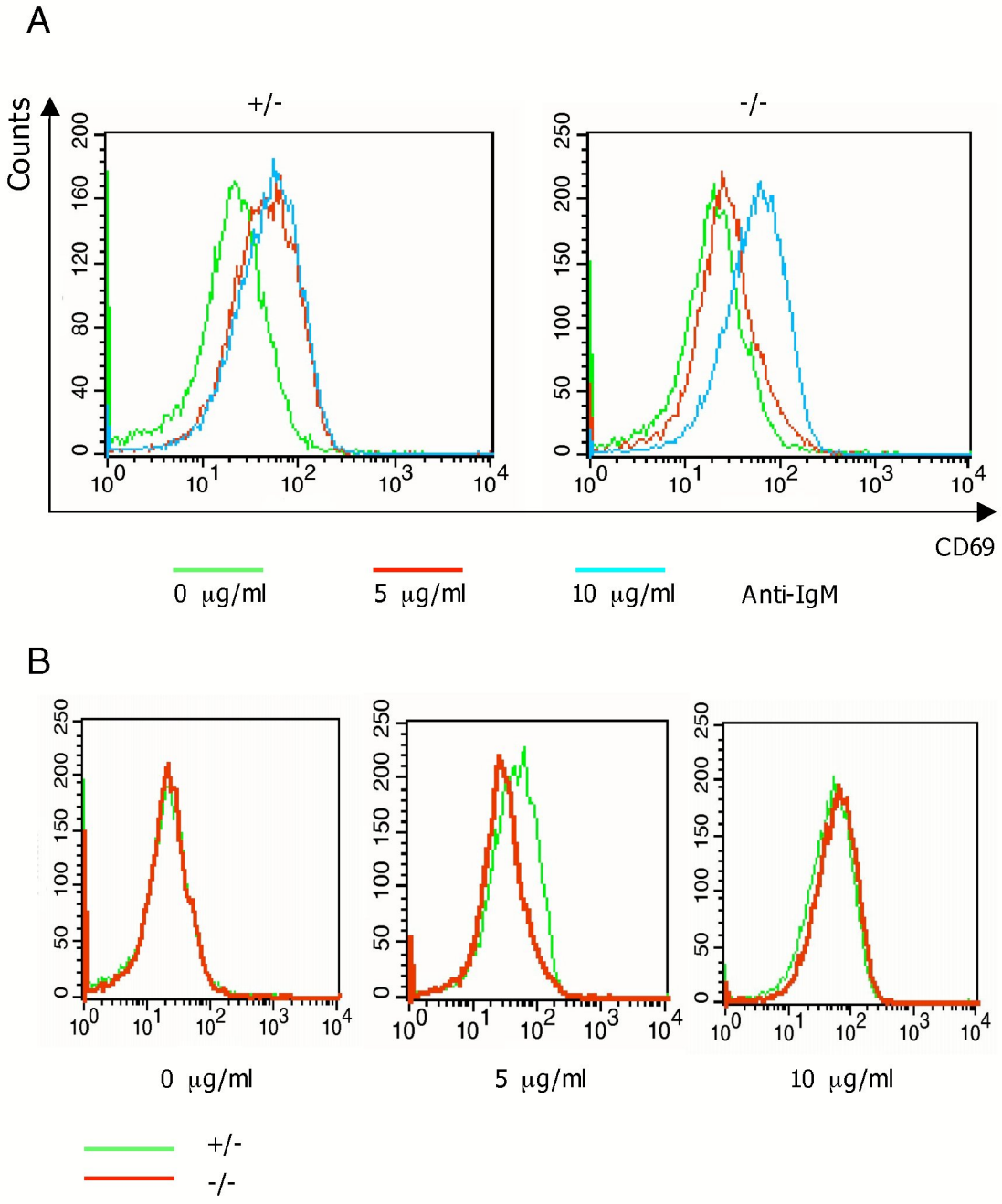

FIGURE 2.8 CD69 EXPRESSION ON STIMULATED B CELLS

(A) Splenic B cells were stimulated by different concentrations of anti-IgM *in vitro* for 48 hours before subjected to flow cytometric analysis for CD69 expression on the surface. The CD69 expression profile from heterozygous B cells had saturated at 5 μg/ml level. Further increase of anti-IgM stimulation to 10 μg/ml level did not shift the profile. Instead, homozygous B cells could express more CD69 molecules on the surface if anti-IgM stimulation was enhanced from 5 μg/ml to 10 μg/ml. The same experiment was repeated twice. (B) Although CD69 was less expressed for homozygous B cells at 5 μg/ml level of anti-IgM stimulation, the expression profile could be compensated by strengthening the challenge to 10 μg/ml. There were no differences between heterozygous and homozygous B cells at 10 μg/ml level of anti-IgM stimulation.

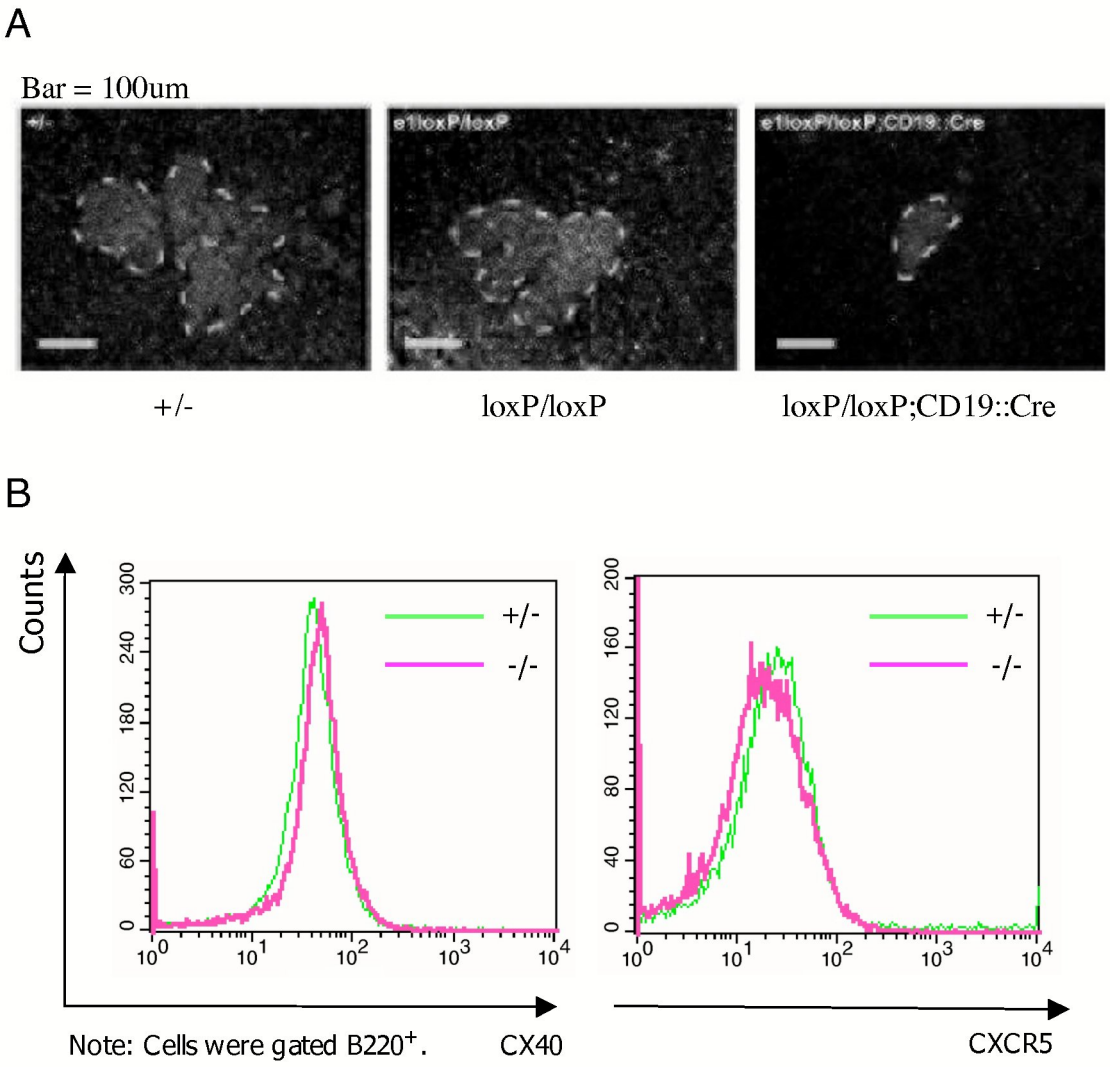

Figure 2.9 Impaired germinal center formation

(A) Germinal centers of popliteal lymph nodes were stained by peanut Lectin-FITC after 10 days' challenge by chicken ovalbumin at hind footpads. Although germinal centers still formed in *loxP/loxP;CD19::Cre* mice, they were much smaller than those in either +/- or *loxP/loxP* mice. Quantification by flow cytometry revealed a 228-fold versus 19-fold increase of $B220^+$ $GL7^+$ GC B lymphocytes per lymph node in response to ovalbumin injections in *loxP/loxP* and *loxP/loxP;CD19::Cre* mice, respectively. (B) Splenic B cells were analyzed for either CD40 or CXCR5 expressions, neither of which had different profiles between homozygous or heterozygous littermates.

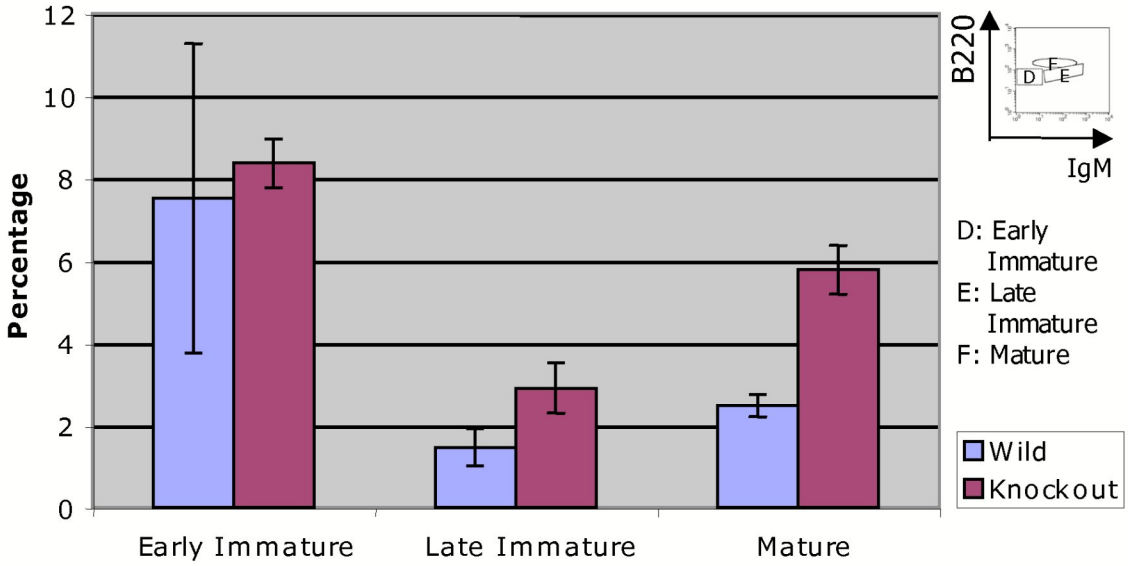

FIGURE 2.10 INCREASED LAMBDA CHAIN USE WITH B CELL MATURATION

Bone marrow cells were analyzed by simplified Hardy's scheme [44]. Early immature *Klhl6*-null B cells ($B200^+$ IgM^-) had comparable use of lambda light chains to wildtype B cells. However, late immature *Klhl6*-null B cells ($B200^+$ IgM^+) selected lambda light chains more frequently in their B cell receptors. The biased selection toward lambda light chains was even more apparent among *Klhl6*-null mature B cells. It is compatible with the concept that *Klhl6*-null B cells failed more frequently in putative positive selections because of presumed threshold elevations in BCR signaling. Each group included 3 mice. See text for more details.

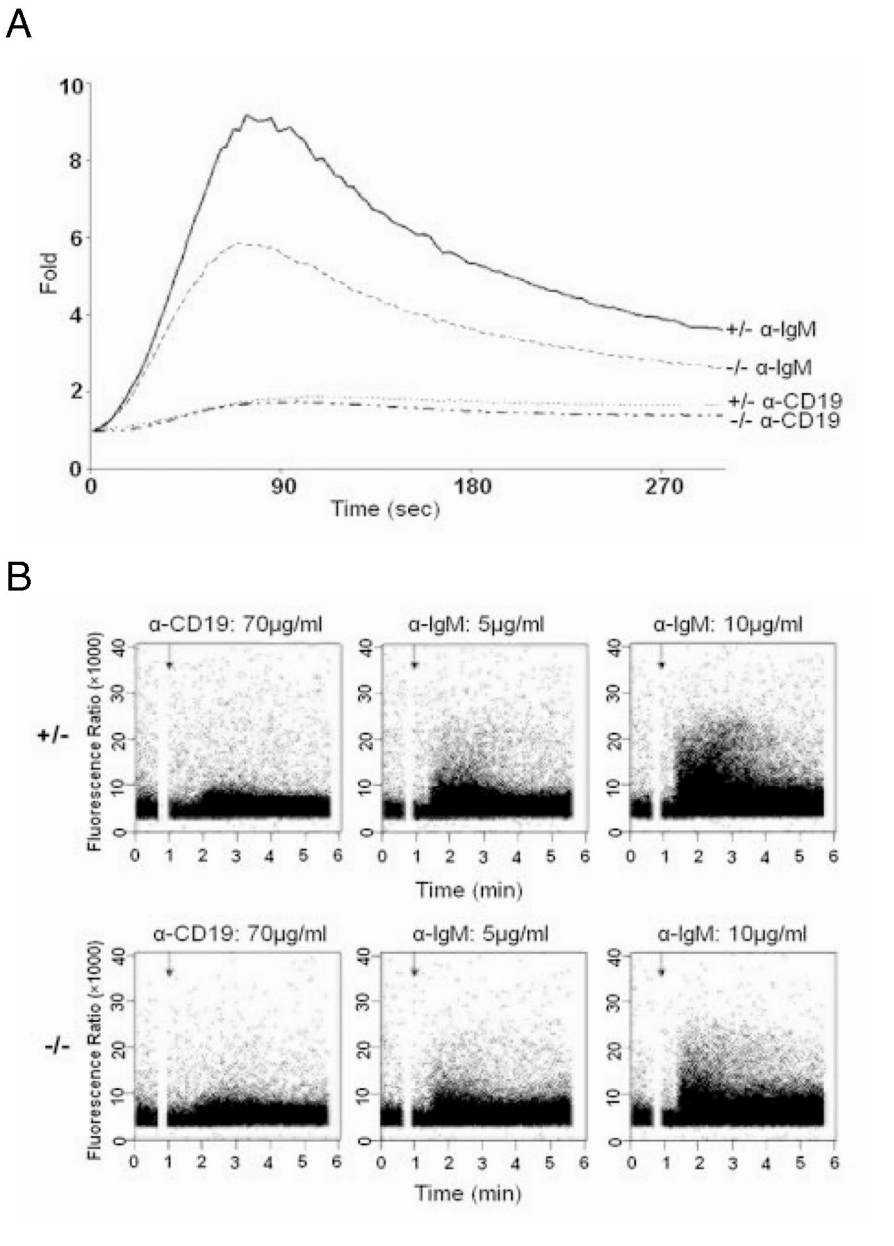

Figure 2.11 Impaired calcium response to anti-IgM stimulation

This figure was contributed by Dr. XZ. Shi. (A) Purified B cells were loaded with Fluo-3 and stimulated with F(ab')$_2$ goat anti-mouse IgM (5 μg/ml) or anti-CD19 (5 μg/ml) at time zero. The fluorescence of Fluo-3 was measured with filters for excitation at 485 nm and for emission at 538 nm. Fold increase is shown as the ratio of internal Ca^{2+} concentration ($[Ca^{2+}]_i$) levels (after/before the stimulation). The results are representative of three independent experiments. The increase in intracellular free calcium in response to BCR stimulation among *Klhl6*-null B cells was apparently compromised. (B) The Ca^{2+} fluxes were analyzed by flow cytometry. Splenocytes were loaded with Indo-1 and stained with phycoerythrin-conjugated anti-B220 monoclonal antibody. $B220^+$ B lymphocytes were examined for the $[Ca2^{2+}]_i$ levels by adding F(ab')$_2$ goat anti-mouse IgM, or anti-CD19 at the indicated time points (arrows). The $[Ca^{2+}]_i$ was determined as the ratio of bound (395 nm) to unbound (530 nm) Indo-1. The results are representative of three independent experiments.

Tables

Table 2.1 Splenic B-lineage Cells.

Number of Splenic B-lineage Cells[a]

Spleen Genotype	Splenocytes* (x10^8)	Marginal Zone (x10^6)	Transitional 1* (x10^5)	Transitional 2* (x10^5)	Follicular* (x10^7)
+/- (n=5)	4.1 ± 1.0	3.1 ± 0.9	14.0 ± 5.8	15.0 ± 3.6	3.8 ± 0.4
-/- (n=5)	2.6 ± 0.3	2.1 ± 0.8	7.0 ± 1.7	6.1 ± 2.5	1.9 ± 0.2

[a] B-lineage cells were sorted by FACS according to the following scheme:
Marginal Zone: $B220^+CD23^-IgM^{high}CD21^{high}$; Transitional 1: $B220^+CD23^-IgM^{high}CD21^{low}$
Follicular: $B220^+CD23^+IgM^{low}CD21^{high}$; Transitional 2: $B220^+CD23^+IgM^{high}CD21^{high}$

* t-test $p<0.05$

Table 2.2 Germinal Center B Cells in Lymph Nodes.

Genotype	-OVA	+OVA	ratio(+OVA/-OVA)
$KLHL6^{+/+}$	$3.77\pm 2.06\times10^3$	$612\pm 137\times10^3$	162 ×
$KLHL6^{-/-}$	$4.18\pm 3.36\times10^3$	$203\pm 76.7\times10^3$	48.6 ×

CHAPTER THREE
mKELCH

Introduction

mKELCH is a novel BTB-kelch protein named after muscle kelch. In a PCR-based expression screening for all predicted BTB-kelch proteins in the mouse genome, *mKelch* was found to be specifically expressed in the heart. Domain analysis of cloned mKELCH sequence identified one BTB domain at the N terminus and several kelch repeats at the C terminus. BACK domain bridged both termini. Northern blotting revealed additional expressions at skeletal muscle. To elucidate the biological function of mKELCH, we took a genetic approach to knock out *mKelch* in all tissues with a knocked-in *LacZ* cassette. Cardiac muscle as well as skeletal muscle were both highly stained by X-Gal. Surprisingly, several photosensitive organs and some smooth muscle had positive staining as well. Although no phenotypes were found in the hearts or muscle, preliminary analyses suggested that mKELCH might play a role in adjusting the sensitivity threshold for phase-shifting circadian rhythms of locomotor behavior in mice.

Materials and Methods

CDD Domain Analysis

NCBI had made available all predicted mRNA and protein sequences by GENSCAN [14] against the mouse genome (MGSCv3 Release 1). CDD is a database storing position-specific scoring matrices for known protein domains. With the following PERL script, I obtained domain structure analyses for all predicted proteins.

```
#! /usr/bin/perl

@list = qw/Mm1 Mm2 Mm3 Mm4 Mm5 Mm6 Mm7 Mm8 Mm9 Mm12 Mm13 Mm14 Mm15 Mm16
             Mm17 Mm18 Mm19 MmUn MmX/;

foreach $item (@list)
{
    @fas = `ls $item`;
    foreach $fasitem (@fas)
    {
        chomp $fasitem;
        `blastall -p blastp -d All -i $item/$fasitem >> ${item}_GS_Pro.blast`;
    }
}
```

The results were filtered through the script below to extract all BTB-kelch protein candidates.

```
#! /usr/bin/perl

if ($ARGV[0])
{
        open (STDIN, $ARGV[0]);
}

while (<STDIN>)
{
    if (/^Query=/)
    {
        $output=1;
```

```
        $block="";
        $domain="";
        $printblock=0;
        $BTB=0;
        $Kelch=0;
        do
        {
            $block="$block$_";
            $_=<STDIN>;
            if (/^gnl/)
            {
                $domain="$domain$_";
                if ($_ =~ /BTB/) {$BTB=1;}
                if ($_ =~ /Kelch/) {$Kelch=1;}
            }
            if (/^>/)
            {
                $output=0;
                if ($BTB && $Kelch) {$printblock=1;}
            }
        }
        while ($output);
        if ($printblock) {print $block;}
    }
}
```

PCR Screening

Predicted mRNA sequences for all BTB-kelch protein candidates were 'BLATted' at UCSC Genome Bioinformatics (http://genome.ucsc.edu), which could easily identify

exon-exon junctions with color letters. Primers were designed in a multiplex manner by Primer3 [82], preferentially crossing exon-exon junctions and had similar annealing temperatures. Every four candidate proteins were grouped together; expected PCR products would appear at around 150 bp, 250 bp, 350 bp, and 450 bp, respectively. There were totally 11 groups plus one β-actin group as a positive control. Reaction conditions were 94°C 5 min, 35 cycles of 94°C 30 seconds, 58°C 30 seconds, 72°C 1 minute, and final 72°C 10 minutes.

in silico Cloning and Bioinformatic Analysis

The cDNA sequence of mouse *mKelch* was used as seeds to 'BLAT' against genome sequences of other species at UCSC Genome Bioinformatics (http://genome.ucsc.edu). Based on the highly conserved exon structures, splicing donors and acceptors could be easily identified by color codes from 'BLATted' results at UCSC. Exon sequences were manually picked out and assembled. The curated exon sequences were then *in silico* translated into protein sequences. Multiple alignments were calculated by ClustalW [22] and outputted as shaded drawings by BOXSHADE (http://www.ch.embnet.org/software/BOX_form.html).

cDNA Synthesis

First strand cDNA was synthesized from total RNA with Invitrogen SUPERSCRIPT II first-strand synthesis kit by poly dT primers. Hearts, spleens, and E12.5 embryos were obtained from conventional KLHL6 knockout mice (J. Kroll). RNA was extracted by QIAGEN RNeasy Midi kit.

Stem Cell and Knockout Mice

The bacterial artificial chromosome (BAC) genomic clone for the *mKelch* gene was obtained from Research Genetics and the targeting vector was constructed as shown in Figure 3.5. Briefly, the ATG exon of *mKelch* was replaced by a fragment containing a Flpase target-flanked *LacZ* cassette [4]. The *LacZ* sequence was followed by a floxed *PGK::neo* cassette. Electroporation, embryonic stem (ES) cell culture, and Southern blot screening

were performed as previously described [102]. Mice were genotyped by PCR using the following primer pairs: aaaacctgcttcttttcttaccc and tgcactcgagtagtccacagg (for the wild type allele); and aaaacctgcttcttttcttaccc and gcgggcctcttcgctattac (for the *LacZ* allele). The PCR conditions were: 94°C for 30 seconds; 58°C for 30 seconds; and 72°C for 1 minute; 35 cycles.

Northern Blotting

Commercial membranes from Clontech were used for tissue blot, embryo blot (Figure 3.4) or dot blot (data not shown). Homemade membrane was transferred from fractionalized total RNA in formaldehyde agarose gel as detailed in the appendix of QIAGEN RNeasy handbook. Each lane was loaded with 20 μg total RNA from hearts, liver, brain, or skeletal muscle.

Genetic Background and Age of the Mice

The mice were studied on CD1 and 129/svEms-+Ter$^{?}$/J mixed backgrounds. The studies were conducted with adult mice at 6 to 10 weeks of age raised at the animal center of University of Southwestern Medical Center at Dallas. The animals for echocardiogram were 4 months old.

X-Gal Staining

Staining procedure was based on Lobe et al. [58]. Briefly, whole mount organs were fixed at 4°C for 4 hours in 0.2% glutaraldehyde, 5 mM EGTA pH 7.3, and 100 mM $MgCl_2$ in PBS. After wash 3 times with 2 mM $MgCl_2$, 0.01% NaDOC, 0.02%NP-40 (*LacZ* wash buffer), organs were incubated at 30°C overnight in *LacZ* wash buffer plus 5 mM potassium ferrocyanide, 5 mM potassium ferricyanide, and 1 mg/ml X-Gal. Stained organs were washed by PBS 3 times, and postfixed in 2% PFA plus 0.1% glutaraldehyde overnight at 4°C. Sections were stained similarly except fixation and postfixation were shortened to 10 minutes at room temperature.

Histology

Frozen sections embedded in OCT were cut at 10 μm thick before staining. Flat mount retinas were detached from eyeballs after whole mount staining by X-Gal. Images were taken under Zeiss Axio-series microscopes, and processed by Openlab.

Circadian Rhythms of Locomotor Activity

Locomotor activity was monitored by wheel running. Mice were entrained to equally divided light-dark cycles for one week before introduced into constant darkness. After another week in darkness, a short pulse of light for 15 minutes was given at 2.5 hour after the predicted activity onset (Zeitgeber Time 14.5, ZT 14.5). Activity was recorded for at least additional 7 days before the next pulse of light for 1 minute at the same time point, i.e. ZT 14.5. Actograms were recorded and analyzed by the Clocklab software package.

Statistics

Student's t-Tests were used for statistical analyses. Data were presented as average $\pm$ standard deviation.

Results

Discovery

Our laboratory had been working on a BTB-kelch protein, KLHL6, before the identification of mKELCH. *Klhl6*-null mice had relatively minor phenotypes in B cells. To exclude the possibility that some other BTB-kelch protein might compensate KLHL6 in null animals, I took a bioinformatic approach to identify all potential BTB-kelch proteins in the mouse genome. A PCR-based expression screening was then performed against cDNA from hearts, spleens, and embryos at E12.5.

Bioinformatic Approach

GENSCAN-predicted protein sequences [14] against the mouse genome (MGSCv3 Release 1) were downloaded from NCBI website. Position-specific scoring matrices for characterizing protein domain structures were also available at CDD of NCBI. All proteins were subject to BLAST analysis locally and results were filtered through PERL script for BTB-kelch combinations. Totally 41 BTB-kelch proteins were identified from the mouse genome, including KLHL6 (Figure 3.1).

PCR Screening

Primers specific for each identified BTB-kelch protein were picked by Primer3 [82], preferentially crossing exon-exon junctions (Table 3.2). cDNA from hearts, spleens, and embryos at E12.5 were subject to expression analysis by multiplex PCR reactions. It turned out every organ had more than 20 BTB-kelch proteins expressed simultaneously, but had different combinations (Figure 3.2). We did not find any specific candidate with higher expressions in *Klhl6*-null spleens. Instead, *mKelch* became a serendipitous finding because of very specific expression in the hearts (arrow in Figure 3.2).

Domain and Distribution

mKelch was cloned from cardiac cDNA by PCR, and subject to sequence verification and domain structure analysis. The result was the same as GENSCAN predictions. Sequences from other species were cloned *in silico*.

Protein Domain Analysis

There is a BTB domain at the N terminus, followed by a BACK domain before the C-terminal kelch repeats (Figure 3.3). However, only 4 kelch repeats were recognized by the Pfam protein families database [8]. Another 2 potential kelch repeats were suspected by inspection, as denoted by fragmented lines in Figure 3.3. Notably the two manually identified repeats did not have the characteristic GG doublets for the typical kelch motif. mKELCH is highly conserved from animals above fish. No homologs were found in species below vertebrates such as *Drosophila*.

Tissue Distribution

Northern blotting with a *mKelch* specific probe showed abundant expression in the heart (Figure 3.4) and faint signals among skeletal muscle and possibly testes. Embryo blots did not give positive results. Tissue dot blots revealed similar findings (data not shown). Signals from homemade Northern membranes were much stronger at skeletal muscle (Figure 3.6). The discrepancy could be due to different normalization methods between the commercial and the homemade membranes. There seemed two bands for each positive tissue, which might represent different splicing variants of *mKelch*.

Knockout Mice

We took a genetic approach to understand mKELCH functions by abolishing mKELCH in all tissues via a knocked-in *LacZ* cassette, which itself served as a reporter under the endogenous promoter of *mKelch*.

Targeting Construct

An *FRT*-flanked *LacZ* cassette, which is removable by yeast-derived recombinase Flipase [4], was targeting at the ATG exon of *mKelch* (Figure 3.5.A). A floxed *PGK::neo* cassette following *LacZ* was used for selection of embryonic stem cells. The lengths of short-arm and long-arm for homologous recombination were 2.5 kb and 4 kb, respectively. The targeted allele can be differentiated from the wildtype allele by Southern blotting after Spe I digestion. The external probe detected the wildtype allele at 6.9 kb and the knocked-in/-out allele at 8.5 kb (Figure 3.5.B).

Mice

Electroporation, culture and selection for homologous recombination among embryonic stem cells are described in Materials and Methods. Out of 280 *neo*-resistant stem cell clones, 5 recombined homologously. Two targeted clones were injected into blastocysts. From chimeras with more than 90% contribution of genetically modified stem cells, one line was maintained for each clone. The chimeras were directly mated to *CAG::Cre* mice to

remove the *PGK::neo* cassette [86]. Offsprings were born normally with Mendelian ratios and gained similar body weights at one month old regardless of genotypes (Table 3.1).

Confirmation of mKelch Knockout

Northern blotting with a *mKelch* specific probe downstream of ATG exon showed complete loss of *mKelch* expression at either hearts or skeletal muscle (Figure 3.6). Heterozygous animals had around half amount of expression levels. Brain and liver remained undetectable for *mKelch* regardless of genotypes.

Distribution Revisited

Knocked-in *LacZ* was driven by endogenous promoter of *mKelch*. X-Gal staining would authentically reflect *LacZ* activity, and presumably revealed the expression pattern of *mKelch* [87].

Whole Mount X-Gal Staining

Fixed organs from heterozygous or wildtype animals were stained by X-Gal. Atria and ventricles of both left and right hearts were strongly stained (Figure 3.7.A). Great arteries were negative, but pulmonary veins and coronary sinuses were positive. Pineal glands and superior colliculi were also highly stained by X-Gal (Figure 3.7.B). Other organs including brain, liver, kidney, pancreas, or intestines were negatively stained (data not shown).

Microscopic View of X-Gal Staining

Frozen tissue sections were subject to X-Gal staining. Skeletal muscle was highly stained, and so was smooth muscle in the lung (Figure 3.8.A). Pineal glands and superior colliculi were again positively stained. Additional positive foci included iris, ciliary body, and some retina ganglia cells in the eye (lower right panels in Figure 3.8.A). Staining on retina ganglia cells were further evaluated on the flat mount preparation (Figure 3.8.B). Only some retina ganglia cells were stained, showing a starry pattern among the whole retina. Notably, this starry pattern on ganglia cells were very similar to the expression

pattern of *Melanopsin* (see below) [45], which is responsible for non-image-forming visual functions such as phase-shifting circadian rhythms of locomotor activity or adjustment of pupil constrictions [see review 71].

Phenotype Search

Search for phenotypes was directed by the expression profile of *mKelch*. Efforts were focused on cardiac performances and non-image-forming visual functions.

Heart

At least at the age of 4 months old, *mKelch*-null mice did not have any detectable abnormalities on cardiac functions or structure (Figure 3.9 and data not shown). Cardiac echo showed normal contraction and relaxation in systole and diastole, respectively.

Non-image-forming Vision

Many physiological functions need cues from environments, such as circadian rhythms of locomotor activity, or adjustment of pupil constriction. Recent studies have shown that *Melanopsin*, which is expressed by a very limited population of retina ganglia cells (1%), plays a major role in this regard [46, 70]. Based on X-Gal staining on the flat mount retina, *mKELCH* and *Melanopsin* have very similar patterns of expression (Figure 3.8.A and 45). It would be possible that *mKELCH* and *Melanopsin* are expressed among the same set of retina ganglia cells, and both might be involved in regulating the same physiological function.

mKelch vs. *Melanopsin*

Although *mKelch* was cloned from hearts, the specific and abundant expressions at several photosensitive organs, including retina, superior colliculi, and pineal glands, had raised the question if *mKelch* is involved in visual functions.

Retina Ganglia

Cones and rods are the two major photosensitive cells to relay light signals through ganglia to the hypothalamus. Recently some retina ganglia cells have been shown to possess the ability to sense light directly [91]. These ganglia cells can influence physiological adjustments to environmental irradiation cues. On the retina, X-Gal staining between *mKelch* and *Melanopsin* were very similar (Figure 3.8.A and 45). It is possible both proteins are expressed by the same type of ganglia cells.

Phase Shift in Constant Darkness

Among the non-image-forming visual functions mediated by *Melanopsin* is the circadian phase shift of locomotor activity [45]. Briefly, endogenous circadian rhythms of locomotor activity in mice could be assayed by wheel-running in constant darkness (actogram). The endogenous rhythm is slightly shorter than 24 hours, so mice would run the wheel a little earlier the next day (Figure 3.10.B). If a short pulse of light was given at around 2 to 3 hours after the activity onset, the next appearance of wheel running would be delayed (Figure 3.10.B). A phase shift would be observed on the actogram.

Light Sensitivity in Setting Phase Shift

mKelch-null and control mice were adapted to constant darkness and recorded for their wheel running activities. A short pulse of light for either 1 minute or 15 minutes were given to each animal on two different occasions. The ratio of phase shifts between 1-minute stimulation and 15-minute stimulation by the same animal was shown in Figure 3.11. Although statistical significance was not reached, it seemed that 1-minute stimulation was as effective as 15-minute stimulation in inducing phase shift for *mKelch*-null mice. The ratio was 1 ± 0.5 for knockout animals, but around 0.6 ± 0.4 for control animals.

Hearts

An interesting question relevant to the presumed coexpression between *mKelch* and *Melanopsin* on ganglia is whether evidences exist for coexpression on the hearts as well. Based on EST search at NCBI, at least 4 records aligned well with *Melanopsin*, whose

accession numbers were 32306165, 4483360, 4373977, and 2249294, respectively. All of these records were derived from cardiac cDNA. One of the alignments was shown in Figure 3.10.A.

Discussion

Bioinformatic Work

I identified totally 41 BTB-kelch proteins in the mouse genome, based on the combination of GENSCAN [14], CDD database, and mouse genome sequences (MGSCv3 Release 1) (Table 3.2). With a similar approach, I found 38 BTB-kelch proteins in the human genome (data not shown). These numbers were higher than we had expected in the laboratory. PCR screening provided expression evidence for these BTB-kelch proteins among several organs (Figure 3.2). Different organs had different combinations of these BTB-kelch proteins. A later study using the more complete genome sequences confirmed the expansion of BTB-kelch proteins in the human genome [74].

mKelch Cloning

3'-RACE cloning of *mKelch* revealed several splicing variants with different numbers of kelch repeats (data not shown). Instead 5'-RACE cloning only identified a single starting exon. Because the promotorless *LacZ* was successfully expressed in *mKelch* mice, the existence of an endogenous promoter upstream of the presumed first exon was justified. In addition, probes downstream of the first exon could not detect *mKelch* expression in the knockout mice (Figure 3.6), so the possibility for *mKelch* mice to have alternate starting exons should be very low. In summary, *mKelch* is completely knocked out by the knocked-in *LacZ* cassette.

However there is a long transcript on the Northern membrane whose sequence is not clear (Figure 3.4. Bioinformatic studies trying to identify implicit downstream exons were

not successful, either. Further experiments would be needed to characterize the sequence of the long transcript.

Light Sensation for Hearts

mKelch was expressed among several photosensitive organs and possibly coexpressed with a photosensing gene, *Melanopsin*, on some of the retina ganglia cells (Figure 3.7 and 3.8). Preliminary studies on circadian locomotor activity of *mKelch* mice implied a possible role for threshold control in sensing the light pulse (Figure 3.11).

Interestingly, bioinformatic studies found expression evidence of *Melanopsin* in the hearts (Figure 3.10.A). A previous report has suggested a direct light-sensing ability of Zebrafish hearts in the *in vitro* culture [121]. In that study, the cardiac circadian clock could be entrained by direct light pulses. However, there have been no molecular explanations for this novel ability. Given the evidence for *Melanopsin* in controlling other circadian activities, it would be intriguing to study the biological role of *Melanopsin* in cardiac functions, assuming the expression evidence could be documented by experiments.

Conclusion

Taken into consideration of experimental data from both BTB-kelch proteins studied in the lab, *Klhl6* and *mKELCH*, it seemed that both genes are involved in the threshold control for environmental stimulations. Loss of *Klhl6* elevated the threshold for BCR signaling, while loss of *mKelch* seemed to lower the threshold for light sensation in some of the retina ganglia cells. With an expanded repertoire of BTB-kelch proteins, vertebrates might be able to respond to environmental cues in a more elaborate manner when there is a specific BTB-kelch protein in accordance to each kind of environmental stimulations. The finer adjustment to the environment probably provide a survival advantage to these animals.

Acknowledgment

I thank Dr. Steven L. McKnight, Dr. Carol A. Dudley and Sandi Jo Estill for their kind help with circadian studies and technical assistance. I also thank John Shelton for his help with histological preparations.

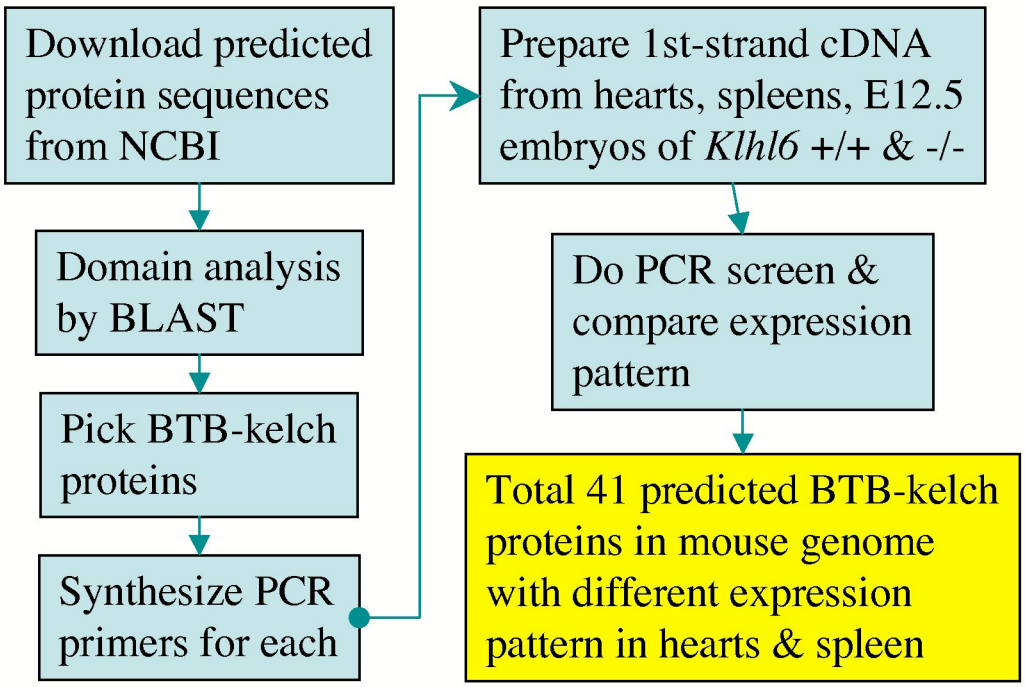

Figure 3.1 Diagram for mKelch discovery

GENSCAN [14]-predicted protein and mRNA sequences against the mouse genome (MGSCv3 Release 1) were downloaded from NCBI. All the predicted sequences were 'BLASTed' by scoring matrices available at the CDD database. Proteins with BTB and kelch combinations were selected for expression screening. Totally 41 such proteins were identified. PCR screening primers were selected by Primer3 [82], as shown in Table 3.2.

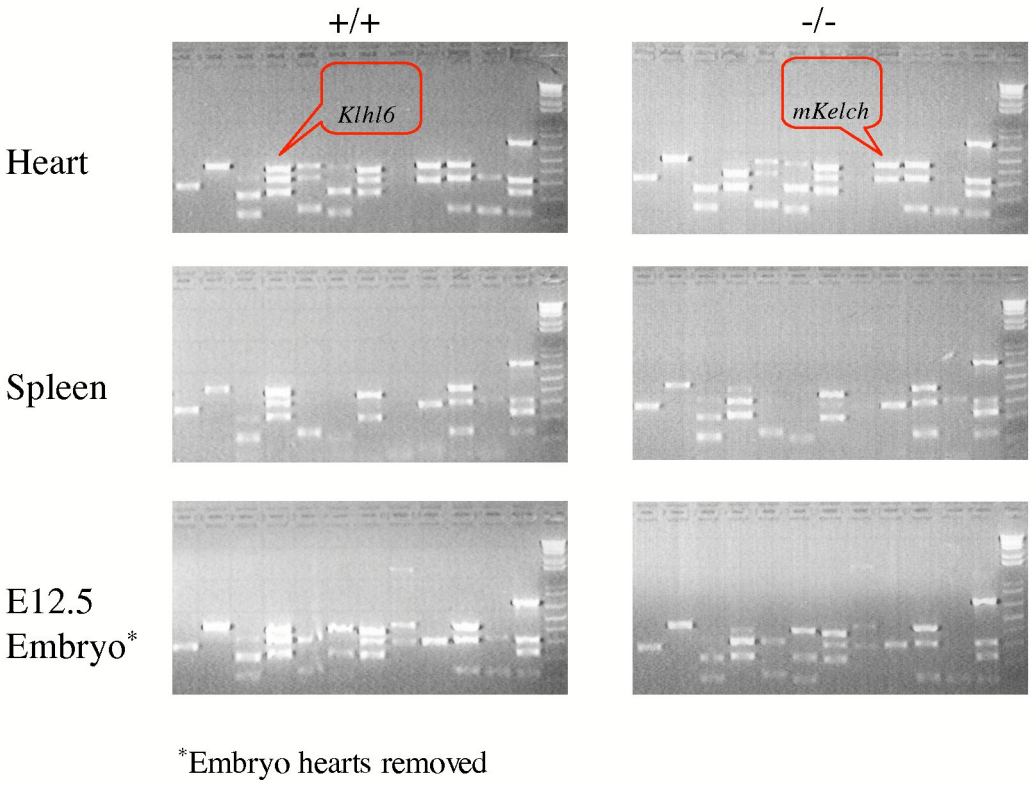

FIGURE 3.2 PCR SCREEN RESULTS

First-strand cDNA from *Klhl6* wildtype and knockout mice (J. Kroll) were synthesized from hearts, spleens, and E12.5 embryos without hearts. Screening primers were grouped into 12 groups, each of which had 1 to 4 pairs of primers with different product sizes (Table 3.2). In each organ, more than 20 different BTB-kelch proteins were identified. Products of *Klhl6* and *mKelch* were pointed out by arrowed rectangles. Notably the *mKelch* band was not seen in either spleens or embryos.

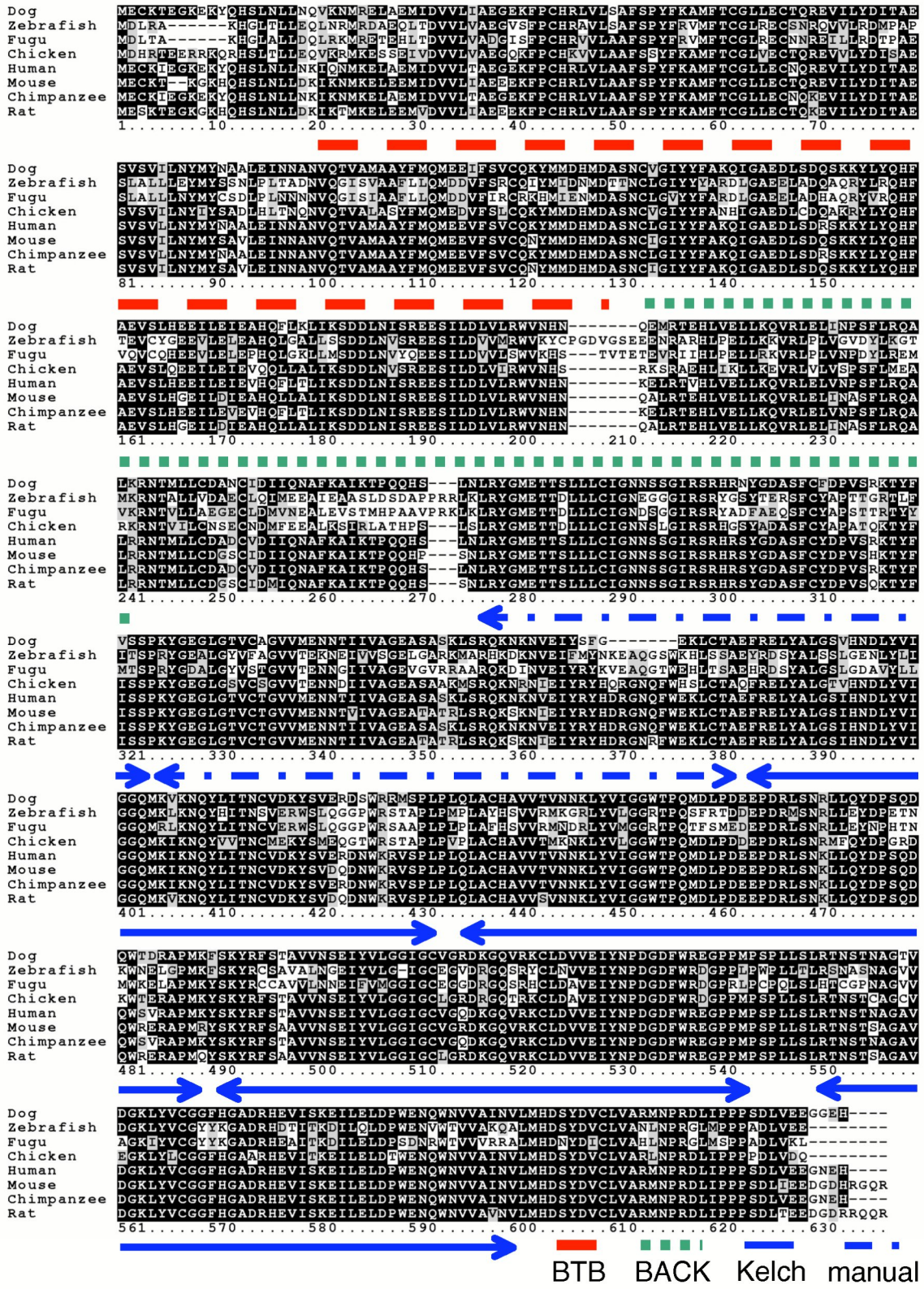
Dog
Zebrafish
Fugu
Chicken
Human
Mouse
Chimpanzee
Rat
BTB
BACK
Kelch
manual

FIGURE 3.3 MULTIPLE ALIGNMENT WITH DOMAIN ANNOTATIONS

mKelch sequences were highly conserved among species above vertebrates. Based on the Pfam protein families database [8], there is a BTB domain at the N terminus (red lines), followed by a BACK domain (green lines) and several kelch repeats at the C terminus (blue lines). Only 4 typical kelch motifs were identified by Pfam (solid blue lines). 2 potential repeats were manually picked up (fragmented blue lines), which did not possess the typical GG doubles in the kelch motif.

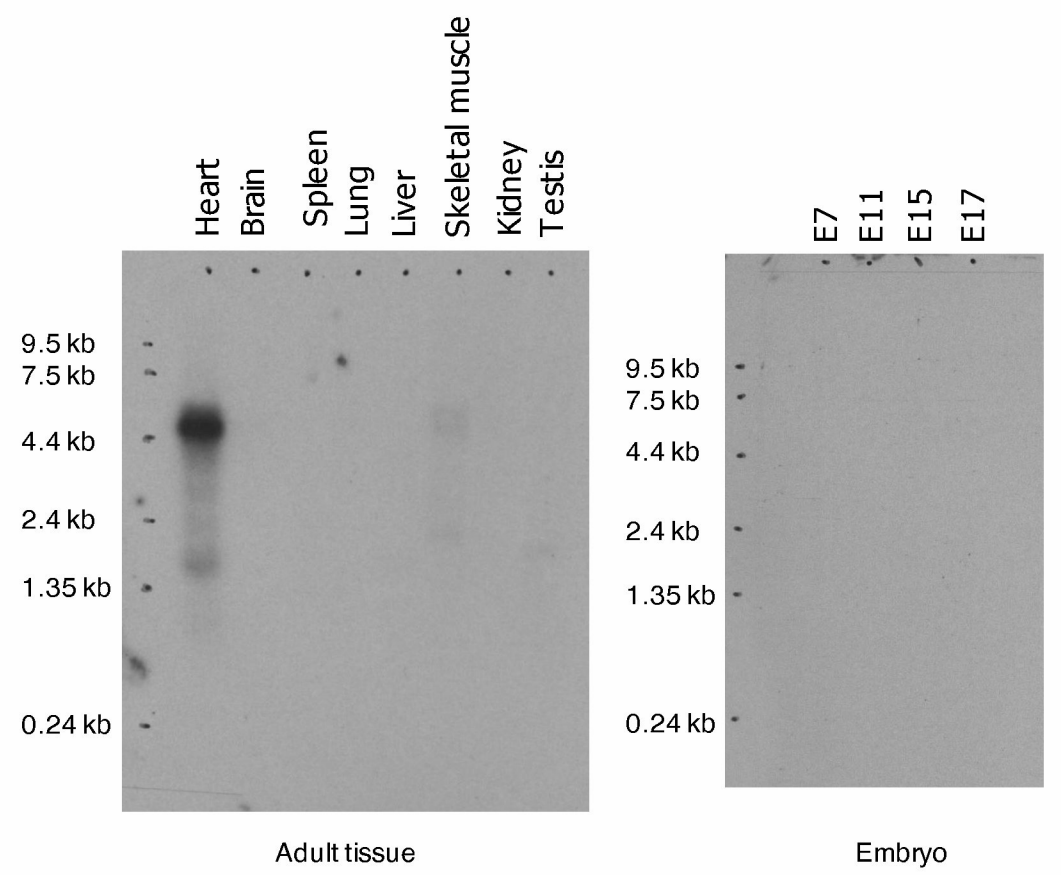

FIGURE 3.4 TISSUE DISTRIBUTION BY NORTHERN BLOTTING

A *mKelch*-specific probe was blotted against commercially available Northern membranes. Expressions were strongly detected at hearts, but only faintly seen in skeletal muscle and possibly testes. No signals were present on embryo membranes. Two bands were present; one was about 1.5 kb, and the other was about 5 kb.

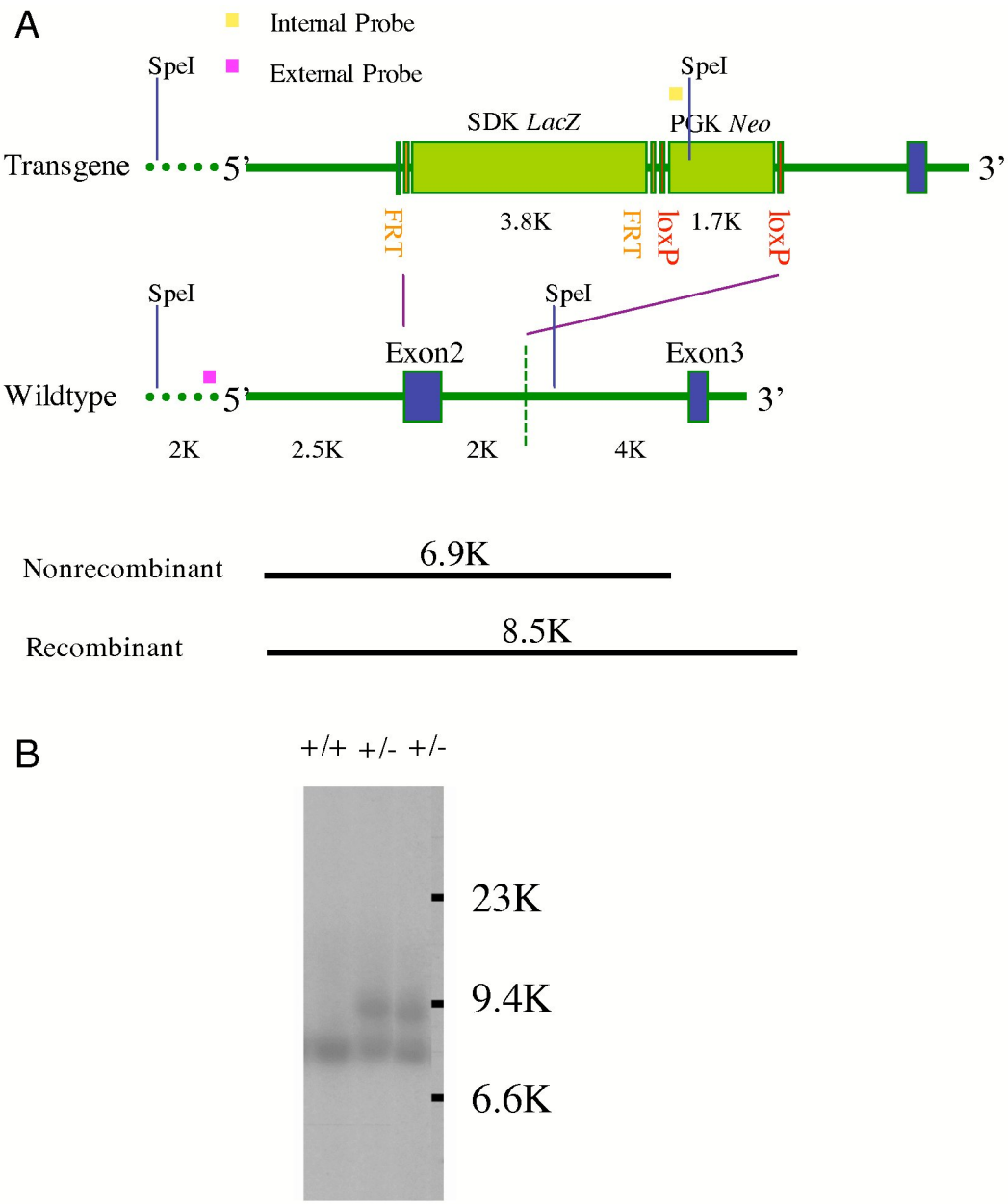

FIGURE 3.5 TARGETING STRATEGY

(A) The ATG exon of *mKelch* was targeted by a construct containing a promotorless *LacZ* and a *PGK*-driven *neo*. *LacZ* and *neo* were flanked by *FRT* and *loxP* sequences, respectively. Homologous arms were 2.5 kb on the 5' side and 4 kb on the 3' side. Recombinant alleles could be detected at 8.5 kb by the external probe against Spe I-digested Southern membranes, but the wildtype alleles were blotted at 6.9 kb. (B) A typical Southern blotting against a Spe I-digested membrane was shown, which contained one nonrecombinant clone and two recombinant clones.

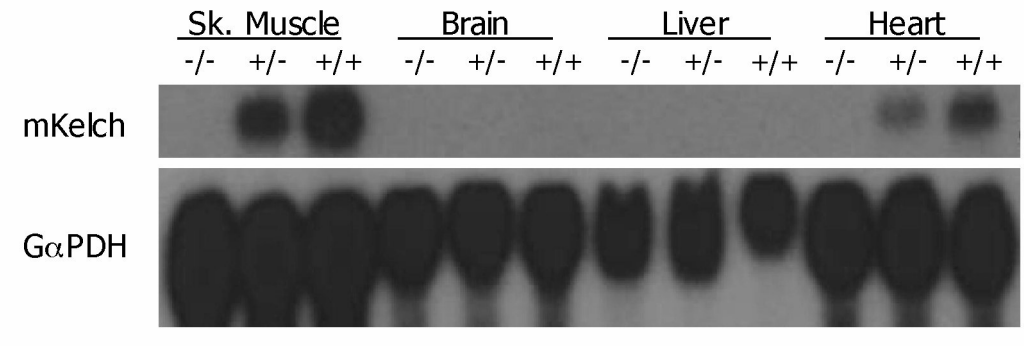

FIGURE 3.6 CONFIRMATION OF KNOCKOUT BY NORTHERN BLOTTING

A Northern membrane was prepared from total RNA extracted from different tissues of *mKelch* mice with various genotypes. In hearts and skeletal muscles, the *mKelch*-specific probe could not detect any signals among knockout mice. Heterozygous mice had roughly half amounts of expression levels of wildtype animals. No blottings were present in brain and liver. GαPDH was used as a loading control.

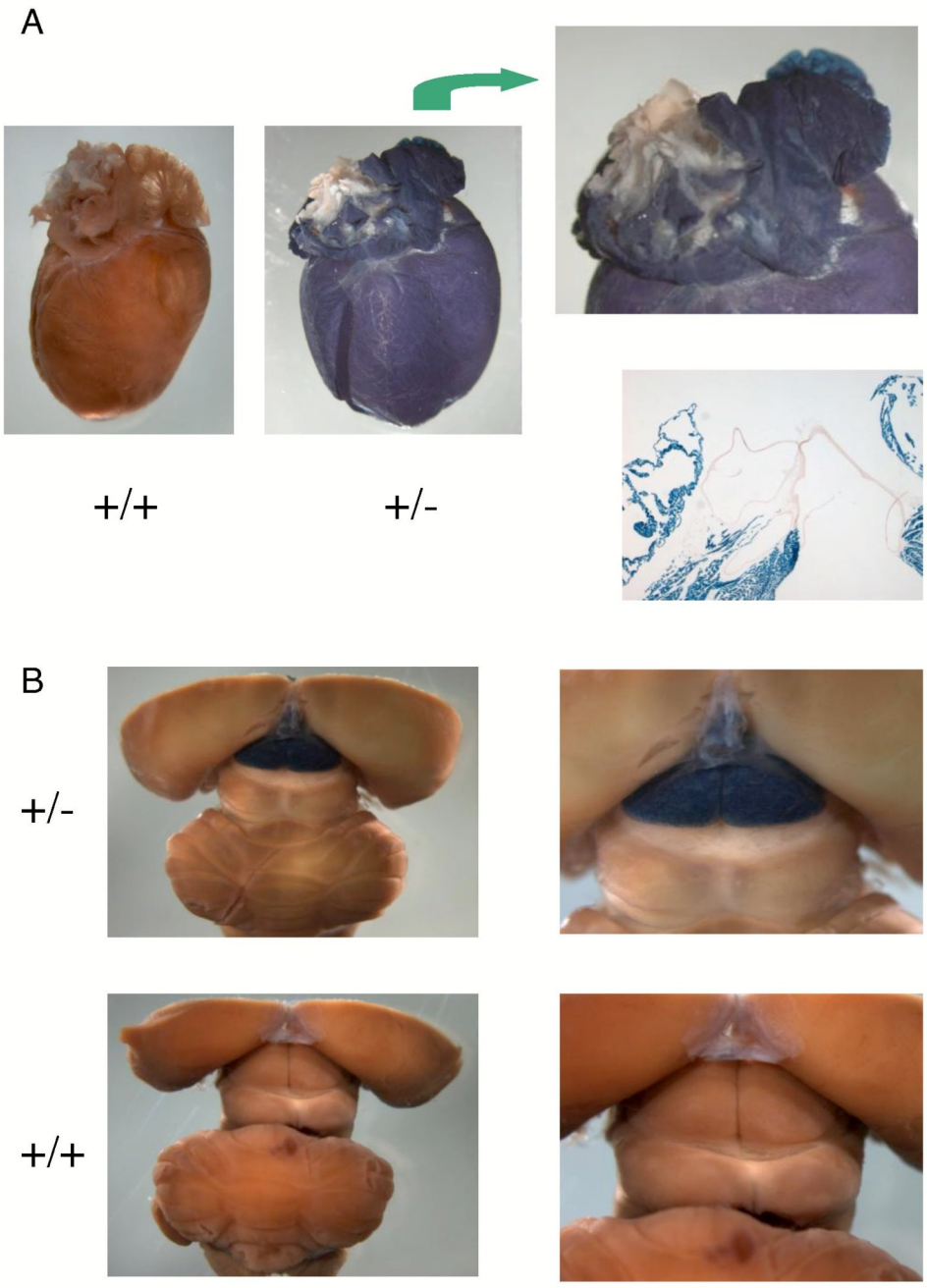

FIGURE 3.7 WHOLE MOUNT *LacZ* STAINING

(A) Hearts from either wildtype or heterozygous animals were subject to X-Gal staining. The whole heart was strongly stained, including both atria and ventricles, pulmonary veins and the coronary sinus. Great arteries were not stained. (B) Brains from both genotypes were stained by X-Gal. Superior colliculi and pineal glands were clearly demarcated in the heterozygous brain.

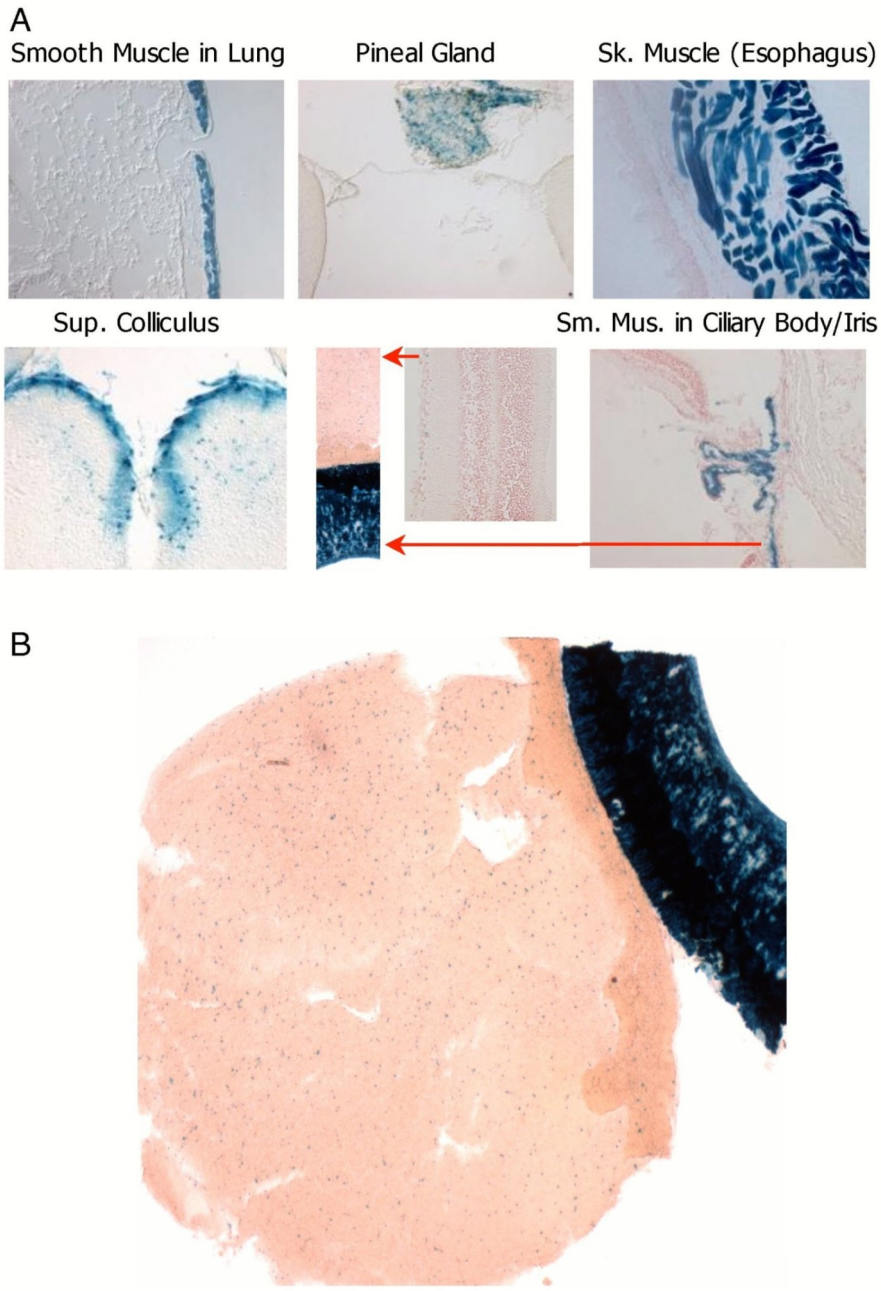

FIGURE 3.8 MICROSCOPIC VIEW OF *LacZ* STAINING

(A) Sections of various organs were stained by X-Gal. Positive tissues included pulmonary smooth muscle, pineal glands, striated muscle at esophagus, and superior colliculi. Intraorbitally ciliary body, iris, and some retina ganglia cells were strongly stained as well. (B) Flat-mount retina was prepared from the X-Gal-stained eyeball. Note only some retina ganglia cells were stained in a starry pattern. Iris was strongly positive.

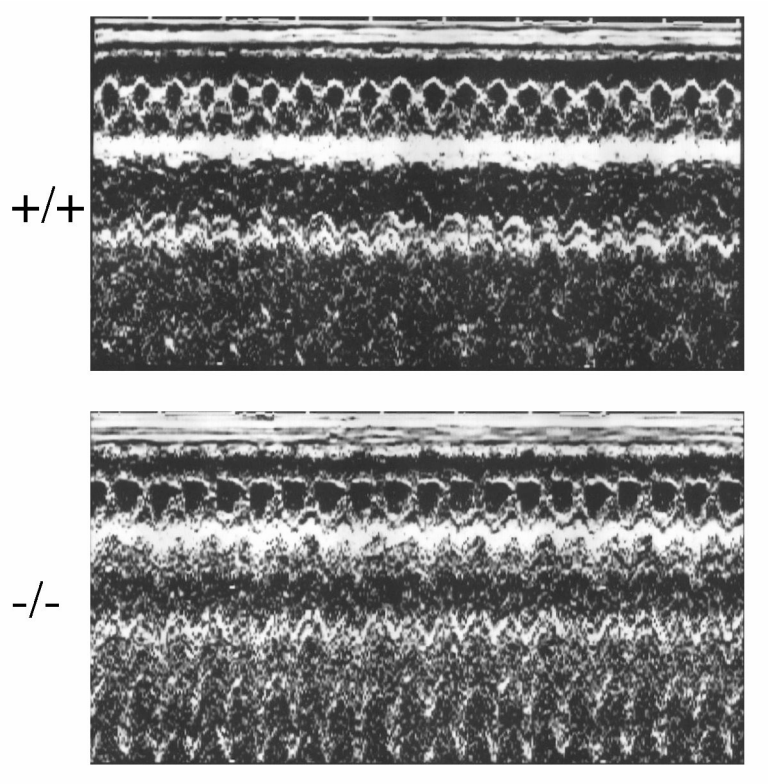

FIGURE 3.9 CARDIAC ECHO

Cardiac echo was performed against *mKelch* mice at 4 months old. Both systolic and diastolic phases were normal. Structurally no abnormalities were identified.

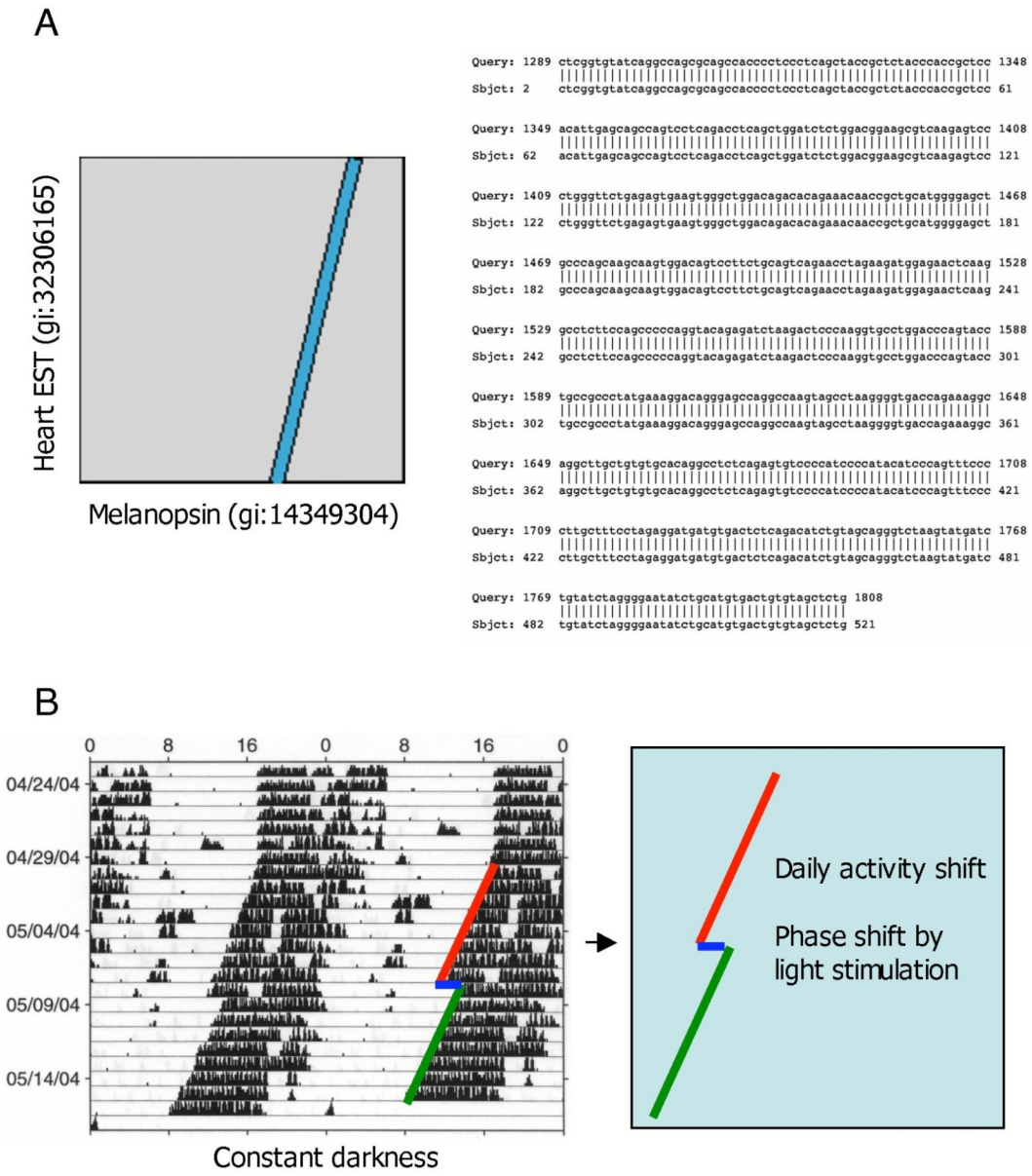

Figure 3.10 Relationship to Melanopsin

(A) *Melanopsin* cDNA aligned well with a record of EST database, which was cloned from hearts. (B) Circadian locomotor activity was monitored by wheel running (actogram). Mice were firstly adapted to equally-divided light-dark cycles for 1 week before entering constant darkness. Endogenous circadian rhythm, which is less than 24 hours, would advance the onset of locomotor activity in constant darkness. If mice were pulsed with light between 2 to 3 hours after onset of activity, there would be a phase delay for the next day's activity onset. The delay could be identified on the actogram, as shown in blue on the right panel.

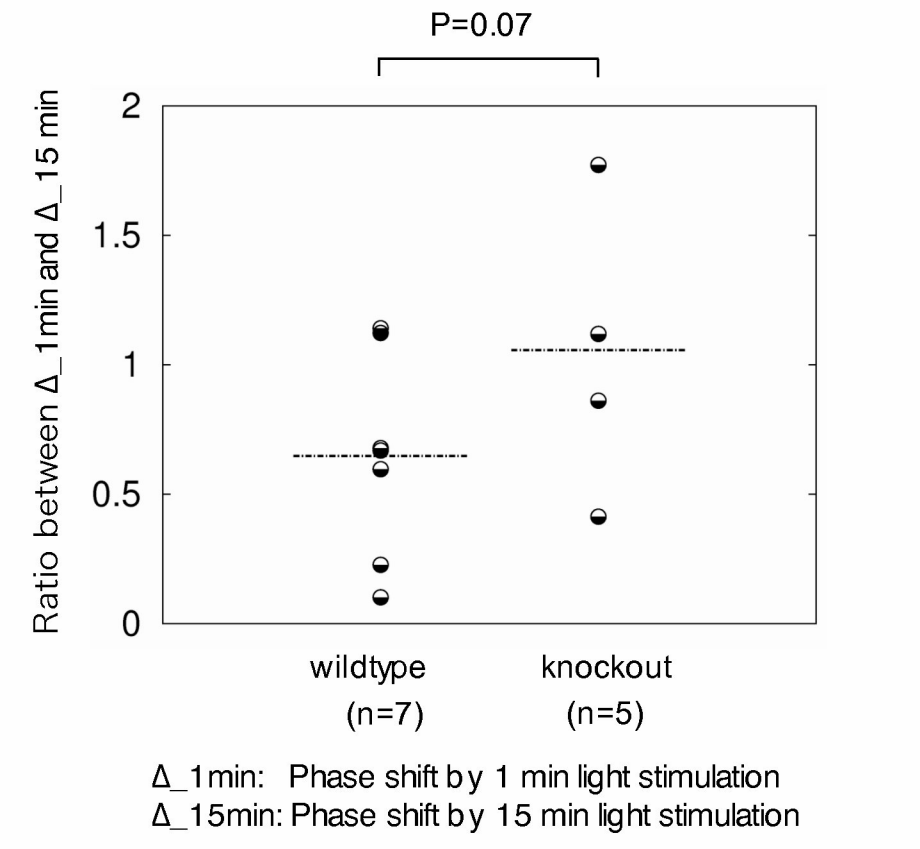

FIGURE 3.11 PHASE SHIFT IN CONSTANT DARKNESS

Each mouse in constant darkness was pulsed with 1-minute and 15-minute light stimulations on two different occasions. The ratio between resultant phase delays (shift from 1-minute stimulation divided by shift from 15-minute stimulation) was plotted in the figure. In knockout animals the ratio was 1±0.5, but the control mice had the ratios at 0.6±0.4. It seemed that knockout animals had a lower threshold for light simulation in phase shift adjustment, though statistical significance was not reached (p=0.07).

Tables

Table 3.1 Genotype and Body Weight Statistics.

	Wild Type	Heterozygous	Homozygous
mKelch +/- x +/-	N = 19 (26.8%) Male 11 Female 8	N = 35 (49.3%) Male 22 Female 13	N = 17 (23.9%) Male 10 Female 7
Body Weight at One m/o (g)	18.7 ± 3.0 (N = 5) M 18.2 ± 1.3 (N = 2) F 19.1 ± 3.7 (N = 3)	19.7 ± 3.4 (N = 10) M 21.6 ± 2.8 (N = 6) F 16.9 ± 1.9 (N = 4)	19.8 ± 2.1 (N = 8) M 20.0 ± 2.5 (N = 5) F 19.3 ± 1.3 (N = 3)

Table 3.2 BTB-kelch Screen Primers.

	Group	1	2	3
Pair 1	Protein Name	Mm1_WIFeb01_14_107_5	Mm2_WIFeb01_27_56_9	Mm4_WIFeb01_60_111_2
	Sense	GTTACGCCTATGGCCACCAAG	AAACCCCTCGTTCCATGTTTG	GCAGCTTTGTTCACTGGAGGA
	Antisense	TGTCCAGGAATCAGTGCGAAT	TTCTTGGGGAAATTCCGTCAT	TGCTGCAACAATCAACTCCTG
	Product Size	138 bp	149 bp	156 bp
Pair 2	Protein Name	Mm1_WIFeb01_17_18_1	Mm2_WIFeb01_27_58_1	Mm4_WIFeb01_71_131_3
	Sense	TTGGAGGTGCAGAATCTTGGA	TGCTCAATGCCAGGTATTACCAC	ACAACCCGAGGACCAACAAGT
	Antisense	CAGCATTGCTCCTTGGTGAAG	GGAGCTGAGGAACCAGGAAGA	TGTTCCAGGTTTTCTGGGTGA
	Product Size	249 bp	249 bp	256 bp
Pair 3	Protein Name	Mm1_WIFeb01_18_30_3	Mm4_WIFeb01_56_35_2	Mm4_WIFeb01_71_64_12
	Sense	AGTGGGAGGGAGAGACGACAC	CACTAAGGGTGACCGGAACCT	CGACTGCTACAATCCGCAGAC
	Antisense	GGTCTTCTGCGCTTACCAGGA	GGTGACACCCCCACATACAAA	GCAGTTGTCCATGGGGTAGGT
	Product Size	336 bp	346 bp	334 bp
Pair 4	Protein Name	Mm1_WIFeb01_7_75_2	Mm4_WIFeb01_58_116_4	Mm5_WIFeb01_73_47_1
	Sense	GCTGGCTCTCCAGTGCTACAG	GCAGCTGCTCTAACGAGGAGA	GCAGCAAATCAGTACCAGATTGAA
	Antisense	GGCCCAGGCATCTCTTACAGT	GCCGTTACCCAGAGACACCTT	CAGCAGATGGTACCTCATTCCA
	Product Size	436 bp	440 bp	459 bp

	Group	4	5	6
Pair 1	Protein Name	Mm5_WIFeb01_80_37_1	Mm7_WIFeb01_173_66_6	Mm8_WIFeb01_194_380_1
	Sense	TGTCAGTCATTGGCTGTGTTCA	GCCTTTGTGAGGCTTTCGAGT	AGCCCCGCAGAAGTTTTACCT
	Antisense	TGTCAGTCATTGGCTGTGTTCA	CGGGTCTCGTGAACACTGACT	ACCTGATCTGCCCACTGAAGA
	Product Size	159 bp	133 bp	171 bp
Pair 2	Protein Name	Mm6_WIFeb01_100_76_4	Mm7_WIFeb01_174_91_6	Mm8_WIFeb01_194_397_1
	Sense	GCCGCCTTGCAGATGATAATA	TCACCAGAAAGGATGGTTGGA	GTCACAATGGAGGCAAGCAAG
	Antisense	AAGTTGTCGCTGCTGAGGATG	CCTTCAGGGGACCTAGGGACT	GCCCAGTGTGAACATGGAGTT
	Product Size	263 bp	241 bp	237 bp
Pair 3	Protein Name	Mm6_WIFeb01_112_137_9	Mm8_WIFeb01_183_107_3	Mm9_WIFeb01_194_5_4
	Sense	CTGGGCAAACTTCTGATGAGG	GCTGAGCCTGGACAACTGCTA	TCCCATGTCATCGTTGTGTGT
	Antisense	ATTGATTTCCCCTGGGCTTCT	CCTCCGCCTGGTAGCAATAAA	GACTGAACAACTGGGCAGAGC
	Product Size	336 bp	311 bp	327 bp
Pair 4	Protein Name	Mm6_WIFeb01_112_72_3	Mm8_WIFeb01_189_49_4	Mm9_WIFeb01_195_72_1
	Sense	GTGCACTGGGGTAGTCATGGA	CTGTTGTTGGCGTCACTGGTC	GGCGGTCATGTACCAGATTGA
	Antisense	ATTGATCTTGGCTGGGGTCAT	GATAGAAAGCCCTGGGCAGAA	GCCTGCAGGATCTCACACTTC
	Product Size	446 bp	464 bp	405 bp

	Group	7	8	9
Pair 1	Protein Name	Mm9_WIFeb01_197_125_2	Mm12_WIFeb01_235_51_5	Mm15_WIFeb01_286_81_3
	Sense	ACCCTGGGCAACAAGCTCTAC	TGGACTCTTTGCCTGTTTGGA	AGCTTGCAGCAGCATTCAGAC
	Antisense	TATCATAGCGCGGTTGGTGAG	CAGGACGCACGCTAGTTTCAA	GGTCTTTGAAGACAACCCCATC
	Product Size	136 bp	161 bp	146 bp
Pair 2	Protein Name	Mm9_WIFeb01_197_221_2	Mm13_WIFeb01_262_61_1	Mm16_WIFeb01_286_114_1
	Sense	ACCCTGAAAATGGATGGAGCA	CGTCTACTTCCAGAGCCACGA	GGACCCTTCGAAACAGTGCAT
	Antisense	GTACAGCAGCCCGTTGAACAC	CTTGCCTCTCCCTGTGATCCT	ATGCTGCTCCCATAGACCACA
	Product Size	248 bp	248 bp	254 bp
Pair 3	Protein Name	Mm9_WIFeb01_203_15_1	Mm13_WIFeb01_266_52_1	Mm16_WIFeb01_286_119_6
	Sense	CATTTCTCCGTGTCGGAGTTG	CCAGTCTCTGTGCTCGTCCTC	CTGGTGGTAGAGGGGAAGCAC
	Antisense	GAACGTGCAGCAAGCATCTTT	CTGTGTGCCCACCGACTACAT	GCTGTTGGGTCAGATGGTTCA
	Product Size	351 bp	342 bp	352 bp
Pair 4	Protein Name	Mm12_WIFeb01_223_24_5	Mm14_WIFeb01_273_43_1	Mm16_WIFeb01_286_162_4
	Sense	GCTTCCTGCAGCTTGTATTTCA	GCACAGCATTGAGCGTCTGTA	TGGAGATGGTTGAAGCAGACC
	Antisense	GGCCTTGGTATTGAGGCTGTC	TGAAAAGGTAGGGCACGAAGC	GCCACCCAATACGACCATCTT
	Product Size	438 bp	457 bp	449 bp

	Group	10	11	12
Pair 1	Protein Name	Mm16_WIFeb01_286_162_7	MmX_WIFeb01_348_21_2	β–Actin
	Sense	CCAGAATTCCCCCGAGTGTTA	GCATCTGGCCTTCTGGAGATT	TGACGTTGACATCCGTAAAGACC
	Antisense	TCACAGCCTCCAACCACAACT	GGCCTGGTAGCCAGTGAGAAG	AAGGGTGTAAAACGCAGCTCA
	Product Size	141 bp	152 bp	307 bp
Pair 2	Protein Name	MmX_WIFeb01_326_85_1		
	Sense	CCGCCAGCTTTCTTCAGATTC		
	Antisense	GCTTAAGGCTGTTGCTGGACA		
	Product Size	243 bp		
Pair 3	Protein Name	MmX_WIFeb01_334_12_1		
	Sense	CTGAAAGATGGCGGCATTG		
	Antisense	GCTCTGAACCCAGCAGAGACA		
	Product Size	350 bp		
Pair 4	Protein Name	MmX_WIFeb01_337_24_9		
	Sense	TATGAGCTGGCCAACCAGATG		
	Antisense	TGGGATTTTAAGAGGTCCAGCA		
	Product Size	477 bp		

CHAPTER FOUR
TAK1 KINASE

INTRODUCTION

The Rel/NF-κB family of transcription factors regulates the expression of a plethora of genes involved in inflammation, immunity, and apoptosis [96, 97]. NF-κB is normally sequestered in the cytoplasm of unstimulated cells through its association with the IκB family of inhibitory proteins. Stimulation of cells with a variety of agents leads to the rapid phosphorylation and subsequent degradation of IκB by the ubiquitin-proteasome pathway, thus allowing NF-κB to enter the nucleus to turn on various target genes.

Phosphorylation of IκB is catalyzed by a large kinase complex consisting of IKKα, IKKβ and NEMO (also known as IKKγ or IKKAP). The IKK complex integrates signals from diverse pathways, including those emanating from the receptors for TNFα and IL-1β, TLRs, and TCR [2, 21, 30, 119]. Stimulation of IL-1β receptors and some TLRs leads to the recruitment of several proteins including the adaptor MyD88, the kinases IRAK4 and IRAK1, and the ubiquitin ligase TRAF6. TRAF6 functions in conjunction with the E2 complex Ubc13-Uev1A to catalyze the synthesis of Lys63-linked polyubiquitin chains on certain protein targets including TRAF6 itself [27, 116]. Polyubiquitinated TRAF6 activates a protein kinase complex consisting of the TAK1 kinase and the adaptor proteins TAB1 and TAB2 [67, 116]. The activation of TAK1 by TRAF6 requires the binding between the K63 polyubiquitin chains and a conserved novel zinc finger domain of TAB2 or its homologue TAB3 [50]. After TAK1 is activated, it phosphorylates IKKβ within the activation loop, resulting in the activation of IKK. TAK1 also phosphorylates and activates MKK6 and MKK7, leading to the activation of p38 and JNK kinase pathways.

Recent studies have shown that TRAF-mediated polyubiquitination and the TAK1 kinase complex also play an important role in NF-κB activation in T cells [101]. Stimulation of TCR by an antigenic peptide and its cognate MHC activates a tyrosine kinase

phosphorylation cascade that in turn leads to the activation of PKCθ. PKCθ then triggers the recruitment of the CARD domain proteins CARMA1 and BCL10, and the paracaspase MALT1 to lipid rafts [56, 60, 105]. MALT1 binds to TRAF6 and promotes TRAF6 oligomerization, which activates its ubiquitin ligase activity [101]. TRAF6-mediated polyubiquitination then leads to the activation of TAK1 and subsequent activation of IKK. This T cell signaling pathway from BCL10 to IKK activation can be reconstituted *in vitro* using purified recombinant proteins, including Ubc13-Uev1A (E2), TRAF6 (E3) and the TAK1 kinase complex [101]. Furthermore, RNAi-mediated silencing of TAK1, TRAF2 and TRAF6 inhibits IKK activation and interleukin-2 production in Jurkat T cells. However, it has been shown that MALT1 can function as a ubiquitin ligase that binds directly to Ubc13-Uev1A and promotes the polyubiquitination of NEMO, thereby leading to IKK activation [126]. According to this model, TRAF proteins and TAK1 are not required for IKK activation by TCR.

The role of TAK1 in NF-κB activation by receptors of the innate immunity pathways, including TNFR, IL-1R and TLR, has been validated *in vivo* through the isolation of *Drosophila* TAK1 mutants [111] and the generation of TAK1 knockout mice [88, 93]. However, conditional deletion of TAK1 in B cells using *Cd19-Cre* did not abolish NF-κB activation by BCR [88], which also signal through the CARMA1-BCL10-MALT1 complex [98]. This result is discordant with another recent study that employed homologous recombination in chicken DT40 cells to delete TAK1 and showed that the complete absence of TAK1 abolished IKK and NF-κB activation by BCR [94]

In this report, we investigated the role of TAK1 in T cell development and activation by engineering a mouse model in which TAK1 was conditionally deleted in T cells. We showed that thymocytes lacking TAK1 failed to survive during the progression from double positive ($CD4^+CD8^+$) to single positive ($CD4^+$ or $CD8^+$) stages, resulting in significant reduction of naïve T cells in the peripheral tissues. The loss of TAK1 in the thymocytes prevented the activation of IKK, NF-κB and JNK, and sensitized the mutant cells to activation-induced apoptosis. Our results provide the genetic evidence that TAK1 is essential for thymocyte development and activation.

Materials and Methods

Gene Targeting and Genotyping of Mice

AB2.2 mouse ES cells were targeted by a construct containing one *loxP* site before the transcription initiation site of *Tak1*, and the other *loxP* site in intron 1. The targeting construct also contained a *FRT-neo-FRT* selection cassette before the intronic *loxP* site. The 5' and 3' homologous regions spanned 2.5 and 3.0 kb, respectively. Targeted ES cells were screened by Southern blotting with both 5' and 3' probes (Figure 4.1), following digestion with EcoR V and Nhe I, respectively. Blastocyst injection was performed at Baylor College of Medicine (Houston). *Lck-Cre* transgenic mice were obtained from the Jackson Laboratory [47]. Floxed *Tak1* mice were crossed to *Lck-Cre* mice at UT Southwestern Medical Center (Dallas). Mice were genotyped by PCR using the following primer pairs: gcacagaaaatgcacagtgctc and gcttgggacaggctggtaaag (for the wild type allele); gcacagaaaatgcacagtgctc and cttacaagccgaattccagca (for the floxed allele); and gcacagaaaatgcacagtgctc and ctcctccactccgcccctac (for the excised allele). The PCR conditions were: 94°C for 30 seconds; 58°C for 30 seconds; and 72°C for 1 minute; 35 cycles. The mice used in this study were 5-10 weeks old. All mice were housed in conventional animal facilities at the University of Texas Southwestern Medical Center or Baylor College of Medicine.

FACS

Spleens, thymi, and lymph nodes were mechanically disrupted by a syringe pump, and filtered through cell strainers (100 μm, BD Biosciences) to obtain suspension cells. Blood cells were isolated by following the online protocol at the Jackson Laboratory (http://www.jax.org/imr/facs.html) except FACS buffer was replaced by 5% FBS in PBS. Cells were stained with a monoclonal antibody for 15 minutes on ice and washed once before FACS analysis. In the event when staining with a secondary antibody was required, cells were stained with the antibody for another 15 minutes on ice followed by another wash step. Data were collected by FACSCalibur or FACScan (Becton Dickinson) flow

cytometers, and analyzed using CellQuest software. Primary antibodies against B220 (RA3-6B2), CD3 (17A2), CD24 (M1/69), CD4 (GK1.5), CD8a (53-6.7), CD69 (H1.2F3) were from BD Bioscience; these antibodies are conjugated with different markers, such as fluorescein isothiocyanate (FITC), phycoerythrin (PE), allophycocyanin (APC), or biotin. Streptavidin coupled to peridinin chlorphyll protein (BD Bioscience) was used as a secondary antibody.

Isolation and Purification of Thymocytes and Lymph Node T Cells

$CD4^+$ SP and $CD4^+CD8^+$ DP thymocytes were directly sorted by FACSVantage SE (with DIVA upgrade) after CD4 and CD8 staining. $CD8^+$ SP thymocytes were purified by depleting $CD4^+$ cells with a magnetic column followed by FACS sorting for $CD8^+$ cells. Briefly, thymocytes were incubated with anti-CD4-PE and anti-PE magnetic beads (Miltenyi Biotec) before applying to a magnetic column. The unbound materials were incubated with anti-CD8a-FITC and then sorted for the $CD8^+$ SP thymocytes by FACS. The purity of the sorted cells was at least 95%. Lymph node T cells were purified using Pan T Cell Isolation Kit (Miltenyi Biotec) from a pool of popliteal, axillary, and mesentery lymph nodes. The purity of the sorted $CD3^+$ cells was at least 96%.

Annexin-V Cell Death Assay

Purified thymocytes at various stages were pelleted and resuspended in complete media (RPMI-1640, 10% FBS, penicillin/streptomycin, 50 μM β-mercaptoethernol) at a density of 5 x 10^5/ml. Aliquots of the cells (5 x 10^4 cells per well) were grown in 96-well plates precoated with either PBS or 10 μg/ml anti-CD3ϵ (145-2C11, BD Bioscience). At indicated times, cells were incubated with Annexin-V-APC (BD Bioscience) in staining buffer (10 mM Hepes pH 7.4, 140 mM NaCl, 2.5 mM $CaCl_2$) for 15 minutes at room temperature and then analyzed by FACS. At least 4000 events were recorded for each sample.

Biochemical Analyses

Immunoblotting was carried out using standard procedures. In Figure 4.1.D, cells (1.6 x 10^6) were lysed directly in SDS sample buffer supplemented with 25 units of Benzonase

(Novagen), which digests genomic DNA to reduce viscosity. After incubation at 4°C for 30 minutes, the samples were boiled and then subjected to SDS-PAGE and Western transfer. In Figure 4.5.B & C, cells were lysed in 200 μl kinase assay buffer per 10^7 cells [20 mM Tris-Cl pH 7.5, 100 mM NaCl, 25 mM β-glycero-phosphate, 1 mM sodium vanadate, 10% glycerol, 0.02% NP-40, and proteinase inhibitor (Roche)]. The antibodies against phospho-ERK and JNK were from Cell Signaling, and the antibody against phospho-JNK was from BioSource. Antibodies for TAK1 (M579), IκBα (C21) and NEMO (FL-419) were from Santa Cruz Biotechnology. Antibodies for tubulin and Cre were from Sigma and Novagen, respectively.

For EMSA, whole cell extracts [3-4 μg protein in 20 mM Tris pH 7.5, 10% glycerol, 0,4 M KCl, 1 mM DTT, 1mM EDTA, 0.1% NP-40, proteinase inhibitor (Roche)] were incubated with radiolabeled DNA probes containing the consensus NF-κB or Oct-1 binding sites (Promega). After incubation at room temperature for 15 minutes, the DNA-protein complexes were resolved by electrophoresis on 5% polyacrylamide gel and analyzed by PhosphorImaging.

For NF-κB and JNK activity assays, thymocytes were prepared at a density of 2 x 10^7/ml in complete media (RPMI-1640, 10% FBS, penicillin/streptomycin, 50 μM β-mercaptoethernol) and stimulated with PMA (100 ng/ml) and ionomycin (200 ng/ml) or mouse TNFα (CHEMICON, 25 ng/ml) for the indicated time periods. The IKK kinase assay was carried out as described before [101]. For plate-bound anti-CD3ϵ stimulation, 10^6/100 μl thymocytes in complete media were stimulated for 16 hours in 96-well plates which had been coated by either PBS or 10 μg/ml anti-CD3ϵ at 37°C for 90 minutes.

Real Time PCR

Thymocytes were stimulated with anti-CD3ϵ for 20 hours as described above, and then total RNA was extracted using the QIAGEN RNeasy Mini kit. First strand cDNA was synthesized using SuperScript III SuperMix for qRT-PCR (Invitrogen). Real time PCR was performed in duplicates in the iQ5 multicolor detection system using SYBR Green supermix (BIO-RAD). *c-myc* primers were gcccaaatcctgtacctcgtc and tgcctcttctccacagacacc. β-actin primers were tgacgttgacatccgtaaagacc and aagggtgtaaaacgcagctca. The PCR conditions

were: 94°C for 30 seconds; 58°C for 30 seconds; and 72°C for 30 seconds; 40 cycles. The expression of *c-myc* was normalized using β-actin as an internal control.

Statistics and Graph Preparation

Student's t-Tests were used for statistical analysis. Data were presented as average $\pm$ standard error. Graphs except FACS analyses were prepared using gnuplot (http://www.gnuplot.info/), Adobe Photoshop, or Microsoft Excel.

Results

Conditional Knockout of TAK1 in T cells

To engineer conditional alleles of *Tak1* in mice, we constructed a targeting vector in which exon 1 of *Tak1* was flanked between a *loxP* site before the transcriptional initiation site and another *loxP* site within intron 1 (Figure 4.1.A). The *FRT-neo-FRT* selection cassette was inserted before the intronic *loxP* site. The 5' and 3' homologous regions were 2.5 and 3.0 kb, respectively. ES cell targeting and the generation of heterologous floxed *Tak1* mice ($Tak1^{+/flox}$) were carried out by standard protocols. The $Tak1^{flox/flox}$ mice were born and lived normally and they expressed TAK1 protein as expected (data not shown). To delete the *Tak1* allele specifically in T cells, we crossed $Tak1^{flox/flox}$ mice with the *Lck-Cre* transgenic mice, which express the Cre recombinase under the control of the T cell-specific Lck promoter [47]. Southern blotting and PCR showed that the floxed *Tak1* alleles were excised in thymocytes, but not in the tail (Figure 4.1.B & C). Western blotting confirmed that TAK1 was not detectable in the thymocytes of *Lck-Cre*/$Tak1^{flox/flox}$ mice, but its expression level in splenocytes was similar to that in control littermates (Figure 4.1.D). Surprisingly, the lymph node T cells from *Lck-Cre*/$Tak1^{flox/flox}$ mice had normal levels of TAK1, but lacked the expression of Cre, whereas the cells from *Lck-Cre*/$Tak1^{+/+}$ mice still had high levels of Cre expression (Figure 4.1.D). Genomic PCR confirmed the presence of the floxed *Tak1* allele in T cells derived from lymph nodes and blood (data not shown),

indicating that these cells have escaped from Cre-mediated recombination. Thus, the loss of Cre expression and the retention of the floxed *Tak1* alleles in *Lck-Cre/Tak1*$^{flox/flox}$ mice likely resulted from counter selection during T cell development in the thymus (see below and Discussion). For the control groups, we observed no phenotypic difference between *Lck-Cre/Tak1*$^{+/+}$ and *Lck-Cre/Tak1*$^{floxed/+}$, indicating that one copy of the Cre transgene did not have any confounding effect on the functional analyses of the mice. For simplicity, the *Lck-Cre/Tak1*$^{flox/flox}$ mice with deletion of the *Tak1* alleles are herein referred to as *Tak1*^{D} or knockout, whereas the control mice still containing the floxed *Tak1* allele are referred to as *Tak1*^{FL} or control.

Reduction of Peripheral T cells

We analyzed peripheral B cells (B220^{+}) and T cells (CD3^{+}) in *Tak1*^{D} and *Tak1*^{FL} by FACS. While the percentage of B cells was similar in both genotypes, the percentage of T cells in the peripheral lymphoid organs, including lymph nodes, spleens and blood, was significantly lower in *Tak1*^{D} mice as compared to controls (Figure 4.2.A). This decrease of T cell percentage was not due to an increase of B cell number because the number of splenocytes was similar in the knockout and control mice ($4.0 \pm 1.0 \times 10^{8}$ in *Tak1*^{D} vs. $4.1 \pm 0.8 \times 10^{8}$ in *Tak1*^{FL}; n=5). The decrease of T cell number was not observed in various control animals, including floxed mice without the *Lck-Cre* transgene and the *Lck-Cre* mice without the floxed *Tak1* allele (Figure 4.2.B). The percentage of T cells in the blood of *Tak1*^{D} mice was about one-fourth of the control mice (5.9 ±(1.1% in *Tak1*^{D} vs. 26.4 ± 1.6% in *Tak1*^{FL}; n=13). The relative abundance of helper (CD4^{+}) versus cytotoxic (CD8^{+}) T cells in the blood was similar for both *Tak1*^{D} and *Tak1*^{FL} mice (CD4^{+}/CD8^{+} ratio: 1.2 ± 0.2 in *Tak1*^{D} vs. 1.3 ± 0.2 in *Tak1*^{FL}; n=6).

TAK1 Is Required for Single Positive Thymocytes

The reduction of T cells in the peripheral lymphoid organs of *Tak1*^{D} mice may be due to defective T cell development in the thymus. Intrathymic T cell precursors develop through several stages before entering the peripheral mature T cell pool [81, 96]. The most immature cells transit from double negative stage (CD4^{-}CD8^{-}, DN) into double positive

stage ($CD4^+CD8^+$, DP) after completion of beta-selection. DP thymocytes go through further selections before committing to single positive cells ($CD4^+$ or $CD8^+$, SP). To determine if TAK1 is required for thymocyte development, we analyzed the expression of CD4 and CD8 by FACS. As shown in Figure 4.3.A and Table 4.1, both $CD4^+$ and $CD8^+$ SP thymocytes in $Tak1^D$ mice were reduced by approximately 50% as compared to the $Tak1^{FL}$ mice. In contrast, there was no significant difference in the number of $CD4^+CD8^+$ DP thymocytes between $Tak1^D$ and $Tak1^{FL}$ mice. We also analyzed the $CD24^{high}CD4^-CD8^-$ thymocytes to examine the transition of thymocytes from DN1 to DN4 (DN1: $CD44^+CD25^-$; DN2: $CD44^+CD25^+$; DN3: $CD44^-CD25^+$; and DN4: $CD44^-CD25^-$). No apparent defect was observed in any of these developmental stages in $Tak1^D$ mice (Figure 4.3.B), consistent with normal TAK1 protein expression in DN thymocytes in which *Lck-Cre* was not turned on until the later stages of DN thymocyte development (data not shown) [16].

To investigate the mechanism underlying the reduction of SP thymocytes in $Tak1^D$ mice, we analyzed the CD69 surface marker, which is expressed on positively selected cells [127]. As shown in Figure 4.3.C, although $Tak1^D$ mice contained fewer $CD4^+$ and $CD8^+$ SP thymocytes, the percentages of $CD69^+$ thymocytes were comparable to those in the wild type mice, indicating that loss of TAK1 did not compromise the positive selection of thymocytes. To determine if the maturation of SP thymocytes is affected by the loss of TAK1, we used FACS to examine the expression of CD24, a surface marker that is gradually downregulated during maturation of SP thymocytes [106]. As shown in Figure 4.3.D, the number of $CD24^{low}$ and $CD24^{intermediate}$ $CD4^+$ or $CD8^+$ SP cells was significantly less in $Tak1^D$ than in $Tak1^{FL}$ mice, indicating that the maturation of SP cells was impaired in $Tak1^D$ thymocytes.

Loss of TAK1 Sensitizes Single Positive Thymocytes to Apoptosis

The reduction in the number of SP thymocytes could be due to survival disadvantages in $Tak1^D$ thymocytes. To investigate this possibility, we carried out *in vitro* survival assay for thymocytes at DP or SP stages. These cells were sorted by FACS and cultured *in vitro* with or without anti-CD3ϵ stimulation. At indicated time points, non-surviving cells were stained by Annexin-V and analyzed by FACS (Figure 4.4.A). After stimulation

with anti-CD3ϵ for 40 hours, both CD4$^+$ and CD8$^+$ SP thymocytes from *Tak1*^{D} mice had a significant increase in apoptosis as compared to thymocytes from the control littermates, as shown by enhanced Annexin-V staining (Figure 4.4.B). In the absence of stimulation, the SP thymocytes from *Tak1*^{D} mice also displayed increased Annexin-V staining than those from the control mice (Figure 4.4.A). In contrast to SP thymocytes, the *Tak1*^{D} DP thymocytes were surviving as well as control DP thymocytes in the absence of anti-CD3ϵ stimulation. Following stimulation, the number of Annexin-V positive DP thymocytes in *Tak1*^{D} mice was slightly less than that of control mice, suggesting that TAK1 might facilitate the apoptosis of DP thymocytes. Cell cycle analysis by 7-AAD staining [107] showed that *Tak1*^{D} SP thymocytes did not have proliferation defects (data not shown), indicating that the decrease of SP thymocytes was primarily due to enhanced apoptosis.

TAK1 Is Required for the Activation of NF-κB and JNK

The defective SP thymocyte development observed in *Tak1*^{D} mice is reminiscent of the phenotypes observed in mice lacking NEMO or expressing a dominant negative mutant of IKKβ in T cells [89]. As *in vitro* and *ex vivo* studies have suggested that TAK1 is required for NF-κB activation in T cells [101], we used EMSA to determine if NF-κB activation was impaired in *Tak1*^{D} thymocytes (Figure 4.5.A). As reported previously [112], NF-κB is active in CD4$^+$ or CD8$^+$ SP thymocytes of wild type mice. In contrast, the NF-κB activity was greatly diminished in the SP thymocytes of *Tak1*^{D} mice. The DP thymocytes from wild type mice also exhibited weak NF-κB activity; this activity was not detectable in the DP thymocytes of *Tak1*^{D} mice. The loss of TAK1 did not affect the DNA binding of the control transcription factor Oct-1. Thus, TAK1 is required for NF-κB activation during the normal development of mouse thymocytes.

To determine if TAK1 is required for the activation of IKK and JNK, we stimulated thymocytes with PMA and ionomycin, which mimic the stimulation of TCR in T cells (Figure 4.5.B & C), or with TNFα (Figure 4.5.D). In both cases, the degradation of IκBα and activation of JNK were severely impaired in thymocytes derived from *Tak1*^{D} mice, whereas the activation of ERK occurred normally in these cells. We also examined NF-κB activation following stimulation of thymocytes with an antibody against CD3ϵ, which

crosslinks TCR. As shown in Figure 4.5.E, NF-κB activation was impaired in thymocytes from *Tak1*^{D} mice. Finally, we used real time PCR to measure the expression of *c-myc*, an NF-κB dependent gene required for the survival of thymocytes [12, 31, 118]. When thymocytes were stimulated with anti-CD3ϵ, *c-myc* was induced by about four fold in the wild type cells but not in *Tak1*^{D} cells (Figure 4.5.F). Collectively, these results indicate that TAK1 is essential for the activation of NF-κB and JNK in thymocytes.

Discussion

In this report, we showed that specific deletion of TAK1 in T cells prevented the development of CD4^{+} and CD8^{+} single positive thymocytes, resulting in significant reduction of T cells in the peripheral tissues including lymph nodes, spleens and blood. The defective development of SP thymocytes was due, at least in part, to the increased apoptosis of these cells, especially under conditions of anti-CD3 stimulation. We further showed that TAK1 was essential for the activation of IKK, NF-κB and JNK, demonstrating the role of TAK1 in T cell development and activation. Thus, TAK1 is an essential IKK kinase in both innate and adaptive immunity.

The defective thymocyte development observed in the conditional *Tak1*^{D} mice is similar to the phenotypes of mice lacking NEMO or expressing a kinase-dead mutant of IKKβ in T cells [89], further supporting the role of TAK1 in IKK activation. However, knockouts of some components of the TCR signaling pathway, such as CARMA1, BCL10 and MALT1, which affect IKK activation in mature T cells, do not severely affect T cell development in the thymus [32, 42, 66, 83, 84, 85]. Thus, TAK1 and IKK may be activated by a TCR-independent signaling pathway in thymocytes. Indeed, NF-κB is constitutively active during intrathymic development at both DN and SP stages. The constitutive activation of NF-κB in DN thymocytes is thought to be mediated by pre-TCR, which is assembled after the rearrangement of TCR β chain during the transition from DN3 to DN4 stages. Pre-TCR signaling is ligand-independent, and may be initiated by the autonomous oligomerization of pre-TCR α chain [123]. However, the mechanism underlying the constitutive activation of NF-κB at the SP stage is currently unknown. As our studies of *Tak1*^{D} mice have now

shown that TAK1 is required for IKK and NF-κB activation in SP thymocytes, further studies should be directed towards understanding how TAK1 is activated in these cells.

Previous studies using transgenic mice expressing an IκBα super-repressor under the control of the *Cd2* promoter have demonstrated that NF-κB is required for the positive selection of $CD8^+$ thymocytes [48]. Furthermore, it was found that the IκBα transgenic mice exhibited a developmental block in the transition from DN3 to DN4 thymocytes [112]. However, we did not observe any obvious developmental defect in the DN thymocytes of $Tak1^D$ mice (Figure 4.3.B). A possible explanation for these distinct phenotypes is that in the IκBα transgenic mice, IκBα can immediately inhibit NF-κB once it is synthesized, whereas in the $Tak1^D$ mice, the TAK1 protein remains in the DN thymocytes until the endogenous TAK1 is degraded following the induction of Cre and the deletion of the floxed *Tak1* locus. Indeed, immunoblotting experiments showed that TAK1 is present in the DN thymocytes of $Tak1^D$ mice (data not shown). Thus, the role of TAK1 in the early stages of thymocyte development remains to be determined.

A recent study employing *Cd19-Cre* to delete *Tak1* in B cells showed that TAK1 is required for JNK but not NF-κB activation in response to B cell receptor stimulation [88]. However, another recent study using chicken DT40 cells to completely remove *Tak1* demonstrated that TAK1 is required for both IKK and JNK activation following BCR stimulation [94]. It is not clear whether these different results reflect the difference of cells (chicken vs. mouse) or the knockout strategies employed in the studies. It is possible that the *Cd19-Cre*-mediated deletion may not be very efficient, resulting in a low level of TAK1 activity that is sufficient for IKK activation, but insufficient for JNK activation. Our current study shows clearly that TAK1 is required for IKK, NF-κB and JNK activation, at least in thymocytes.

The defective T cell development in $Tak1^D$ mice results in a significant decrease of mature T cells in the peripheral tissues. In fact, when T cells isolated from the lymph nodes of $Tak1^D$ mice were analyzed, they were found to express TAK1 and lack the expression of Cre (Figure 4.1.D), implying that only T cells that escape from Cre-mediated excision were able to emigrate from the thymus and populate the peripheral tissues. The requirement of TAK1 for the development of mature T cells precludes the analysis of the role of TAK1 in

the activation of these cells. Conditional deletion of TAK1 specifically in mature T cells, such as the use of a tamoxifen-inducible Cre, will be required to examine the function of TAK1 in these cells.

In sum, our results provide the genetic evidence that TAK1 is required for the activation of IKK, NF-κB and JNK in mouse thymocytes, and that TAK1 plays an essential role in thymocyte development and activation. These results extend the pivotal role of TAK1 in the innate immune system to the adaptive immune system.

Acknowledgment

We thank Gabriel Pineda for help with the IKK kinase assay. This work was supported by grants from NIH (RO1-AI60919), American Cancer Society (RSG0219501TBE), and the Welch Foundation (I-1389). Z.J.C. is an Investigator of Howard Hughes Medical Institute and a Burroughs Wellcome Fund Investigator in Pathogenesis of Infectious Diseases.

Figures

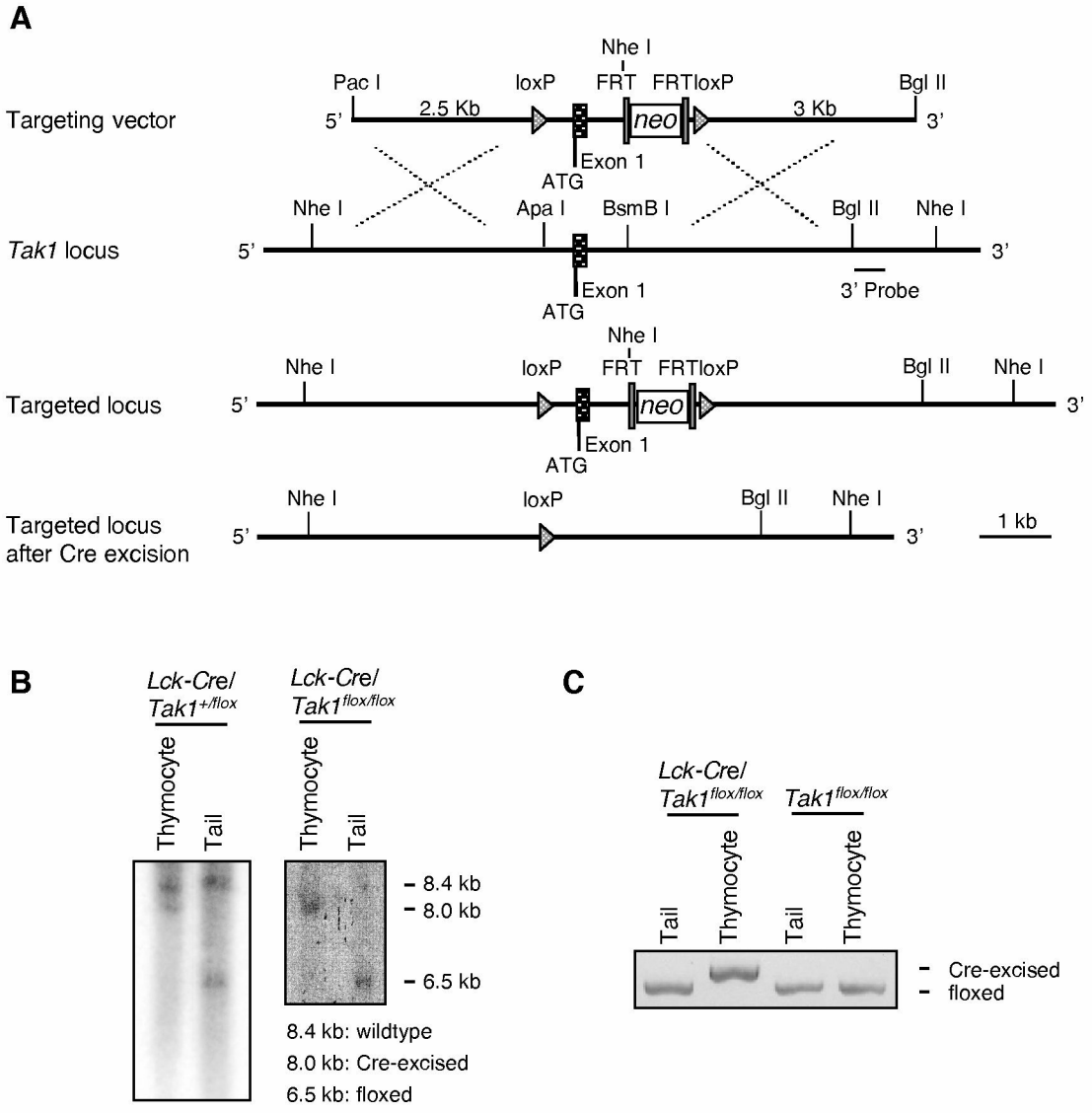
A
Nhe I
Pac I
loxP
FRT
FRTloxP
Bgl II
Targeting vector
5'
2.5 Kb
neo
3 Kb
3'
Exon 1
ATG
Nhe I
Apa I
BsmB I
Bgl II
Nhe I
Tak1 locus
5'
3'
Exon 1
ATG
3' Probe
Nhe I
Nhe I
loxP
FRT
FRTloxP
Bgl II
Nhe I
Targeted locus
5'
neo
3'
Exon 1
ATG
Nhe I
loxP
Bgl II
Nhe I
Targeted locus
after Cre excision
5'
3'
1 kb
B
Lck-Cre/
Tak1+/flox
Thymocyte
Tail
Lck-Cre/
Tak1flox/flox
Thymocyte
Tail
8.4 kb
8.0 kb
6.5 kb
8.4 kb: wildtype
8.0 kb: Cre-excised
6.5 kb: floxed
C
Lck-Cre/
Tak1flox/flox
Tak1flox/flox
Tail
Thymocyte
Tail
Thymocyte
Cre-excised
floxed

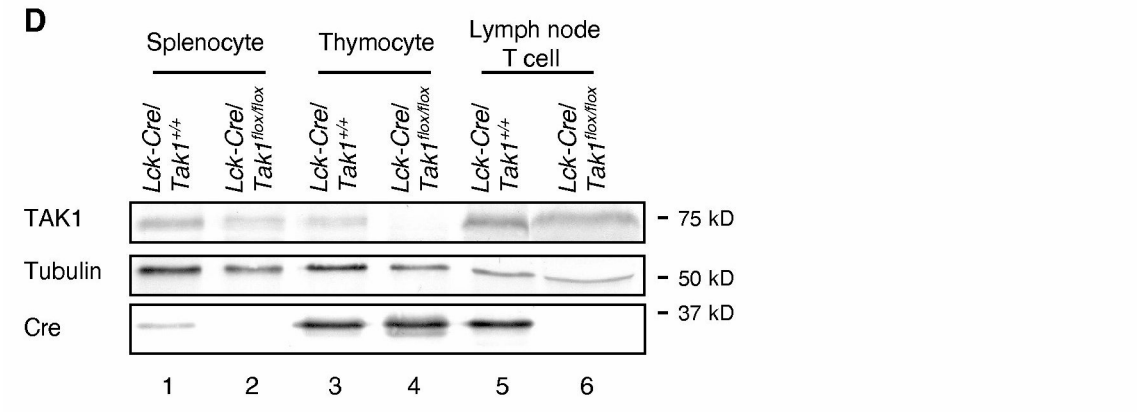

FIGURE 4.1 CONDITIONAL DELETION OF *Tak1* IN MOUSE THYMOCYTES

(A) Strategies for the generation and deletion of floxed *Tak1* alleles. (B) Southern blotting of genomic DNA after digestion with Nhe I. (C) PCR of genomic DNA isolated from the tails or thymocytes of the mice as indicated. (D) Western blotting of whole cell lysates from splenocytes, thymocytes and lymph node T cells. Lysates from 1.6 x 10^6 cells were loaded on each lane. In lane 6, lymph node T cells for *Lck-Cre/Tak1*$^{flox/flox}$ were pooled from 3 mice. The expression of TAK1 and loss of expression of Cre in these cells likely resulted from the selective expansion of TAK1-expressing cells that escaped from Cre-mediated excision.

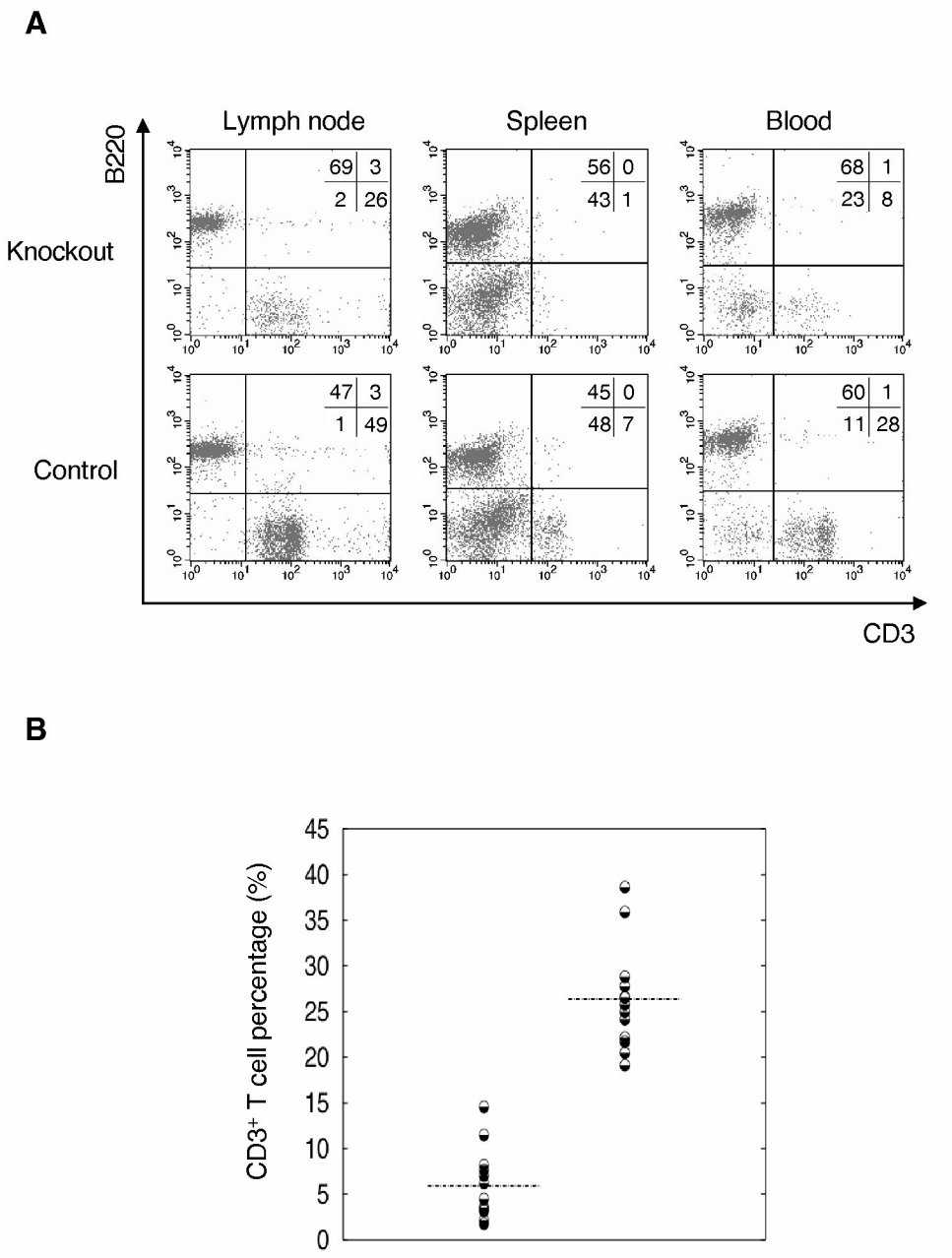

FIGURE 4.2 REDUCTION OF PERIPHERAL T CELLS IN *Tak1^D* MICE

(A) Suspension cells from Lymph nodes, spleens and blood were analyzed by FACS using antibodies against CD3 and B220, respectively. (B) The percentages of CD3$^+$ T cells in the blood from the TAK1 knockout (*Tak1^D*) mice and their control littermates (n=13).

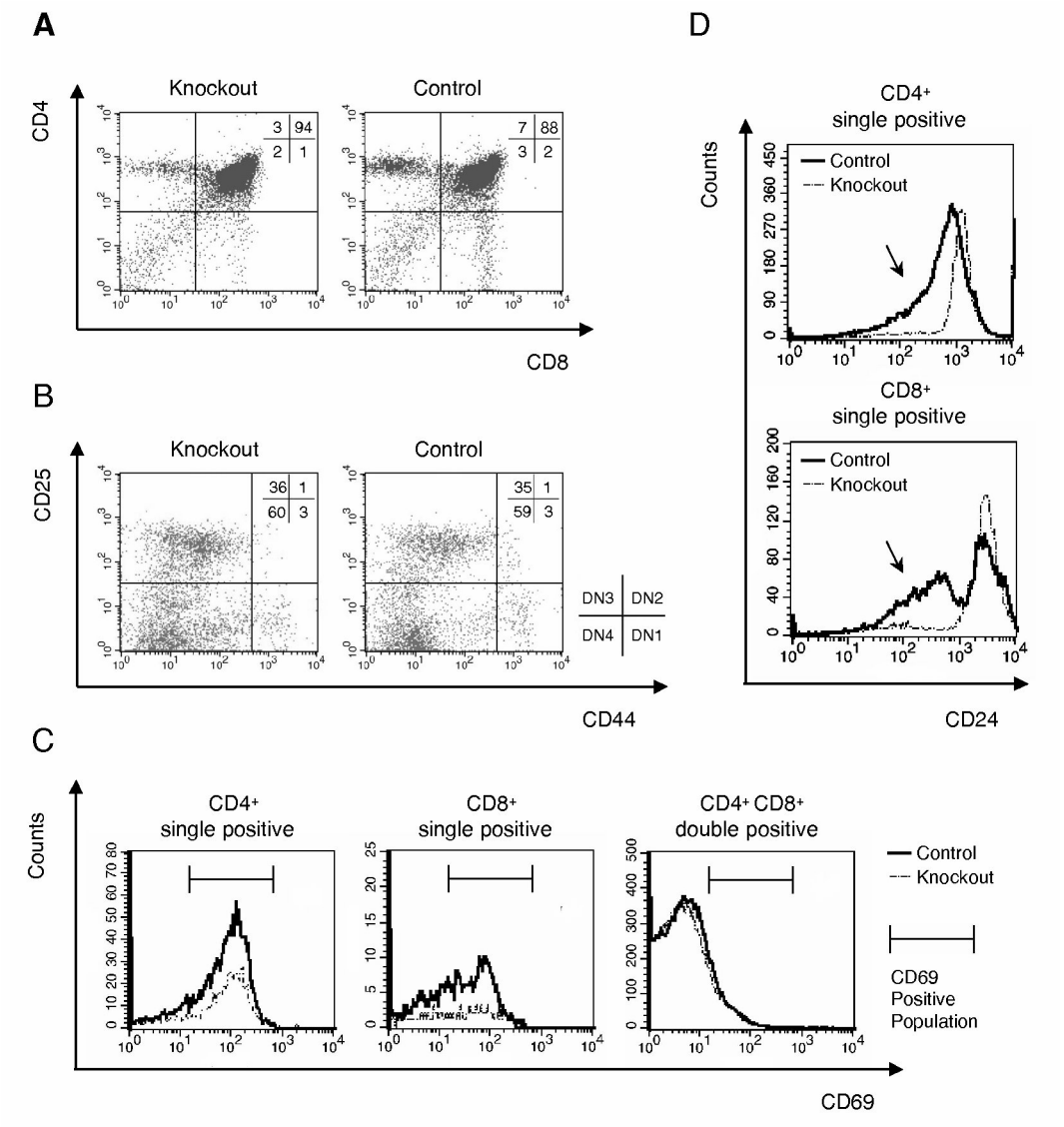

FIGURE 4.3 DEFECTIVE DEVELOPMENT OF $CD4^+$ AND $CD8^+$ SINGLE POSITIVE THYMOCYTES IN *Tak1*^{D} MICE

(A) Thymocytes from *Tak1*^{D} (knockout) and wild type (control) littermates were analyzed by FACS using antibodies against CD4 and CD8. The percentages of thymocytes at different stages are shown in the inlet, whereas the absolute number of each type of thymocytes is shown in Table 4.1. (B) CD24^{high}CD4^{-}CD8^{-} double negative (DN) thymocytes were analyzed by FACS using antibodies against CD25 and CD44. Different developmental stages of thymocytes (DN1-4) are indicated on the lower right corner. (C) SP and DP thymocytes were analyzed for CD69 expression. Percentages of CD69^{+} populations were 89% in *Tak1*^{D} vs. 87% in *Tak1*^{FL} for CD4^{+} SP, 60% in *Tak1*^{D} vs. 64% in *Tak1*^{FL} for CD8^{+} SP, and 11% in *Tak1*^{D} vs. 10% in *Tak1*^{FL} for CD4^{+}CD8^{+} DP. (D) FACS analysis of CD24 expression in CD4^{+} or CD8^{+} SP thymocytes. High expression of CD24 is inversely correlated with the maturation of SP thymocytes. The results are normalized for the total numbers of thymocytes.

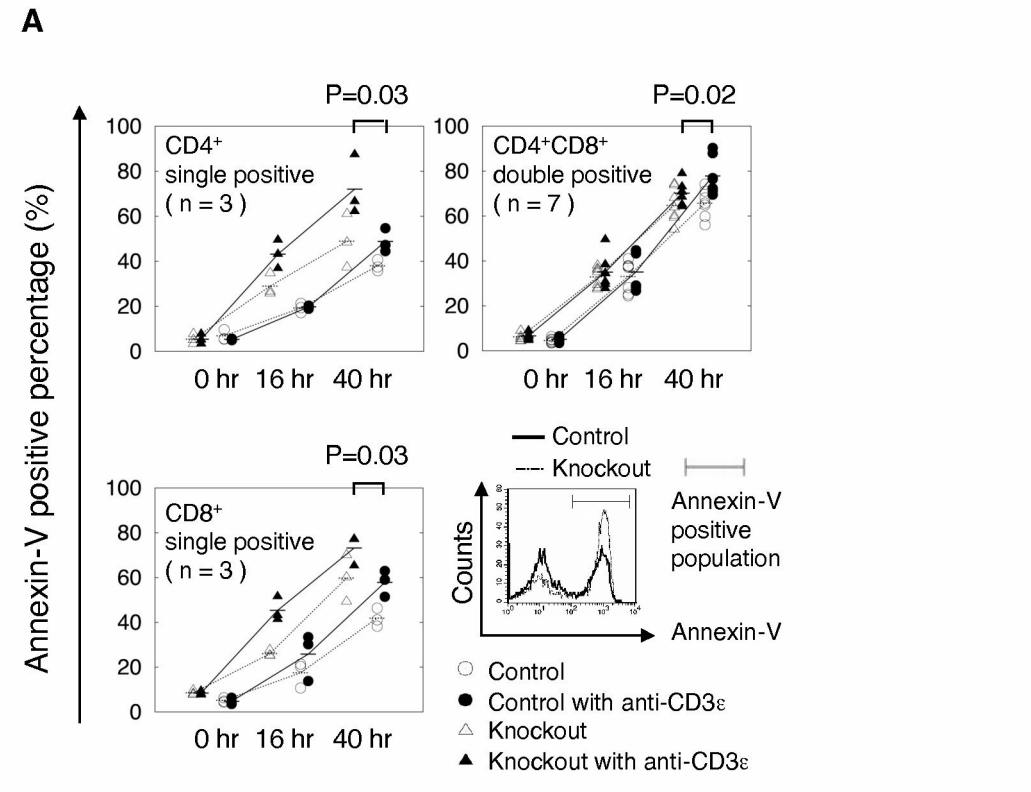

B

Percentage of Annexin-V positive cells				
Genotype	Thymocytes	0hr (%)	anti-CD3ε stimulation (10 μg/ml) 16hr (%)	40hr (%)
Knockout	$CD4^+$ SP	5.39 ± 2.22	43.14 ± 6.31	72.04 ± 13.49
	$CD8^+$ SP	8.38 ± 0.88	45.32 ± 5.44	73.18 ± 6.86
	$CD4^+CD8^+$	6.65 ± 1.73	34.96 ± 7.35	70.17 ± 4.99
Control	$CD4^+$ SP	5.35 ± 0.32	19.74 ± 0.73	48.81 ± 5.27
	$CD8^+$ SP	4.74 ± 1.42	25.80 ± 10.51	57.78 ± 5.85
	$CD4^+CD8^+$	5.11 ± 1.04	35.09 ± 8.53	77.79 ± 8.22

$CD4^+$ SP : $CD4^+$ single positive
$CD8^+$ SP : $CD8^+$ single positive
$CD4^+CD8^+$: $CD4^+CD8^+$ double positive

FIGURE 4.4 SURVIVAL DISADVANTAGE OF $CD4^+$ AND $CD8^+$ SINGLE POSITIVE THYMOCYTES IN *Tak1*^{D} MICE

(A) Single positive (SP) and double positive (DP) thymocytes from *Tak1*^{D} mice (knockout) or control littermates were purified and sorted by FACS, and then cultured in 96-well plates coated with an anti-CD3ϵ antibody or PBS buffer (as a control). Cells were harvested at indicated time points, incubated with Annexin-V, and then analyzed by FACS. At least 4000 events were analyzed for each sample. Probabilities shown in the diagrams represent samples stimulated with anti-CD3ϵ for 40 hours. Inlet shown at the lower right corner is a typical FACS diagram from $CD4^+$ thymocytes stimulated with anti-CD3ϵ for 40 hours. (B) Tabulation of Annexin-V positive thymocytes after anti-CD3ϵ stimulation.

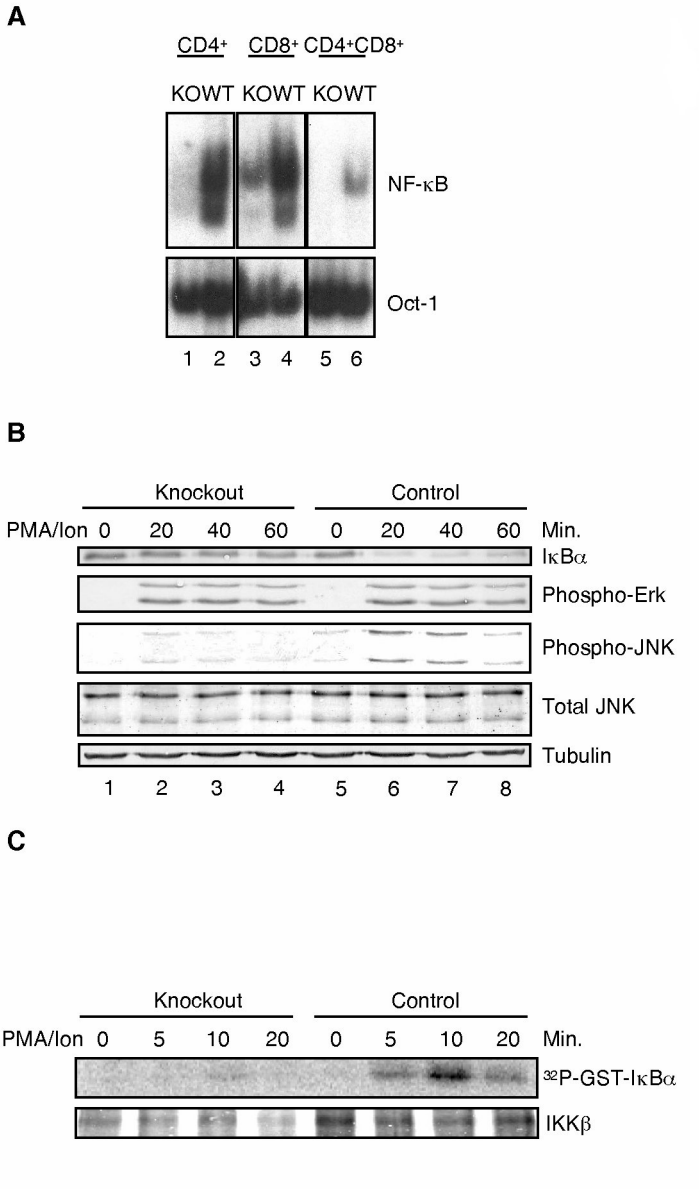
A
CD4+ CD8+ CD4+CD8+
KOWT KOWT KOWT
NF-κB
Oct-1
1 2 3 4 5 6
B
Knockout
Control
PMA/Ion 0 20 40 60 0 20 40 60 Min.
IκBα
Phospho-Erk
Phospho-JNK
Total JNK
Tubulin
1 2 3 4 5 6 7 8
C
Knockout
Control
PMA/Ion 0 5 10 20 0 5 10 20 Min.
32P-GST-IκBα
IKKβ

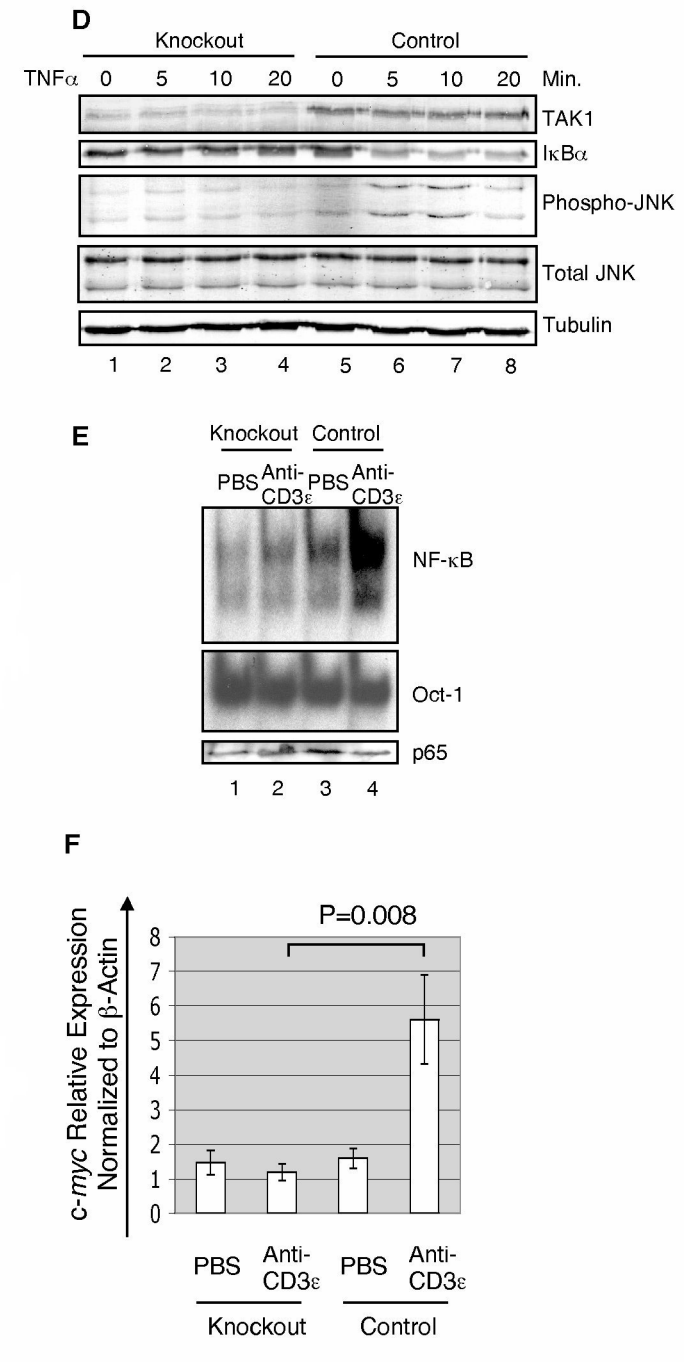

FIGURE 4.5 TAK1 IS REQUIRED FOR THE ACTIVATION OF NF-κB AND JNK IN THYMOCYTES

(A) Electrophoretic mobility shift assays for NF-κB DNA binding activity using whole cell extracts from single positive or double positive thymocytes isolated from *Tak1*^{D} mice (lanes 1, 3 & 5) or control littermates (lanes 2, 4 & 6). In the bottom panel, the same extracts were assayed for DNA binding of the constitutive transcription factor Oct-1. (B) Thymocytes were stimulated with PMA (100 ng/ml) and ionomycin (200 ng/ml) for the indicated time periods, and then cell lysates were harvested for analysis by immunoblotting using antibodies specific for IκBα, phosphorylated JNK or ERK, or tubulin (as a loading control). (C) Thymocytes were stimulated with PMA and ionomycin as described above, and then the IKK complex was immunoprecipitated using a NEMO specific antibody. IKK activity was measured using GST-IκBα-NT (N-terminus) and γ-^{32}P-ATP as the substrates. Aliquots of the immunoprecipitated complexes were subject to immunoblotting using an antibody against IKKβ. (D) Thymocytes were stimulated with TNFα for the indicated time periods, and then cell lysates were harvested for analysis by immunoblotting using antibodies specific for TAK1, IκBα, phosphorylated JNK, or tubulin. (E) Thymocytes were incubated with PBS or plate-bound anti-CD3ϵ for 16 hours and then whole cell extracts were prepared for analyses of NF-κB or OCT-1 DNA binding by EMSA. The same extracts were also subjected to immunoblotting with an antibody against p65. (F) Thymocytes from *Tak1*^{D} mice or control littermates were incubated with PBS or plate-bound anti-CD3ϵ for 20 hours before total RNA was extracted for real time PCR analyses. Two mice were used in each group. The *c-myc* expression levels were normalized to the levels of β-actin. The error bars indicate standard errors.

Tables

Table 4.1 Comparison of thymocyte numbers in *Tak1*^{D} (knockout) mice and control littermates.

Numbers of CD4 and CD8 Thymocytes				
Thymus / Genotype	Total thymocytes (x 10^8)	$CD4^+CD8^+$ double positive (x 10^8)	$CD4^+$ single positive * (x 10^7)	$CD8^+$ single positive * (x 10^7)
control (n=5)	2.81 ± 0.27	2.40 ± 0.26	1.98 ± 0.21	0.71 ± 0.07
knockout (n=5)	2.04 ± 0.47	1.82 ± 0.45	0.82 ± 0.22	0.32 ± 0.03
* t-test p<0.005				

CHAPTER FIVE
Perspectives

In this chapter, I would like to provide more perspectives to my thesis work. For the part of BTB-kelch proteins, corollaries from the structural observations would be discussed. For the part of TAK1 kinase, more issues about lymphocyte development and NF-κB activity would be addressed.

BTB-kelch Proteins

Keap1 is the most well studied BTB-kelch protein. It is an adaptor to Cullin3-mediated ubiquitination and degradation of the Nrf2 transcription factor [24, 51, 125]. Structurally the kelch domain of Keap1 has been resolved [55, 69]. Results from those investigations might provide useful hints for further understanding of KLHL6 and mKelch.

Structural Hints

The crystal structure of the kelch domain of Keap1 is a six-bladed β-propeller. Each blade has four strands linked by out-reaching loops. An interesting feature is a positively-charged surface at the bottom, which is contributed by several Arginine and Histidine residues on the connecting loops between strand 2 and 3 or strand 4 and 1 of various blades. Many of the residues are also responsible for protein-protein interaction to the ETGE motif on Nrf2 [69]. Interestingly the same surface binds to another region on Nrf2 at a lower affinity as well [108]. Therefore stoichiometry between Keap1-Nrf2 interaction is possibly a dimer to monomer relationship [108], which corresponds well to the dimerizing function of the N-terminal BTB domain of Keap1. Another biochemical study has also documented the two-to-one stoichiometry between Keap1 and Nrf2 [33].

Hypothesis: Combinatorial Kelch Codes by BTB Dimerization

The interaction between Keap1 and Nrf2 is contributed to a major extent by electrostatic forces with low specificity, which is much enhanced by a two-site recognition scheme

plus stereotactic stringency by dimerized Keap1 [108]. Potentially the BTB domain can do heterodimerization in addition to homodimerization [7]. Different kelch domains with low specificity could be assembled into a high specificity adaptor by BTB dimerization. Assuming all BTB-kelch proteins are adaptors for Cullin3-based E3, a single kelch domain could be used for different substrates; in the mean while, various combinations of kelch domains could achieve high specificity for lots of protein substrates. It would be an efficient use of genome space for efficient and specific protein degradation. A recent paper documented interaction between KLHL12 and KLHL21 in a pull-down experiment, both of which belong to BTB-kelch proteins [5]. However, the authors did not analyze their binding relationship further.

Hypothesis: Localization by BACK Domain

The BACK domain was found to bridge the N-terminal BTB domain and the C-terminal kelch domain in a bioinformatic study [99]. So far there have been no defined functions for this domain. However, several sulfhydryl groups which are suggested to sense oxidants for Keap1 do reside on this segment [29]. In the literature, the interaction between BTB and Cullin3 seems not under regulation. For example, KLHL12 binds to Cullin-3 in a constitutive manner [5]. There has been no evidence for conditional interaction between the kelch domain and its cognate substrates, either. Therefore the decision between degradation or not for relevant substrates very likely depends on the BACK domain. One possible mechanism is to approximate the whole complex to the vicinity of proteasomes. In the case of Keap1, oxidized BACK domain might lose the approximation to proteasomes and thus increase the level of Nrf2. Alternatively, the BACK domain might control the approximation between the BTB-kelch adaptor and its cognate substrate. For example, KLHL12 reaches Dishevelled in a Wnt-dependent manner [5].

TAK1 in B Cell Development and Activation

The role of TAK1 in B cells have been investigated by crossing floxed *Tak1* mice to the *CD19::Cre* strain [77]. During the breeding period, a similar study in B-cell specific

knockout of *Tak1* was published [88].

B Cell Activation

NF-κB is activated by BCR stimulation through CARD11, BCL10, and MALT1 [see review 104]. The importance of TAK1 in this cascade is suggested by a study of Jurkat T cells in which TCR stimulation leads to NF-κB activation via the same adaptor complex upstream of TAK1 [101]. Unexpectedly, *Tak1*-null murine B cells were still able to activate the NF-κB pathway after anti-IgM stimulation *in vitro* (Figure 5.1). However, a DT40 cell line based study confirmed instead the essential role of TAK1 in NF-κB activation after BCR stimulation [94]. It is unknown if this discrepancy resulted from different species (mouse vs. chicken) or from different TAK1 residual levels (incomplete knockout vs. complete knockout).

B Cell Development

B cells develop through several stages from bone marrow to the periphery [see review 10]. Unlike T cells, loss of TAK1 seemed not important for B cell development (Figure 5.2). Similar results were also found in the published study [88].

TAK1 for Regulatory T Cells, Double Positive Thymocytes, and Peripheral T cells

Another study of TAK1 in T cells has been published recently [115]. In addition to reduced mature T cells, the authors noted compromised development of regulatory T cells, severe disadvantage for *Tak1*-null double positive thymocytes in a competitive bone marrow transplantation experiment, and intact NF-κB activation among *Tak1*-null effector T cells.

Regulatory T Cells

Regulatory T cells is a subset of $CD4^+$ cells which are important for maintaining self-tolerance and immune suppression [see review 36]. In Wan's study [115], loss of TAK1

was accompanied by compromised development of regulatory T cells. However, my studies did not find either reduced $CD4^+CD25^+$ regulatory T cells in the thymus (Figure 5.3) or enlarged spleens as observed by Wan et al [57]. A possible explanation could be due to different Cre lines in both studies; Wan used *CD4::Cre* in their study while I adopted *Lck::Cre* in my study. It seemed that *CD4::Cre*-induced nullity of *Tak1* had different effects on CD4 or CD8 single positive (SP) thymocytes (CD4 SP around 40% of controls and CD8 SP around 16% of controls). In my study, both CD4 and CD8 SP thymocytes were reduced to around half in knockout mice. Therefore the possibility could not be ruled out that Wan's observation on regulatory T cells were due to biased impacts upon CD4-bearing thymocytes by *CD4::Cre* rather than a direct result of nullity of *Tak1* itself.

Double Positive Thymocytes

Wan et al. also used competitive transplantation of bone marrow cells to demonstrate developmental abnormality for *Tak1*-null thymocytes at the double positive stage. However, the phenotype seemed so severe that only 6% double positive thymocytes came from null donors after 8 weeks. The authors did not provide sufficient negative controls such as relative percentages of B cell population after the 8-week period, or relative contributions of bone marrow stem cells from both control and null donors after the 8-week engraftment. If the *Tak1*-null double positive thymocytes do have such severe survival disadvantages, the thymocytes which escape from the Cre excision would have the same advantages in Wan's knockout animals. However, even genomic PCR for CD4 single positive thymocytes from null animals did not detect intact floxed alleles in their study. More experiments would be needed in evaluating the impacts on double positive thymocytes in the absence of TAK1.

Peripheral T Cells

By treating floxed T effector cells with Cre-expressing viruses, Wan et al. could evaluate TAK1 functions among peripheral effector cells. Notably TAK1 level was not knocked down satisfactorily by this approach. Nevertheless, the authors did see compromised JNK activation but relatively intact IκBα degradation after PMA/Ionomycin stimulations. I myself tried to get *Tak1*-null peripheral naïve T cells by using Tamoxifen-inducible Cre

[6]. Though TAK1 was knocked down to some extent, IκBα degradation was still intact after PMA/Ionomycin stimulation (data now shown). Because TAK1 was not completely knocked out in both Wan's study and my own trial, it would be difficult to make a convincing statement about the contribution of TAK1 in activating NF-κB pathway upon peripheral T cells.

NF-κB Activation in Thymocyte Development

NF-κB pathway is activated several times along the developmental stages for T cells [see review 23]. In conditional knockout of IKKβ or IKKγ, thymocytes fail to survive beyond the single positive stage [89]. Similar phenotypes were observed in my conditional knockout of TAK1. In addition, *Tak1*-null thymocytes failed to activate IKK complex after PMA/ionomycin stimulation. Therefore TAK1 is upstream of IKK complex in activating NF-κB during thymocyte development. An interesting observation is that positive selections are not affected in *Tak1*-null thymocytes as CD69 selection markers were expressed normally among single positive cells from knockout animals. Negative selections appeared not to be affected, either, because thymocyte numbers were very similar, and TUNEL stain did not show apparent differences (data not shown). With these arguments, it is worth considering more carefully about the relationship between selections and NF-κB activation.

NF-κB Activation vs. Thymocyte Selections

Previous studies suggested that NF-κB activation is necessary for positive selection of thymocytes [105]. In that study, a superinhibitory IκB was expressed under *CD2* promotor. CD69$^+$ thymocytes were reduced, but total thymocyte numbers were nearly doubled in the transgenic mice. Therefore the absolute number of CD69$^+$ thymocytes were roughly the same between mutant and control mice. Actually the phenotype of increased thymocytes was not observed in other *in vivo* knockout studies, including conditional ablation of IKKβ, IKKγ, or TAK1. A possible explanation was mutant IκB had helped immature thymocytes bypass earlier checkpoints, such as pre-TCR at double negative stages. Therefore many of 'inappropriate' thymocytes at double positive stage failed to pass positive selection not

because of loss of NF-κB activation but because of doomed failure inherited from earlier checkpoint escape. Those which should pass the selections still succeeded so the absolute numbers of CD69$^+$ thymocytes were actually similar.

Another example in favor of uncoupling TCR-induced NF-κB activity from TCR-centered selections came from the knockout study of CARD11 [42]. CARD11 is essential for TCR-induced NF-κB activation for both immature thymocytes and peripheral T cells. However, neither positive selections nor negative selections were impaired in CARD11 knockout animals. Nevertheless, the authors clearly demonstrated impaired NF-κB activation for both immature and mature T-lineage cells after TCR stimulation. Therefore it would be plausible that TCR-induced NF-κB activity is not essential for TCR-centered selections, at least not in a TCR-autonomous manner.

Rescue of *Tak1*-null Thymocytes

Apparently NF-κB activity is essential for thymocytes to pass through the single positive stage during development [57, 115]. However, TCR-induced NF-κB activity seems not required for thymocyte development [42]. It would be possible that NF-κB activity at the single positive stage was actually induced by other receptors. A recent paper which conditionally knocked out TAK1 in epidermis with resultant apoptosis was rescued by abolishing TNFα receptor 1 [68]. A similar developmental scenario could possibly be applied to single positive thymocytes as well.

Stimulated TNFα receptors initiate both NF-κB activation and apoptotic cascades [see review 61]. Without the balance from NF-κB activity, cells would be prone to death after TNFα stimulation. RIP is an important death domain kinase mediating NF-κB activation for TNFα receptors. In a reconstitution experiment, *Rip*-null hematopoietic stem cells failed to populate the recipient with donor T cells unless TNFα receptor 2 was knocked out [25]. Another reconstitution experiment with *IKKβ*-null cells could have mature T cells only after TNFα receptor 1 was also knocked out [92]. Based on these observations, the survival disadvantage for *Tak1*-null thymocytes could possibly be reversed by abolishing the TNFα pathway as well.

If that was the scenario, could there be any functional coupling between TCR and

TNFα receptors? Alternatively, could there be an independent biological role for TNFα activity at that particular stage? There has been a report of increased hyperinflammatory T cells in knockout mice of TNFα receptor 1 [34]. Actually treatment with TNFα inhibitors among patients with rheumatoid arthritis could induce the development of anti-double strand DNA antibodies significantly [35]. A plausible role for TNFα as an independent selection factors for T cell development could not be ruled out.

Figures

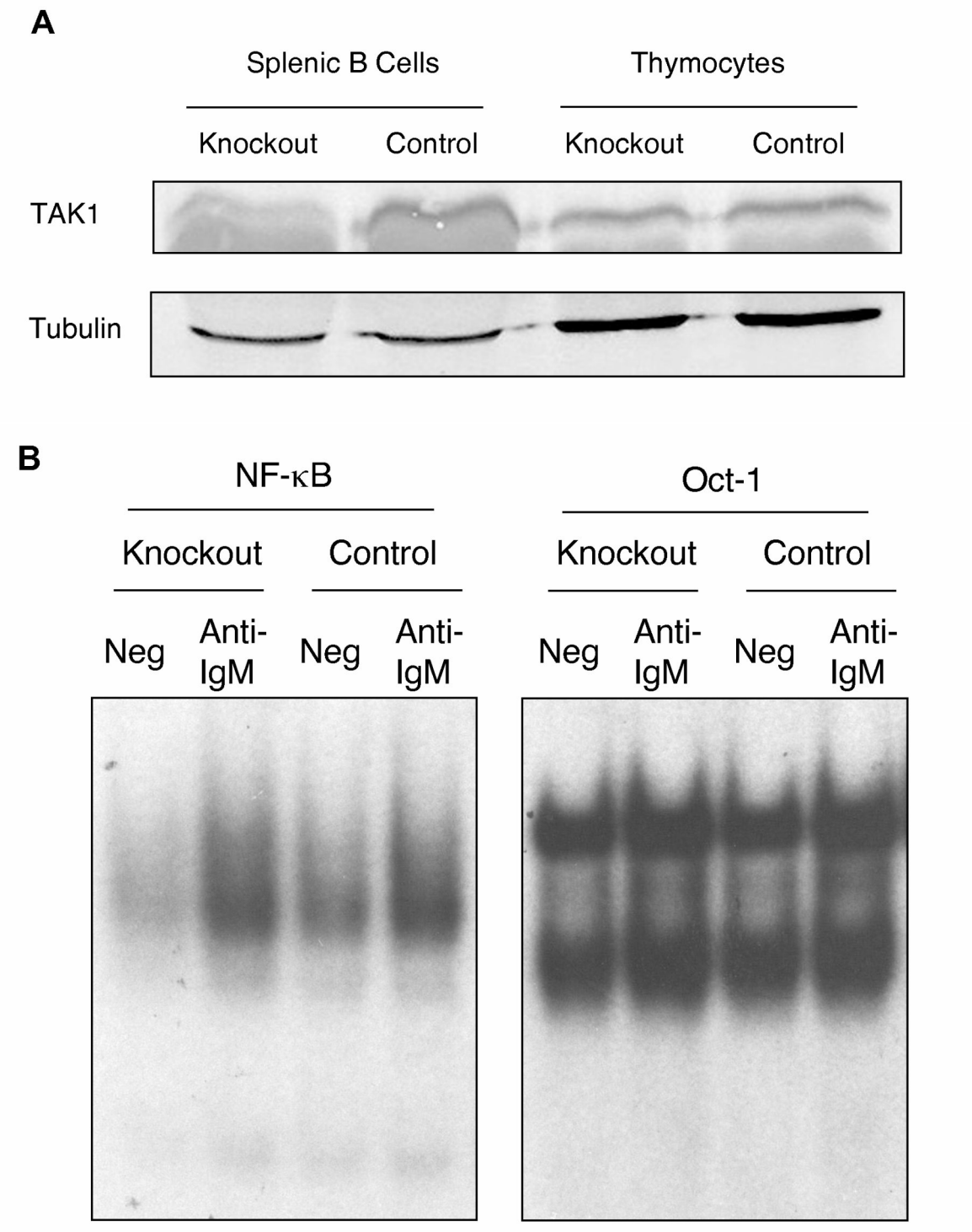
A
Splenic B Cells
Thymocytes
Knockout
Control
Knockout
Control
TAK1
Tubulin
B
NF-κB
Oct-1
Knockout
Control
Knockout
Control
Neg
Anti-IgM
Neg
Anti-IgM
Neg
Anti-IgM
Neg
Anti-IgM

FIGURE 5.1 TAK1 IS NOT REQUIRED FOR NF-κB ACTIVATION AMONG PERIPHERAL B CELLS

(A) Splenic naïve B cells and thymocytes of *Tak1* floxed mice carrying *CD19::Cre* were subject to Western blotting. TAK1 level was much lower among splenic B cells from knockout mice, but not among thymocytes of the same animal. Tubulin was used as loading controls. (B) Lymph node naïve B cells were subject to anti-IgM stimulation. Whole cell lysates were used for gel shift assay. Shift by NF-κB binding in knockout mice was comparable to that in controls. Gel shift by Oct-1 binding was used as loading controls.

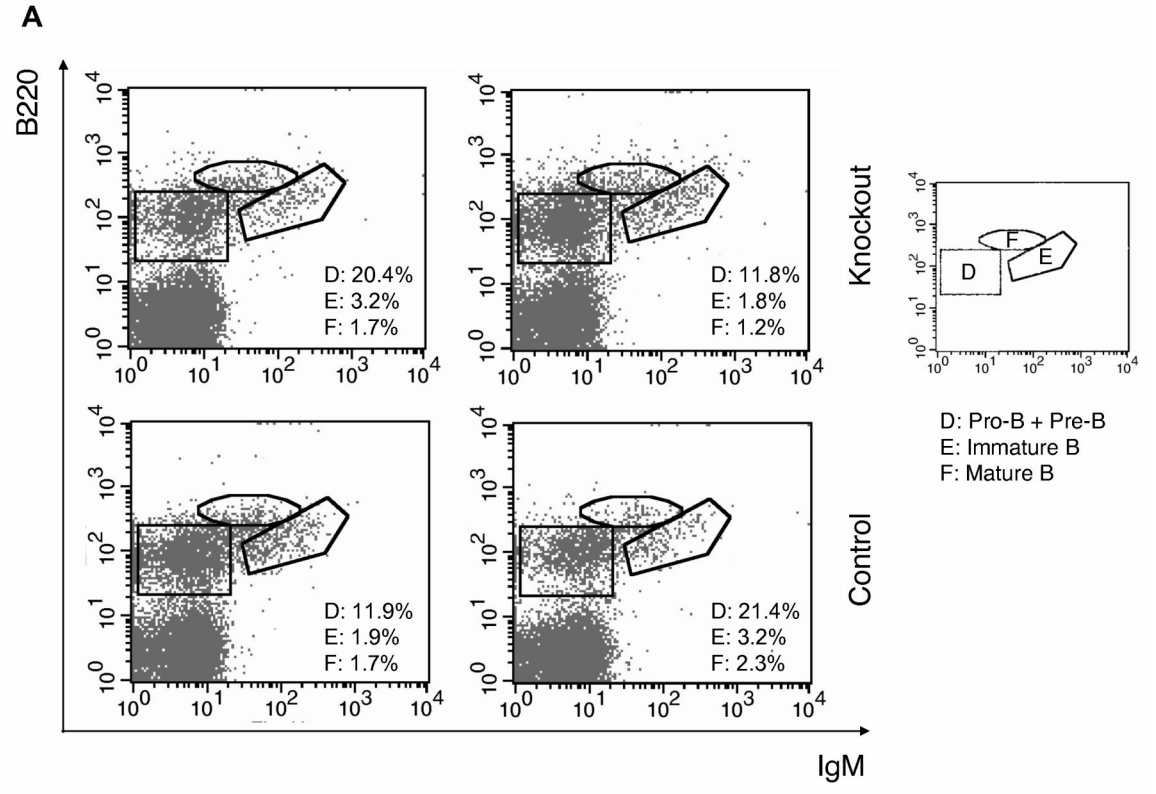

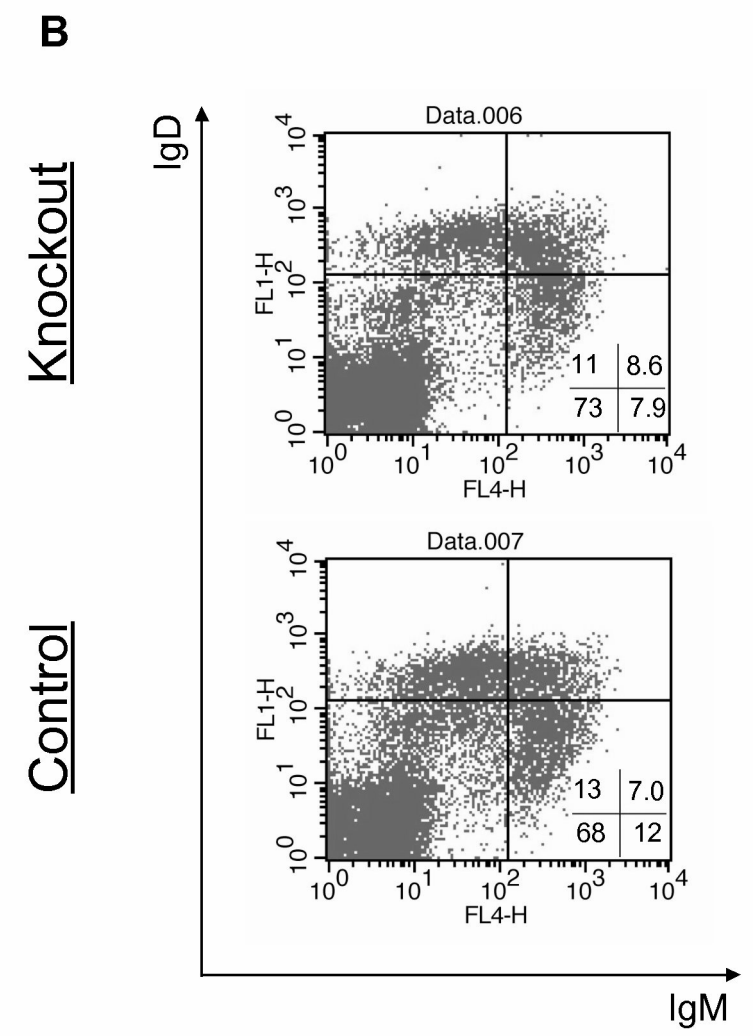

FIGURE 5.2 TAK1 IS NOT IMPORTANT FOR B CELL DEVELOPMENT

(A) Bone marrow B lineages were characterized by anti-IgM and anti-B220 two color FACS. Fraction D contains Pro-B and Pre-B cells. Fraction E contains immature B cells, and fraction F contains mature B cells. (B) Splenic B lineages were characterized by anti-IgM and anti-IgD two color FACS. B cells mature from $IgM^{high}IgD^{low}$, $IgM^{high}IgD^{high}$, to $IgM^{low}IgD^{high}$. Inlets denote percentages.

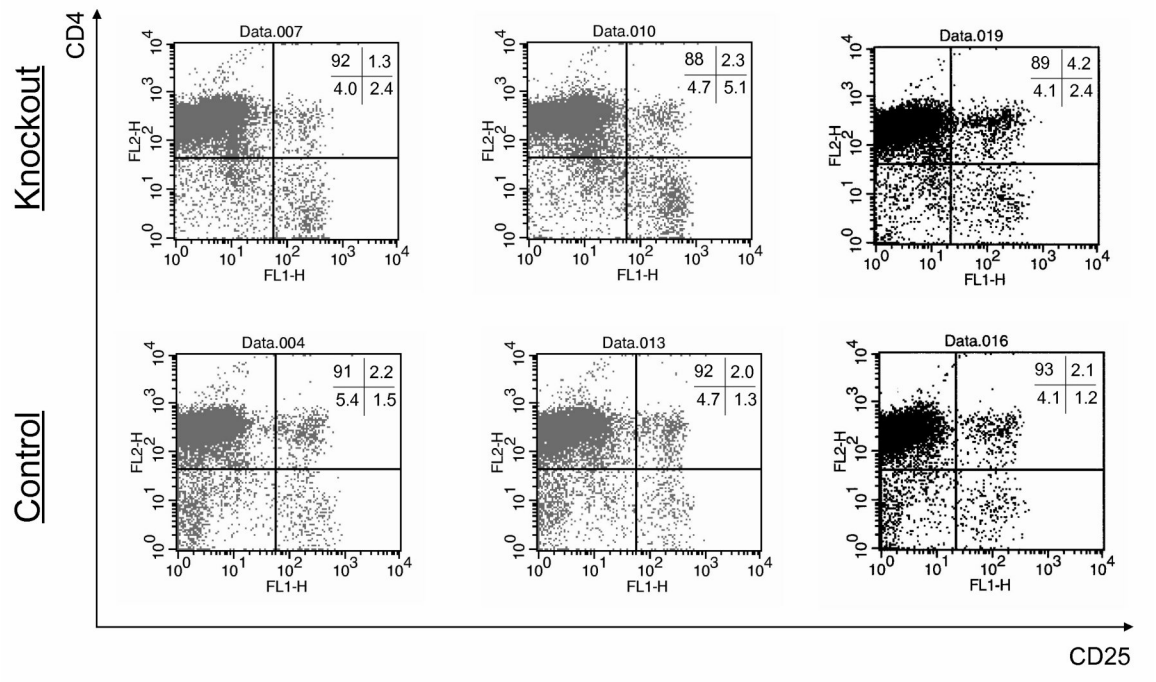

FIGURE 5.3 REGULATORY T CELLS ARE PRESERVED IN *Tak1*-NULL THYMOCYTES BY *Lck::Cre*-INDUCED EXCISION OF *Tak1*

Regulatory T cells in the thymi were characterized by anti-CD4 and anti-CD25 two color FACS. Each genotype comprised of three mice. There were no differences for $CD4^+CD25^+$ regulatory T cells. Inlets denote percentages.

BIBLIOGRAPHY

[1] Adams, J., Kelso, R., and Cooley, L. (2000). The kelch repeat superfamily of proteins: propellers of cell function. Trends Cell Biol, 10(1):17–24.

[2] Akira, S. and Takeda, K. (2004). Toll-like receptor signalling. Nat Rev Immunol, 4(7):499–511.

[3] Allen, E., Ding, J., Wang, W., Pramanik, S., Chou, J., Yau, V., and Yang, Y. (2005). Gigaxonin-controlled degradation of MAP1B light chain is critical to neuronal survival. Nature, 438(7065):224–228.

[4] Andrews, B. J., Proteau, G. A., Beatty, L. G., and Sadowski, P. D. (1985). The FLP recombinase of the 2 micron circle DNA of yeast: interaction with its target sequences. Cell, 40(4):795–803.

[5] Angers, S., Thorpe, C. J., Biechele, T. L., Goldenberg, S. J., Zheng, N., MacCoss, M. J., and Moon, R. T. (2006). The KLHL12-Cullin-3 ubiquitin ligase negatively regulates the Wnt-beta-catenin pathway by targeting Dishevelled for degradation. Nat Cell Biol, 8(4):348–357.

[6] Badea, T. C., Wang, Y., and Nathans, J. (2003). A noninvasive genetic/pharmacologic strategy for visualizing cell morphology and clonal relationships in the mouse. J Neurosci, 23(6):2314–2322.

[7] Bardwell, V. J. and Treisman, R. (1994). The POZ domain: a conserved protein-protein interaction motif. Genes Dev, 8(14):1664–1677.

[8] Bateman, A., Birney, E., Cerruti, L., Durbin, R., Etwiller, L., Eddy, S. R., Griffiths-Jones, S., Howe, K. L., Marshall, M., and Sonnhammer, E. L. L. (2002). The Pfam protein families database. Nucleic Acids Res, 30(1):276–280.

[9] Batlle, M., Lu, A., Green, D. A., Xue, Y., and Hirsch, J. P. (2003). Krh1p and Krh2p act downstream of the Gpa2p G(alpha) subunit to negatively regulate haploid invasive growth. J Cell Sci, 116(Pt 4):701–710.

[10] Blom, B. and Spits, H. (2006). Development of human lymphoid cells. Annu Rev Immunol, 24:287–320.

[11] Bomont, P., Cavalier, L., Blondeau, F., Hamida, C. B., Belal, S., Tazir, M., Demir, E., Topaloglu, H., Korinthenberg, R., Tysz, B., Landrieu, P., Hentati, F., and Koenig, M. (2000). The gene encoding gigaxonin, a new member of the cytoskeletal BTB/kelch repeat family, is mutated in giant axonal neuropathy. Nat Genet, 26(3):370–374.

[12] Broussard-Diehl, C., Bauer, S. R., and Scheuermann, R. H. (1996). A role for c-myc in the regulation of thymocyte differentiation and possibly positive selection. J Immunol, 156(9):3141–3150.

[13] Buhl, A. M., Pleiman, C. M., Rickert, R. C., and Cambier, J. C. (1997). Qualitative regulation of B cell antigen receptor signaling by CD19: selective requirement for PI3-kinase activation, inositol-1,4,5-trisphosphate production and Ca2+ mobilization. J Exp Med, 186(11):1897–1910.

[14] Burge, C. and Karlin, S. (1997). Prediction of complete gene structures in human genomic DNA. J Mol Biol, 268(1):78–94.

[15] Butcher, E. C., Rouse, R. V., Coffman, R. L., Nottenburg, C. N., Hardy, R. R., and Weissman, I. L. (1982). Surface phenotype of Peyer's patch germinal center cells: implications for the role of germinal centers in B cell differentiation. J Immunol, 129(6):2698–2707.

[16] Cantrell, D. A. (2002). Transgenic analysis of thymocyte signal transduction. Nat Rev Immunol, 2(1):20–27.

[17] Carsetti, R. (2004). Characterization of B-cell maturation in the peripheral immune system. Methods Mol Biol, 271:25–35.

[18] Carsetti, R., Khler, G., and Lamers, M. C. (1995). Transitional B cells are the target of negative selection in the B cell compartment. J Exp Med, 181(6):2129–2140.

[19] Carsetti, R., Rosado, M. M., and Wardmann, H. (2004). Peripheral development of B cells in mouse and man. Immunol Rev, 197:179–191.

[20] Carter, R. H., Spycher, M. O., Ng, Y. C., Hoffman, R., and Fearon, D. T. (1988). Synergistic interaction between complement receptor type 2 and membrane IgM on B lymphocytes. J Immunol, 141(2):457–463.

[21] Chen, G. and Goeddel, D. V. (2002). TNF-R1 signaling: a beautiful pathway. Science, 296(5573):1634–1635.

[22] Chenna, R., Sugawara, H., Koike, T., Lopez, R., Gibson, T. J., Higgins, D. G., and Thompson, J. D. (2003). Multiple sequence alignment with the Clustal series of programs. Nucleic Acids Res, 31(13):3497–3500.

[23] Claudio, E., Brown, K., and Siebenlist, U. (2006). NF-kappaB guides the survival and differentiation of developing lymphocytes. Cell Death Differ, 13(5):697–701.

[24] Cullinan, S. B., Gordan, J. D., Jin, J., Harper, J. W., and Diehl, J. A. (2004). The Keap1-BTB protein is an adaptor that bridges Nrf2 to a Cul3-based E3 ligase: oxidative stress sensing by a Cul3-Keap1 ligase. Mol Cell Biol, 24(19):8477–8486.

[25] Cusson, N., Oikemus, S., Kilpatrick, E. D., Cunningham, L., and Kelliher, M. (2002). The death domain kinase RIP protects thymocytes from tumor necrosis factor receptor type 2-induced cell death. J Exp Med, 196(1):15–26.

[26] DeLano, W. L. (2002). The pymol molecular graphics system. http://www.pymol.org. DeLano Scientific, San Carlos, CA, USA.

[27] Deng, L., Wang, C., Spencer, E., Yang, L., Braun, A., You, J., Slaughter, C., Pickart, C., and Chen, Z. J. (2000). Activation of the IkappaB kinase complex by TRAF6 requires a dimeric ubiquitin-conjugating enzyme complex and a unique polyubiquitin chain. Cell, 103(2):351–361.

[28] Ding, J., Allen, E., Wang, W., Valle, A., Wu, C., Nardine, T., Cui, B., Yi, J., Taylor, A., Jeon, N. L., Chu, S., So, Y., Vogel, H., Tolwani, R., Mobley, W., and Yang, Y. (2006). Gene targeting of GAN in mouse causes a toxic accumulation of microtubule-associated protein 8 and impaired retrograde axonal transport. Hum Mol Genet.

[29] Dinkova-Kostova, A. T., Holtzclaw, W. D., Cole, R. N., Itoh, K., Wakabayashi, N., Katoh, Y., Yamamoto, M., and Talalay, P. (2002). Direct evidence that sulfhydryl groups of Keap1 are the sensors regulating induction of phase 2 enzymes that protect against carcinogens and oxidants. Proc Natl Acad Sci U S A, 99(18):11908–11913.

[30] Dunne, A. and O'Neill, L. A. J. (2003). The interleukin-1 receptor/Toll-like receptor superfamily: signal transduction during inflammation and host defense. Sci STKE, 2003(171):re3.

[31] Duyao, M. P., Buckler, A. J., and Sonenshein, G. E. (1990). Interaction of an nf-kappa b-like factor with a site upstream of the c-myc promoter. Proc Natl Acad Sci U S A, 87(12):4727–4731.

[32] Egawa, T., Albrecht, B., Favier, B., Sunshine, M.-J., Mirchandani, K., O'Brien, W., Thome, M., and Littman, D. R. (2003). Requirement for CARMA1 in antigen receptor-induced NF-kappa B activation and lymphocyte proliferation. Curr Biol, 13(14):1252–1258.

[33] Eggler, A. L., Liu, G., Pezzuto, J. M., van Breemen, R. B., and Mesecar, A. D. (2005). Modifying specific cysteines of the electrophile-sensing human Keap1 protein is insufficient to disrupt binding to the Nrf2 domain Neh2. Proc Natl Acad Sci U S A, 102(29):10070–10075.

[34] Ehlers, S., Kutsch, S., Ehlers, E. M., Benini, J., and Pfeffer, K. (2000). Lethal granuloma disintegration in mycobacteria-infected tnfrp55-/- mice is dependent on t cells and il-12. J Immunol, 165(1):483–492.

[35] Eriksson, C., Engstrand, S., Sundqvist, K.-G., and Rantap-Dahlqvist, S. (2005). Autoantibody formation in patients with rheumatoid arthritis treated with anti-tnf alpha. Ann Rheum Dis, 64(3):403–407.

[36] Fehrvari, Z. and Sakaguchi, S. (2004). CD4+ Tregs and immune control. J Clin Invest, 114(9):1209–1217.

[37] Fischer, M. B., Goerg, S., Shen, L., Prodeus, A. P., Goodnow, C. C., Kelsoe, G., and Carroll, M. C. (1998). Dependence of germinal center B cells on expression of CD21/CD35 for survival. Science, 280(5363):582–585.

[38] Furukawa, M., He, Y. J., Borchers, C., and Xiong, Y. (2003). Targeting of protein ubiquitination by BTB-Cullin 3-Roc1 ubiquitin ligases. Nat Cell Biol, 5(11):1001–1007.

[39] Geyer, R., Wee, S., Anderson, S., Yates, J., and Wolf, D. A. (2003). BTB/POZ domain proteins are putative substrate adaptors for cullin 3 ubiquitin ligases. Mol Cell, 12(3):783–790.

[40] Gulbins, E., Coggeshall, K. M., Baier, G., Katzav, S., Burn, P., and Altman, A. (1993). Tyrosine kinase-stimulated guanine nucleotide exchange activity of Vav in T cell activation. Science, 260(5109):822–825.

[41] Gupta-Rossi, N., Storck, S., Griebel, P. J., Reynaud, C.-A., Weill, J.-C., and Dahan, A. (2003). Specific over-expression of deltex and a new Kelch-like protein in human germinal center B cells. Mol Immunol, 39(13):791–799.

[42] Hara, H., Wada, T., Bakal, C., Kozieradzki, I., Suzuki, S., Suzuki, N., Nghiem, M., Griffiths, E. K., Krawczyk, C., Bauer, B., D'Acquisto, F., Ghosh, S., Yeh, W. C., Baier, G., Rottapel, R., and Penninger, J. M. (2003). The MAGUK family protein CARD11 is essential for lymphocyte activation. Immunity, 18(6):763–775.

[43] Harashima, T. and Heitman, J. (2002). The Galpha protein Gpa2 controls yeast differentiation by interacting with kelch repeat proteins that mimic Gbeta subunits. Mol Cell, 10(1):163–173.

[44] Hardy, R. R., Carmack, C. E., Shinton, S. A., Kemp, J. D., and Hayakawa, K. (1991). Resolution and characterization of pro-B and pre-pro-B cell stages in normal mouse bone marrow. J Exp Med, 173(5):1213–1225.

[45] Hattar, S., Liao, H. W., Takao, M., Berson, D. M., and Yau, K. W. (2002). Melanopsin-containing retinal ganglion cells: architecture, projections, and intrinsic photosensitivity. Science, 295(5557):1065–1070.

[46] Hattar, S., Lucas, R. J., Mrosovsky, N., Thompson, S., Douglas, R. H., Hankins, M. W., Lem, J., Biel, M., Hofmann, F., Foster, R. G., and Yau, K.-W. (2003). Melanopsin and rod-cone photoreceptive systems account for all major accessory visual functions in mice. Nature, 424(6944):76–81.

[47] Hennet, T., Hagen, F. K., Tabak, L. A., and Marth, J. D. (1995). T-cell-specific deletion of a polypeptide N-acetylgalactosaminyl-transferase gene by site-directed recombination. Proc Natl Acad Sci U S A, 92(26):12070–12074.

[48] Hettmann, T. and Leiden, J. M. (2000). NF-kappa B is required for the positive selection of CD8+ thymocytes. J Immunol, 165(9):5004–5010.

[49] Itoh, K., Wakabayashi, N., Katoh, Y., Ishii, T., Igarashi, K., Engel, J. D., and Yamamoto, M. (1999). Keap1 represses nuclear activation of antioxidant responsive elements by Nrf2 through binding to the amino-terminal Neh2 domain. Genes Dev, 13(1):76–86.

[50] Kanayama, A., Seth, R. B., Sun, L., Ea, C.-K., Hong, M., Shaito, A., Chiu, Y.-H., Deng, L., and Chen, Z. J. (2004). TAB2 and TAB3 activate the NF-kappaB pathway through binding to polyubiquitin chains. Mol Cell, 15(4):535–548.

[51] Kobayashi, A., Kang, M.-I., Okawa, H., Ohtsuji, M., Zenke, Y., Chiba, T., Igarashi, K., and Yamamoto, M. (2004). Oxidative stress sensor Keap1 functions as an adaptor for Cul3-based E3 ligase to regulate proteasomal degradation of Nrf2. Mol Cell Biol, 24(16):7130–7139.

[52] Kobayashi, M., Itoh, K., Suzuki, T., Osanai, H., Nishikawa, K., Katoh, Y., Takagi, Y., and Yamamoto, M. (2002). Identification of the interactive interface and phylogenic conservation of the Nrf2-Keap1 system. Genes Cells, 7(8):807–820.

[53] Kutuzov, M. A. and Andreeva, A. V. (2002). Protein Ser/Thr phosphatases with kelch-like repeat domains. Cell Signal, 14(9):745–750.

[54] Levine, M. H., Haberman, A. M., Sant'Angelo, D. B., Hannum, L. G., Cancro, M. P., Janeway, C. A., and Shlomchik, M. J. (2000). A B-cell receptor-specific selection step governs immature to mature B cell differentiation. Proc Natl Acad Sci U S A, 97(6):2743–2748.

[55] Li, X., Zhang, D., Hannink, M., and Beamer, L. J. (2004). Crystal structure of the Kelch domain of human Keap1. J Biol Chem, 279(52):54750–54758.

[56] Lin, X. and Wang, D. (2004). The roles of CARMA1, Bcl10, and MALT1 in antigen receptor signaling. Semin Immunol, 16(6):429–435.

[57] Liu, H.-H., Xie, M., Schneider, M. D., and Chen, Z. J. (2006). Essential role of tak1 in thymocyte development and activation. Proc Natl Acad Sci U S A, 103(31):11677–11682.

[58] Lobe, C. G., Koop, K. E., Kreppner, W., Lomeli, H., Gertsenstein, M., and Nagy, A. (1999). Z/AP, a double reporter for cre-mediated recombination. Dev Biol, 208(2):281–292.

[59] Loder, F., Mutschler, B., Ray, R. J., Paige, C. J., Sideras, P., Torres, R., Lamers, M. C., and Carsetti, R. (1999). B cell development in the spleen takes place in discrete steps and is determined by the quality of B cell receptor-derived signals. J Exp Med, 190(1):75–89.

[60] Lucas, P. C., McAllister-Lucas, L. M., and Nunez, G. (2004). NF-kappaB signaling in lymphocytes: a new cast of characters. J Cell Sci, 117(Pt 1):31–39.

[61] MacEwan, D. J. (2002). TNF receptor subtype signalling: differences and cellular consequences. Cell Signal, 14(6):477–492.

[62] McPherson, M. J., Ogel, Z. B., Stevens, C., Yadav, K. D., Keen, J. N., and Knowles, P. F. (1992). Galactose oxidase of Dactylium dendroides. Gene cloning and sequence analysis. J Biol Chem, 267(12):8146–8152.

[63] Mora-Garca, S., Vert, G., Yin, Y., Cao-Delgado, A., Cheong, H., and Chory, J. (2004). Nuclear protein phosphatases with Kelch-repeat domains modulate the response to brassinosteroids in Arabidopsis. Genes Dev, 18(4):448–460.

[64] Nacak, T. G., Leptien, K., Fellner, D., Augustin, H. G., and Kroll, J. (2006). The BTB-kelch protein LZTR-1 is a novel golgi protein that is degraded upon induction of apoptosis. J Biol Chem, 281(8):5065–5071.

[65] Nagro, C. J. D., Otero, D. C., Anzelon, A. N., Omori, S. A., Kolla, R. V., and Rickert, R. C. (2005). CD19 function in central and peripheral B-cell development. Immunol Res, 31(2):119–131.

[66] Newton, K. and Dixit, V. M. (2003). Mice lacking the CARD of CARMA1 exhibit defective B lymphocyte development and impaired proliferation of their B and T lymphocytes. Curr Biol, 13(14):1247–1251.

[67] Ninomiya-Tsuji, J., Kishimoto, K., Hiyama, A., Inoue, J., Cao, Z., and Matsumoto, K. (1999). The kinase TAK1 can activate the NIK-I kappaB as well as the MAP kinase cascade in the IL-1 signalling pathway. Nature, 398(6724):252–256.

[68] Omori, E., Matsumoto, K., Sanjo, H., Sato, S., Akira, S., Smart, R. C., and Ninomiya-Tsuji, J. (2006). TAK1 is a master regulator of epidermal homeostasis involving skin inflammation and apoptosis. J Biol Chem.

[69] Padmanabhan, B., Tong, K. I., Ohta, T., Nakamura, Y., Scharlock, M., Ohtsuji, M., Kang, M.-I., Kobayashi, A., Yokoyama, S., and Yamamoto, M. (2006). Structural basis for defects of keap1 activity provoked by its point mutations in lung cancer. Mol Cell, 21(5):689–700.

[70] Panda, S., Provencio, I., Tu, D. C., Pires, S. S., Rollag, M. D., Castrucci, A. M., Pletcher, M. T., Sato, T. K., Wiltshire, T., Andahazy, M., Kay, S. A., Gelder, R. N. V., and Hogenesch, J. B. (2003). Melanopsin is required for non-image-forming photic responses in blind mice. Science, 301(5632):525–527.

[71] Peirson, S. and Foster, R. G. (2006). Melanopsin: another way of signaling light. Neuron, 49(3):331–339.

[72] Petroski, M. D. and Deshaies, R. J. (2005). Function and regulation of cullin-RING ubiquitin ligases. Nat Rev Mol Cell Biol, 6(1):9–20.

[73] Pintard, L., Willis, J. H., Willems, A., Johnson, J.-L. F., Srayko, M., Kurz, T., Glaser, S., Mains, P. E., Tyers, M., Bowerman, B., and Peter, M. (2003). The BTB protein MEL-26 is a substrate-specific adaptor of the CUL-3 ubiquitin-ligase. Nature, 425(6955):311–316.

[74] Prag, S. and Adams, J. C. (2003). Molecular phylogeny of the kelch-repeat superfamily reveals an expansion of BTB/kelch proteins in animals. BMC Bioinformatics, 4:42.

[75] Rameh, L. E., Rhee, S. G., Spokes, K., Kazlauskas, A., Cantley, L. C., and Cantley, L. G. (1998). Phosphoinositide 3-kinase regulates phospholipase Cgamma-mediated calcium signaling. J Biol Chem, 273(37):23750–23757.

[76] Rickert, R. C., Rajewsky, K., and Roes, J. (1995). Impairment of T-cell-dependent B-cell responses and B-1 cell development in CD19-deficient mice. Nature, 376(6538):352–355.

[77] Rickert, R. C., Roes, J., and Rajewsky, K. (1997). B lymphocyte-specific, Cre-mediated mutagenesis in mice. Nucleic Acids Res, 25(6):1317–1318.

[78] Robinson, D. N. and Cooley, L. (1997). Drosophila kelch is an oligomeric ring canal actin organizer. J Cell Biol, 138(4):799–810.

[79] Rodrguez, C. I., Buchholz, F., Galloway, J., Sequerra, R., Kasper, J., Ayala, R., Stewart, A. F., and Dymecki, S. M. (2000). High-efficiency deleter mice show that FLPe is an alternative to Cre-loxP. Nat Genet, 25(2):139–140.

[80] Rolink, A., Grawunder, U., Haasner, D., Strasser, A., and Melchers, F. (1993). Immature surface Ig+ B cells can continue to rearrange kappa and lambda L chain gene loci. J Exp Med, 178(4):1263–1270.

[81] Rothenberg, E. V. and Taghon, T. (2005). Molecular genetics of T cell development. Annu Rev Immunol, 23:601–649.

[82] Rozen, S. and Skaletsky, H. (2000). Bioinformatics Methods and Protocols: Methods in Molecular Biology. Humana Press, Totowa, NJ, pp 365-386.

[83] Ruefli-Brasse, A. A., French, D. M., and Dixit, V. M. (2003). Regulation of NF-kappaB-dependent lymphocyte activation and development by paracaspase. Science, 302(5650):1581–1584.

[84] Ruland, J., Duncan, G. S., Elia, A., del Barco Barrantes, I., Nguyen, L., Plyte, S., Millar, D. G., Bouchard, D., Wakeham, A., Ohashi, P. S., and Mak, T. W. (2001). Bcl10 is a positive regulator of antigen receptor-induced activation of NF-kappaB and neural tube closure. Cell, 104(1):33–42.

[85] Ruland, J., Duncan, G. S., Wakeham, A., and Mak, T. W. (2003). Differential requirement for Malt1 in T and B cell antigen receptor signaling. Immunity, 19(5):749–758.

[86] Sakai, K. and Miyazaki, J. (1997). A transgenic mouse line that retains Cre recombinase activity in mature oocytes irrespective of the cre transgene transmission. Biochem Biophys Res Commun, 237(2):318–324.

[87] Sanes, J. R., Rubenstein, J. L., and Nicolas, J. F. (1986). Use of a recombinant retrovirus to study post-implantation cell lineage in mouse embryos. EMBO J, 5(12):3133–3142.

[88] Sato, S., Sanjo, H., Takeda, K., Ninomiya-Tsuji, J., Yamamoto, M., Kawai, T., Matsumoto, K., Takeuchi, O., and Akira, S. (2005). Essential function for the kinase TAK1 in innate and adaptive immune responses. Nat Immunol, 6(11):1087–1095.

[89] Schmidt-Supprian, M., Courtois, G., Tian, J., Coyle, A. J., Isral, A., Rajewsky, K., and Pasparakis, M. (2003). Mature T cells depend on signaling through the IKK complex. Immunity, 19(3):377–389.

[90] Schulman, B. A., Carrano, A. C., Jeffrey, P. D., Bowen, Z., Kinnucan, E. R., Finnin, M. S., Elledge, S. J., Harper, J. W., Pagano, M., and Pavletich, N. P. (2000). Insights into SCF ubiquitin ligases from the structure of the Skp1-Skp2 complex. Nature, 408(6810):381–386.

[91] Sekaran, S., Foster, R. G., Lucas, R. J., and Hankins, M. W. (2003). Calcium imaging reveals a network of intrinsically light-sensitive inner-retinal neurons. Curr Biol, 13(15):1290–1298.

[92] Senftleben, U., Li, Z. W., Baud, V., and Karin, M. (2001). IKKbeta is essential for protecting T cells from TNFalpha-induced apoptosis. Immunity, 14(3):217–230.

[93] Shim, J.-H., Xiao, C., Paschal, A. E., Bailey, S. T., Rao, P., Hayden, M. S., Lee, K.-Y., Bussey, C., Steckel, M., Tanaka, N., Yamada, G., Akira, S., Matsumoto, K., and Ghosh, S. (2005). TAK1, but not TAB1 or TAB2, plays an essential role in multiple signaling pathways in vivo. Genes Dev, 19(22):2668–2681.

[94] Shinohara, H., Yasuda, T., Aiba, Y., Sanjo, H., Hamadate, M., Watarai, H., Sakurai, H., and Kurosaki, T. (2005). PKC beta regulates BCR-mediated IKK activation by facilitating the interaction between TAK1 and CARMA1. J Exp Med, 202(10):1423–1431.

[95] Shivtiel, S., Leider, N., Sadeh, O., Kraiem, Z., and Melamed, D. (2002). Impaired light chain allelic exclusion and lack of positive selection in immature B cells expressing incompetent receptor deficient of CD19. J Immunol, 168(11):5596–5604.

[96] Siebenlist, U., Brown, K., and Claudio, E. (2005). Control of lymphocyte development by nuclear factor-kappaB. Nat Rev Immunol, 5(6):435–445.

[97] Silverman, N. and Maniatis, T. (2001). NF-kappaB signaling pathways in mammalian and insect innate immunity. Genes Dev, 15(18):2321–2342.

[98] Simeoni, L., Kliche, S., Lindquist, J., and Schraven, B. (2004). Adaptors and linkers in T and B cells. Curr Opin Immunol, 16(3):304–313.

[99] Stogios, P. J. and Priv, G. G. (2004). The BACK domain in BTB-kelch proteins. Trends Biochem Sci, 29(12):634–637.

[100] Sun, L. and Chen, Z. J. (2004). The novel functions of ubiquitination in signaling. Curr Opin Cell Biol, 16(2):119–126.

[101] Sun, L., Deng, L., Ea, C.-K., Xia, Z.-P., and Chen, Z. J. (2004). The TRAF6 ubiquitin ligase and TAK1 kinase mediate IKK activation by BCL10 and MALT1 in T lymphocytes. Mol Cell, 14(3):289–301.

[102] Swiatek, P. J. and Gridley, T. (1993). Perinatal lethality and defects in hindbrain development in mice homozygous for a targeted mutation of the zinc finger gene Krox20. Genes Dev, 7(11):2071–2084.

[103] Testi, R., D'Ambrosio, D., Maria, R. D., and Santoni, A. (1994). The CD69 receptor: a multipurpose cell-surface trigger for hematopoietic cells. Immunol Today, 15(10):479–483.

[104] Thome, M. (2004). CARMA1, BCL-10 and MALT1 in lymphocyte development and activation. Nat Rev Immunol, 4(5):348–359.

[105] Thome, M. and Tschopp, J. (2003). TCR-induced NF-kappaB activation: a crucial role for Carma1, Bcl10 and MALT1. Trends Immunol, 24(8):419–424.

[106] Tian, T., Zhang, J., Gao, L., Qian, X. P., and Chen, W. F. (2001). Heterogeneity within medullary-type TCRalphabeta(+)CD3(+)CD4(-)CD8(+) thymocytes in normal mouse thymus. Int Immunol, 13(3):313–320.

[107] Toba, K., Winton, E. F., Koike, T., and Shibata, A. (1995). Simultaneous three-color analysis of the surface phenotype and DNA-RNA quantitation using 7-amino-actinomycin D and pyronin Y. J Immunol Methods, 182(2):193–207.

[108] Tong, K. I., Katoh, Y., Kusunoki, H., Itoh, K., Tanaka, T., and Yamamoto, M. (2006). Keap1 recruits neh2 through binding to etge and dlg motifs: characterization of the two-site molecular recognition model. Mol Cell Biol, 26(8):2887–2900.

[109] Tsokos, G. C., Lambris, J. D., Finkelman, F. D., Anastassiou, E. D., and June, C. H. (1990). Monovalent ligands of complement receptor 2 inhibit whereas polyvalent ligands enhance anti-Ig-induced human B cell intracytoplasmic free calcium concentration. J Immunol, 144(5):1640–1645.

[110] Turner, M., Mee, P. J., Walters, A. E., Quinn, M. E., Mellor, A. L., Zamoyska, R., and Tybulewicz, V. L. (1997). A requirement for the Rho-family GTP exchange factor Vav in positive and negative selection of thymocytes. Immunity, 7(4):451–460.

[111] Vidal, S., Khush, R. S., Leulier, F., Tzou, P., Nakamura, M., and Lemaitre, B. (2001). Mutations in the Drosophila dTAK1 gene reveal a conserved function for MAPKKKs in the control of rel/NF-kappaB-dependent innate immune responses. Genes Dev, 15(15):1900–1912.

[112] Voll, R. E., Jimi, E., Phillips, R. J., Barber, D. F., Rincon, M., Hayday, A. C., Flavell, R. A., and Ghosh, S. (2000). NF-kappa B activation by the pre-T cell receptor serves as a selective survival signal in T lymphocyte development. Immunity, 13(5):677–689.

[113] Wakabayashi, N., Itoh, K., Wakabayashi, J., Motohashi, H., Noda, S., Takahashi, S., Imakado, S., Kotsuji, T., Otsuka, F., Roop, D. R., Harada, T., Engel, J. D., and Yamamoto, M. (2003). Keap1-null mutation leads to postnatal lethality due to constitutive Nrf2 activation. Nat Genet, 35(3):238–245.

[114] Wall, M. A., Coleman, D. E., Lee, E., Iiguez-Lluhi, J. A., Posner, B. A., Gilman, A. G., and Sprang, S. R. (1995). The structure of the G protein heterotrimer Gi alpha 1 beta 1 gamma 2. Cell, 83(6):1047–1058.

[115] Wan, Y. Y., Chi, H., Xie, M., Schneider, M. D., and Flavell, R. A. (2006). The kinase TAK1 integrates antigen and cytokine receptor signaling for T cell development, survival and function. Nat Immunol, 7(8):851–858.

[116] Wang, C., Deng, L., Hong, M., Akkaraju, G. R., Inoue, J., and Chen, Z. J. (2001). TAK1 is a ubiquitin-dependent kinase of MKK and IKK. Nature, 412(6844):346–351.

[117] Wang, W., Ding, J., Allen, E., Zhu, P., Zhang, L., Vogel, H., and Yang, Y. (2005). Gigaxonin interacts with tubulin folding cofactor B and controls its degradation through the ubiquitin-proteasome pathway. Curr Biol, 15(22):2050–2055.

[118] Wang, W., Wykrzykowska, J., Johnson, T., Sen, R., and Sen, J. (1999). A nf-kappa b/c-myc-dependent survival pathway is targeted by corticosteroids in immature thymocytes. J Immunol, 162(1):314–322.

[119] Weil, R. and Isral, A. (2004). T-cell-receptor- and B-cell-receptor-mediated activation of NF-kappaB in lymphocytes. Curr Opin Immunol, 16(3):374–381.

[120] Weng, W. K., Jarvis, L., and LeBien, T. W. (1994). Signaling through CD19 activates Vav/mitogen-activated protein kinase pathway and induces formation of a CD19/Vav/phosphatidylinositol 3-kinase complex in human B cell precursors. J Biol Chem, 269(51):32514–32521.

[121] Whitmore, D., Foulkes, N. S., and Sassone-Corsi, P. (2000). Light acts directly on organs and cells in culture to set the vertebrate circadian clock. Nature, 404(6773):87–91.

[122] Xu, L., Wei, Y., Reboul, J., Vaglio, P., Shin, T.-H., Vidal, M., Elledge, S. J., and Harper, J. W. (2003). BTB proteins are substrate-specific adaptors in an SCF-like modular ubiquitin ligase containing CUL-3. Nature, 425(6955):316–321.

[123] Yamasaki, S., Ishikawa, E., Sakuma, M., Ogata, K., Sakata-Sogawa, K., Hiroshima, M., Wiest, D. L., Tokunaga, M., and Saito, T. (2006). Mechanistic basis of pre-T cell receptor-mediated autonomous signaling critical for thymocyte development. Nat Immunol, 7(1):67–75.

[124] Yan, W., Ma, L., Burns, K. H., and Matzuk, M. M. (2004). Haploinsufficiency of kelch-like protein homolog 10 causes infertility in male mice. Proc Natl Acad Sci U S A, 101(20):7793–7798.

[125] Zhang, D. D., Lo, S.-C., Cross, J. V., Templeton, D. J., and Hannink, M. (2004). Keap1 is a redox-regulated substrate adaptor protein for a Cul3-dependent ubiquitin ligase complex. Mol Cell Biol, 24(24):10941–10953.

[126] Zhou, H., Wertz, I., O'Rourke, K., Ultsch, M., Seshagiri, S., Eby, M., Xiao, W., and Dixit, V. M. (2004). Bcl10 activates the NF-kappaB pathway through ubiquitination of NEMO. Nature, 427(6970):167–171.

[127] Ziegler, S. F., Ramsdell, F., and Alderson, M. R. (1994). The activation antigen CD69. Stem Cells, 12(5):456–465.

[128] Zollman, S., Godt, D., Priv, G. G., Couderc, J. L., and Laski, F. A. (1994). The BTB domain, found primarily in zinc finger proteins, defines an evolutionarily conserved family that includes several developmentally regulated genes in Drosophila. Proc Natl Acad Sci U S A, 91(22):10717–10721.

VITAE

Hong-Hsing Liu was born in Taichung, Taiwan on September 2^{nd}, 1971, the son of Zhen-Gui Liu and Bi-Ru Huang. After completing his work at Viator high School, Taichung in 1989, he entered Medical School of National Taiwan University at Taipei. He received the degree of Medicine from National Taiwan University in June, 1996. During the following two years he fulfilled obligatory military service at Chungli. In 1998, he married YenJu, Connie, Tsuei. From 1998 to 2001, he did his residency in the Pediatrics Department of National Taiwan University Hospital. Twin boys, Chih-Wei, Joshua, and Chih-Lun, Julian, were born in 2000. In 2001, he was certified by the Board of Pediatrics in Taiwan. In August 2001, he entered the Graduate School of Biomedical Sciences, The University of Texas Southwestern Medical Center at Dallas.

Permanent Address: No. 11, Alley 7, Lane 402,
Sec. 1, Zhongshan Rd.,
Pinlin Village, Taiping City,
Taichung County, Taiwan 411